2013

Feedback control of sector-bound nonlinear systems with applications to aeroengine control

Luis Donaldo Alvergue
Louisiana State University and Agricultural and Mechanical College

FEEDBACK CONTROL OF SECTOR-BOUND NONLINEAR SYSTEMS WITH APPLICATIONS TO AEROENGINE CONTROL

A Dissertation

Submitted to the Graduate Faculty of the
Louisiana State University and
Agricultural and Mechanical College
in partial fulfillment of the
requirements for the degree of
Doctor of Philosophy

in

The Division of Electrical and Computer Engineering

by
Luis Donaldo Alvergue
B.S., McNeese State University, USA, 2004
M.S., Louisiana State University, USA, 2008
May 2012

Acknowledgments

I would like to thank my advisor, Professor Guoxiang Gu, for his goodwill, patience, encouragement, and guidance by example that have made this dissertation possible. His support has been essential and I have been very fortunate to have him as my main advisor. I'd also like to thank Professor Sumanta Acharya for his trust in me that this project could be completed and for the generous financial support that I received through the IGERT fellowship. Professors Kemin Zhou and Dimitris Nikitopoulos have also helped me much along the way, thank you. Finally, I'd like to thank the late Professor Jorge Aravena for his advice and motivation, and Professor Jorge Pullin for serving in this dissertation committee.

I also greatly appreciate the work of the LS-LAMP program at McNeese State University and Louisiana State University. The program coordinators at both institutions, Dr. Stevenson and Ms. Stevenson, and Dr. Su-Seng Pang, constantly provided me with opportunities and guidance throughout my undergraduate and graduate studies.

I'd also like extend my thanks to my friends from the EE office, Laurentiu, Xiaobo, Lili, and Xi; the IGERT group, Sam, Kevin, Wes, Farid, Mike, Tyler, Nathan, and Adey; and my good friend Hessam for his generous help and advice.

Finally, I would like to thank my family for their unconditional love and support, I cannot find the words to describe how grateful I am to have them.

Table of Contents

List of Tables

List of Figures

List of Nomenclature

$\{\,\}$	set
$\in,\ \notin$	is an element of, is not an element of
$\subseteq,\ \subset$	is a subset of, is a proper subset of
$\mathcal{X} \setminus \mathcal{Y}$	$\{x \in \mathcal{X} :\ x \notin \mathcal{Y}\}$ for sets $\mathcal{X}$ and $\mathcal{Y}$
$\mathbb{R}$	set of real numbers
$\mathbb{R}^{n\times m}$	set of $n \times m$ real matrices
$\mathbb{R}^n$	$\mathbb{R}^{n\times 1}$ (real column vectors)
$f : \mathcal{X} \to \mathcal{Y}$	function with domain $\mathcal{X}$ and codomain $\mathcal{Y}$
$\|\cdot\|$	vector or matrix norm, vector or matrix operator norm
A^T, a^T	matrix, vector transpose
$\mathrm{sym}\,(\mathrm{A})$	$A + A^T$
$\Re\{z\}$	real part of a complex number z
$\Im\{z\}$	real part of a complex number z
$det(A)$	determinant of matrix A
$\lambda_i(A)$	i^{th} eigenvalue of matrix A
$\lambda_{\max}(A), \lambda_{\min}(A)$	maximum, minimum eigenvalue of matrix A
$\sigma_i(A)$	i^{th} singular value of A
$\overline{\sigma}(A),\ \underline{\sigma}(A)$	maximum, minimum singular value of A
$Q \in \mathbb{R}^{n\times n} > 0$	strictly positive definite matrix Q
$\|v\|_Q$	$\sqrt{v^TQv}$, Q weighted 2-norm of v for $Q > 0$
$\mathcal{B}_P(\rho)$	$\{v \in \mathbb{R}^n :\ \ \|v\|_P < \rho\}$, open ellipsoid of size ρ
$\overline{\mathcal{B}}_P(\rho)$	$\{v \in \mathbb{R}^n :\ \ \|v\|_P \le \rho\}$, closed ellipsoid of size ρ
$\mathcal{L}_2$	space of piecewise continuous square integrable functions on $[0, \infty)$
$\mathcal{H}_\infty$	Hardy space of real-rational transfer function matrices bounded on the imaginary axis and analytic in the right half plane

Abstract

This dissertation is divided into two parts. In the first part we consider the problem of feedback stabilization of nonlinear systems described by state-space models. This approach is inherited from the methodology of sector bounded or passive nonlinearities, and influenced by the concept of absolute and quadratic stability. It aims not only to regionally stabilize the nonlinear dynamics asymptotically but also to maximize the estimated region of quadratic attraction and to ensure nominal performance at each equilibrium. In close connection to gain scheduling and switching control, a path of equilibria is programmed based on the assumption of centered-ϵ-cover which leads to a sequence of linear controllers that regionally stabilize the desired equilibrium asymptotically.

In the second part we tackle the problem of control for fluid flows described by the incompressible Navier-Stokes equation. We are particularly interested in film cooling for gas turbine engines which we model with the jet in cross-flow problem setup. In order to obtain a model amenable to the controller design presented in the first part, the well-known Proper Orthogonal Decomposition (POD)/Galerkin projection is employed to obtain a nonlinear state-space system called the reduced order model (ROM). We are able to stabilize the ROM to an equilibrium point via our design method and we also present direct numerical simulation (DNS) results for the system under state feedback control.

Chapter 1
Introduction

1.1 Motivation and Historical Perspective

Modern science and engineering are model-based. Many of these models are mathematically described by nonlinear differential equations. The majority of engineering applications depend on these models which is especially true for control system. Consequently there has been much focus on developing mathematical models and control strategies for nonlinear systems. While modeling is important, this dissertation assumes the existence of system models that are derived from either physical principles or experimental data. We focus on the control aspect of nonlinear systems. The first part of this dissertation describes the development of a linearization-based control system for nonlinear systems using state-space models (Chapters 2 and 3). The second part deals with a flow control application, the controlled "jet in cross-flow" (Chapter 4).

Nonlinear control theory has had a rich and successful history that includes Lie algebra and differential geometry [Isi89], singular perturbation [KK99], backstepping [KKK95], and more recently constructive methods [SJK97], among many others. Despite the success of nonlinear control theory, the linearization method is still widely used due to its simplicity and the availability of many design tools. It is a fact that linear methods perform well and most of the engineering applications are based on linear methods, including gain scheduling and adaptive control [rW95, RS00], which are widely used in practice. The main drawback of the linearization method lies in the difficulty in estimating the region where the local linear approximation is valid. An early and influential approach to this problem consisted in decomposing the nonlinear system into a linear and nonlinear part in a feedback interconnection. This approach, developed in the 1960s and 70s, became known as "absolute stability theory" [AG64, NT73, Pop62] and still attracts considerable attention. See for example [HHL04], [DHTZ09], [WIOv98], and references therein. The

seminal papers of Zames [Zam66a], [Zam66b] considered sector bounded nonlinearities and introduced the small gain theorem to stability analysis and feedback stabilization for a class of nonlinear systems under input/output or operator descriptions. The notion of passivity [Wil72a, Wil72b, HM76] contributed further to stability analysis of nonlinear systems along this thread of research by stating similar results in terms of state space models. Later developments in nonlinear control focused more on state-space systems, including feedback linearization [Isi89], nonlinear observers [AK99, Raj98, XG89], and optimal and robust control [IA92, IK95, vdS92], in addition to the aforementioned references. It is worth mentioning that the notion of input to state stability (ISS) surveyed in [Son07] provided a way to merge the state-space description with the operator approach in study of nonlinear system stability, and led to the small gain theorem for nonlinear state-space systems [MH92, JTP94]. It is important to note that all nonlinear control methods, to this date, are only applicable to certain classes of nonlinear systems. There is no universal method that can be applied to all nonlinear systems. This is in stark contrast to the linear methods that are applicable to all linear systems.

A linearization-based method that has been very effective in engineering applications is gain scheduling. Gain scheduling consists in designing several linear controllers (one for each operating point of interest) that cover the system's operating regions and implementing them by interpolating the controller gains over this range [rW95, RS00]. Although stability of the system can be established for states near the operating condition, stability of the gain scheduled nonlinear feedback system is usually derived by repeated simulations. Some approaches that do not rely on simulations may be found in [SA90] and [LHC01], where the latter presents an alternative to gain scheduling and points to a view of gain scheduling as a special type of a switched system. The main limitation of the gain scheduled design is hinged to the limitations of the linear method where the domain of operation of the nonlinear state-space is approximated by a set of linear regions.

The jet in cross-flow is an important fluid flow problem setup that is used as a model for various engineering applications. We are interested in this problem setup since it can be used to model film cooling of gas turbine blades although it is also used, among many others, as a model for fuel injection systems, smokestacks in the atmosphere, and dilution jets in combustors. Film cooling refers to the process of injecting cool air on the surface of gas turbine blades through small holes. If it is done right, a thin protective layer of cool air will form on the surface of the blades reducing heat transfer from the environment into the surface of the blade, allowing the turbine to operate at a high temperature without damaging the blades.

The jet in cross-flow is described by the 3D incompressible Navier-Stokes (N-S) equation, a non-linear, partial differential equation (PDE) that describes the conservation of momentum of a fluid. Although it is not yet known if this equation has a unique, continuously differentiable solution, it is routinely approximately solved by direct numerical simulation (DNS). A DNS is basically a set of coupled discrete-time ordinary differential equations (ODEs) obtained by temporally and spatially discretizing the N-S equation. Due to the fine spatial discretizations required to obtain meaningful DNS solutions, the number of ODEs is typically in the order of millions. This poses a challenge for control system design, as well as understanding the dynamics of the jet. We focus on control design and in particular, model based control design, which in the context of flow control includes: Adjoint based iterative optimization and estimation (or model predictive control) and Riccati equation based feedback control and estimation. The survey paper [KB07] and the book [Gun03] provide a good overview of these two approaches.

We follow the path of Riccati equation based feedback control and estimation via reduced order modeling. It is possible to project the ODEs to a lower dimensional subspace by expressing the solution obtained by DNS as a series expansion of a small number of basis functions, typically less than 100. The POD/Galerkin method achieves this reduction and the resulting low dimensional model is termed a reduced order model (ROM).

Feedback control design is then carried out based on this ROM and finally the controller is implemented in the full order DNS.

1.2 Overview of Contributions

This dissertation focuses on the design of sequences of linear controllers that semi-globally stabilize sector-bounded nonlinear systems. We propose a linear controller design method (state and output feedback) for the regional control of sector-bounded nonlinear systems. Under an ϵ-cover assumption on the location of the operating points in the state space, we complement the linear design with a switching strategy to stabilize the system semi-globally [AGA13]. We also present a controller design method (state feedback) for quadratic nonlinear systems [AG12]. Preliminary results were applied to a driven cavity problem [AGA11].

For the jet in crossflow problem, we investigate the construction of a ROM for control system design. To our knowledge, this is the first investigation of the jet in cross-flow where the POD expansion is augmented with a control mode. The purpose of our controller is to reduce the perturbation energy of the flow which in turn should reduce mixing of the cold and hot fluids. In this sense, our controller stabilizes some unstable operating point that has desirable cooling characteristics. We are able to stabilize the ROM flow to a steady state, and when implemented in the DNS simulation, it achieves stabilization for a period of time before diverging to a limit cycle. This highlights the difficulties that are encountered when designing controllers based on ROMs and implementing them in full dimensional models.

1.3 Organization of the Dissertation

In Chapter 2 we survey the systems theory background material that will be used throughout this dissertation. They include stability, signal and system norms, linear matrix inequalities, and switched systems. In Chapter 3 we develop the linear feedback stabilization methods that form the main part of the first part of this dissertation. Two methods are presented, one based on generalized sector-bounds and the other on the polytopic de-

scription of a quadratic nonlinear system. In addition, the switching strategy is described and simulation results for a simplified fluid convection model are presented. In Chapter 4 we employ the well-known POD/Galerkin model reduction method to obtain a ROM of the jet in cross-flow problem amenable to feedback control design. The controller designed in Chapter 3 is implemented and the results are discussed. Finally, Chapter 5 contains the conclusion of the work as well as a recommended agenda for future research.

Chapter 2

Background Material

2.1 Systems

This chapter covers standard material and many parts have been quoted from [Kha02]. In this work our main concern is to analyze and control physical phenomena that can be described by a finite number of first order ordinary differential equations (ODEs)

$$\begin{aligned} \dot{x}_1 &= f_1(t, x_1, \ldots, x_n, u_1, \ldots, u_m) \\ &\vdots \\ \dot{x}_n &= f_n(t, x_1, \ldots, x_n, u_1, \ldots, u_m). \end{aligned} \tag{2.1}$$

Often there is another set of algebraic equations related to (2.1)

$$\begin{aligned} y_1 &= h_1(t, x_1, \ldots, x_n, u_1, \ldots, u_m) \\ &\vdots \\ y_p &= h_p(t, x_1, \ldots, x_n, u_1, \ldots, u_m) \end{aligned} \tag{2.2}$$

that consist of variables that are of particular interest for analysis or control. By defining vectors

$$x := \begin{pmatrix} x_1(t) \\ \vdots \\ x_n(t) \end{pmatrix}, \; u := \begin{pmatrix} u_1(t) \\ \vdots \\ u_m(t) \end{pmatrix}, \; y := \begin{pmatrix} y_1(t) \\ \vdots \\ y_p(t) \end{pmatrix}, \; f := \begin{pmatrix} f_1(t, x, u) \\ \vdots \\ f_n(t, x, u) \end{pmatrix}, \; h := \begin{pmatrix} h_1(t, x, u) \\ \vdots \\ h_p(t, x, u) \end{pmatrix}$$

where $x(t)$ is called the state, $u(t)$ is called the input, and $y(t)$ is called the output, we may write (2.1) and (2.2) in a more compact notation.

Definition 1 (Nonlinear state-space system)**.** *A nonlinear state-space system is a set of differential equations consisting of a dynamics equation with an initial condition and an output equation*

$$\dot{x} = f(t, x, u),\ x(0) = x_0 \tag{2.3}$$

$$y = h(t, x, u) \tag{2.4}$$

We use the notation $\phi(t, x_0)$ to denote the solution to (2.3) at time t with initial condition x_0. For details on existence and uniqueness of solutions of ordinary differential equation see [Kha02] and [MM07], among others. In this dissertation we will mostly work with the following special cases of the nonlinear state-space system:

1. Autonomous nonlinear system: When $f(\cdot)$ and $h(\cdot)$ are not explicit functions of time, i.e., time only enters through the state.

$$\begin{aligned} \dot{x} &= f(x, u), \quad x(0) = x_0 \\ y &= h(x, u) \end{aligned} \tag{2.5}$$

2. Linear time varying system (LTV): When $f(\cdot)$ and $h(\cdot)$ are linear functions.

$$\begin{aligned} \dot{x} &= A(t)x + B(t)u \\ y &= C(t)x + D(t)u \end{aligned} \tag{2.6}$$

3. Linear time invariant system (LTI): When $f(\cdot)$ and $h(\cdot)$ are linear functions and do not explicitly depend on time.

$$\begin{aligned} \dot{x} &= Ax + Bu \\ y &= Cx + Du \end{aligned} \tag{2.7}$$

An alternative representation of an LTI system may be obtained through the Laplace transform. The Laplace transform of a single variable function $f(t)$ is defined as

$$F(s) = \int_0^\infty f(t)e^{-st}dt.$$

If $\dot{f}(t)$ has a well defined Laplace transform, it is given by

$$sF(s) - f(0).$$

Therefore, the Laplace transform of (2.7) is

$$\begin{aligned} sX(s) - x_0 &= AX(s) + BU(s) \\ Y(s) &= CX(s) + DU(s) \end{aligned}$$

In the special case of $x_0 = 0$, we have the *input/output* description of (2.7)

$$Y(s) = G(s)U(s)$$

where $G(s) = C(sI - A)^{-1}B + D$ is called the *transfer function* of (2.7).

2.2 Lyapunov Stability

The method developed by the Russian mathematician Lyapunov (1857-1918) for studying stability of differential equations is fundamental for much of modern stability analysis. It is not only used for analysis, but also for control system design. The simplest notion of stability is the one related to stability of equilibrium points.

Definition 2 (Equilibrium point)**.** *A point $x(t) = x_e$ in the state space is said to be an equilibrium point of the autonomous system*

$$\dot{x} = f(x)$$

if and only if it has the property that whenever the state of the system starts at x_e, it remains at x_e for all future time.

According to the definition, the equilibrium points of (2.5) are the real roots of the equation $f(x_e) = 0$. This is made clear by noting that if

$$\dot{x}_e = f(x_e) = 0$$

then it follows that x_e is constant and, by definition, an equilibrium point. Without loss of generality, we assume that 0 is an equilibrium point of the system. If the equilibrium point under study, x_e, is not at zero we may define a new (shifted) coordinate system $x_s(t) = x(t) - x_e$ and note that

$$\dot{x}_s(t) = \dot{x}(t) = f(x(t)) = f(x_s(t) + x_e) =: f_s(x_s(t)), \;\; x_s(0) = x_0 - x_e$$

The claim follows by noting that $f_s(0) = f(x_e) = 0$. In summary, the study of the zero equilibrium point of $\dot{x}_s(t) = f_s(x_s(t))$ is equivalent to the study of the nonzero equilibrium point x_e of $\dot{x} = f(x(t))$. We now define what is meant by stability of an equilibrium point of an autonomous system.

Definition 3 (Stability of equilibrium point)**.** *The equilibrium point $x = 0$ of (2.5) is*

- *Stable, if for every $\epsilon > 0$ there exists a $\delta = \delta(\epsilon) > 0$ such that*

$$\|x(0)\| < \delta \Rightarrow \|x(t)\| < \epsilon, \; \forall \, t \geq 0.$$

- *Unstable if it is not stable.*

- *Asymptotically stable if it is stable and δ can be chosen such that*

$$\|x(0)\| < \delta \Rightarrow \lim_{t \to \infty} x(t) = 0.$$

The following result is a particular version of Lyapunov's stability theorem. It characterizes the stability of an equilibrium point in terms of a scalar 'energy function' that decreases along every trajectory of the system. To state the definition we first assume that in (2.5), $\mathcal{D}$ is an open and connected subset of $\mathbb{R}^n$ and $f : \mathcal{D} \to \mathbb{R}^n$ is a locally Lipshchitz map.

Theorem 2.2.1 (Lyapunov asymptotic stability theorem)**.** *Let $x = 0$ be an equilibrium point of $\dot{x} = f(x)$, $f : \mathcal{D} \to \mathbb{R}^n$, and let $V : \mathcal{D} \to \mathbb{R}$ be a continuously differentiable function such that*

1. $V(0) = 0$
2. $V(x) > 0 \quad in \quad \mathcal{D} \setminus \{0\}$
3. $\dot{V}(x) < 0 \quad in \quad \mathcal{D} \setminus \{0\}$

then $x = 0$ is asymptotically stable.

Since Lyapunov's stability theorem presents only sufficient conditions, the main difficulty in applying the theorem boils down to finding Lyapunov functions and there is no general systematic procedure for constructing Lyapunov functions. For linear systems, quadratic Lyapunov functions are necessary and sufficient to prove stability.However there are no such results for nonlinear systems. Backstepping [KKK95] and feedback passivation [SJK97], among others, are systematic design methods for certain classes of nonlinear systems.

Often it is not enough to determine if an equilibrium point is stable. Having an idea of the set of initial conditions that converge to the equilibrium is also important. The region of attraction (RoA) makes this idea explicit.

Definition 4 (Region of attraction)**.** *Let the origin $x = 0$ be an asymptotically stable equilibrium point for (2.5). The region of attraction (RoA) of the origin of (2.5) is defined by the set*

$$RoA = \{x_0 \in \mathcal{D} : \phi(t, x_0) \text{ is defined } \forall t \geq 0 \text{ and } x(t) \to 0 \text{ as } t \to \infty\}$$

The RoA is an invariant set that is typically difficult to represent and much effort has been devoted to methods for estimating the RoA [Bla99, GTV85, CT89].

In addition to an equilibrium point, a periodic solution is an important structural property of a system that characterizes oscillatory behavior.

Definition 5 (Periodic solution)**.** *The solution $x(t)$ is a nontrivial periodic solution if it satisfies*

$$x(t + T) = x(t), \ \forall \ t \geq 0$$

The 'nontrivial' quantifier is included in the definition to exclude constant solutions corresponding to an equilibrium point.

2.2.1 Quadratic Stability

The notion of quadratic stability was introduced in [Bar85] and has been thoroughly studied in the literature since then. It has found substantial applications in $\mathcal{H}_\infty$ control problems and in determining stability margins for a variety of linear systems (uncertain, uncertain LTV, and interval systems). For a good overview see [Cor94] and its bibliography. We are motivated to introduce the quadratic stability idea and use it to study uncertain LTV systems described by state equations of the form

$$\begin{aligned} \dot{x} &= (A + B_1 \Delta_t C_1)x + Bu, \\ \Delta_t^T \Delta_t &\leq \delta^2 I, \quad \delta > 0 \end{aligned} \tag{2.8}$$

where $x(t) \in \mathbb{R}^n$ is the *state*, $u(t) \in \mathbb{R}^m$ is the *control* and $\Delta_t \in \mathbb{R}^{q_1 \times q_2}$ is *a matrix of uncertain time-varying parameters.* The notation $\Delta_t \in \mathbf{\Delta}(\delta)$ is also regularly used. In this case,

$$\mathbf{\Delta}(\delta) := \{\Delta_t \ : \ \overline{\sigma}(\Delta_t) \leq \delta\}, \ \delta > 0 \tag{2.9}$$

is the *set of admissible* Δ_t.

Definition 6 (Quadratic stability)**.** *The uncertain linear time-varying system (2.8) (with* $u(t) = 0$*) is said to be quadratically stable if and only if there exists a* $P > 0$ *and a constant* $\alpha > 0$ *such that for any admissible uncertainty* Δ_t*, the Lyapunov derivative for the Lyapunov function* $V(x) = x^T P x$ *satisfies*

$$\dot{V} = 2x^T P \left(A + B_1 \Delta_t C_1\right) x \leq -\alpha \left\|x(t)\right\|^2$$

for all state variables $x(t) \in \mathbb{R}^n$ *and* $t \in \mathbb{R}$*. The system is said to be quadratically stabilizable if there exists a state feedback control* $u(t) = Fx(t)$ *such that the closed loop system is quadratically stable.*

Remark 1. *The concept of quadratic stability requires the existence of a fixed quadratic Lyapunov function for all possible choices of the uncertain parameters.*

Since it is very difficult to compute the RoA, we introduce a tractable estimate for it which we call region of quadratic attraction.

Definition 7 (RoQA)**.** *The system (2.8) is said to admit a* RoQA *of Q-weighted size* $\varepsilon_m > 0$ *at the equilibrium point* $x_\mathrm{e} = 0$*, if there exist square matrices* $P > 0$ *and* $Q > 0$ *such that the Lyapunov derivative of the Lyapunov function* $V[x(t)] = \|x(t)\|_P^2 = x(t)^T P x(t)$ *satisfies* $\dot{V}(t) < 0$ *for all* $t \geq 0$ *and* $x_0 \in \mathcal{B}_Q(\varepsilon_m), x_0 \neq 0$*.*

Regarding feedback stabilization, the following notions are important since they quantify the stability properties of a closed loop system [Kha02]. If a nonlinear system is

stabilized via linearization, then the RoA may be infinitely small. In this case, feedback control achieves *local stabilization*. If the feedback control guarantees that a certain set is included in the region of attraction or if an estimate of the region of attraction is given, the feedback control achieves *regional stabilization*. If the origin of the closed-loop system is globally asymptotically stable, the control achieves *global stabilization*. If feedback control does not achieve global stabilization, but can be designed such that any given compact set (no matter how large) can be included in the region of attraction, the feedback control achieves *semi-global stabilization*.

2.3 Norms for Signals and Systems

The norm function, $\|s\|$, is used to measure the size of a signal. It satisfies the following three properties:

1. $\|s\| \geq 0$ and $\|s\| = 0$ if and only if $s = 0$.
2. $\|s_1 + s_2\| \leq \|s_1\| + \|s_2\|$ for all s_1 and s_2.
3. $\|\alpha s\| = |\alpha| \, \|s\|$ for all $\alpha \in \mathbb{C}$.

For the space of piecewise continuous square integrable functions, $\mathcal{L}_2$, the norm is defined by

$$\|s\|_2 = \sqrt{\int_0^\infty \|s(t)\|^2 \, dt}.$$

A fundamental question that arises in the study of systems described by ODEs or transfer functions is the following: If we know that the input signal has some property, what can we say about the output signal? For example, if the input $u(t) \in \mathcal{L}_2$, is $y(t) \in \mathcal{L}_2$ also?

In this dissertation we will only make use of the $\mathcal{H}_\infty$ norm. If we let T be the Lyapunov stable linear system (i.e., all the eigenvalues of A have strictly negative real parts)

$$\dot{x} = Ax + Bu$$
$$y = Cx + Du$$

or its corresponding transfer function $T(s) = C(sI - A)^{-1}B + D$, then the $\mathcal{H}_\infty$-norm of T is defined as

$$\|T\|_{\mathcal{H}_\infty} := \sup_{\mathrm{Re}\{s\}>0} \overline{\sigma}[T(s)]$$

where $\overline{\sigma}(\cdot)$ is the maximum singular value or equivalently as

$$\|T\|_{\mathcal{H}_\infty} := \sup_{0<\|u\|_2<\infty} \frac{\|y\|_2}{\|u\|_2} \tag{2.10}$$

As such, the $\mathcal{H}_\infty$ norm measures how much a system amplifies the $\mathcal{L}_2$ norm of an input signal. In addition, it is a fundamental tool in small-gain stability arguments. Essentially, these arguments prove stability of a feedback loop if the product of the $\mathcal{H}_\infty$ norm of the components in the feedforward and feedback paths is less than unity.

The following is a version of the Kalman-Yakubovich-Popov (KYP) lemma which can be found in [DP00], among others. This version is known as the strictly bounded real lemma and it characterizes the $\mathcal{H}_\infty$ norm of a system in terms of an algebraic Riccati inequality.

Lemma 2.3.1 (Strictly bounded real lemma)**.** *Suppose that $T(s) = C(sI - A)^{-1}B + D$, then $\|T\|_{\mathcal{H}_\infty} < \delta^{-1}$, if and only if there exists a matrix $P > 0$ such that*

$$\begin{bmatrix} A^TP + PA + \delta^2 C^TC & PB + \delta^2 C^TD \\ B^TP + \delta^2 D^TC & \delta^2 D^TD - I \end{bmatrix} < 0. \tag{2.11}$$

2.4 Linear Matrix Inequalities and Schur Complement

A Linear Matrix Inequality (LMI) has the form

$$F(x) = F_0 + \sum_{i=1}^{m} x_i F_i > 0,$$

where $x = \begin{bmatrix} x_1 & \dots & x_m \end{bmatrix}^T \in \mathbb{R}^m$ is the vector variable and $F_i = F_i^T \in \mathbb{R}^{n \times n},\ i = 0, \dots, m$ are given symmetric matrices. LMIs appear in many control problems, from Lyapunov stability constraints to controller synthesis to interpolation and system realization problems. The book [BGFB94] is a good reference and contains a wide variety of control problems that can be posed as LMIs.

Nonlinear (convex) inequalities arising in control problems can be converted to an LMI using the Schur factorization. First, let M be a 2×2 block matrix,

$$M = \begin{bmatrix} A & B \\ C & D \end{bmatrix}.$$

If D is square and nonsingular, then it is straightforward to verify that

$$\begin{bmatrix} A & B \\ C & D \end{bmatrix} = \begin{bmatrix} I & BD^{-1} \\ 0 & I \end{bmatrix} \begin{bmatrix} A - BD^{-1}C & 0 \\ 0 & D \end{bmatrix} \begin{bmatrix} I & 0 \\ D^{-1}C & I \end{bmatrix}.$$

The matrix $A - BD^{-1}C$ is called the *Schur complement* of D in M, and this decomposition motivates the strict Schur complement formula stated next.

Theorem 2.4.1. *Given any symmetric matrix*

$$M = \begin{bmatrix} A & B \\ B^T & D \end{bmatrix}$$

The following are equivalent

(a) $M > 0$

(b) $A - BD^{-1}B^T > 0$ *and* $D > 0$

Now it is clear that the LMI

$$\begin{bmatrix} Q(x) & S(x) \\ S(x)^T & R(x) \end{bmatrix} > 0$$

is equivalent to the set of nonlinear inequalities

$$R(x) > 0, \;\; Q(x) - S(x)R(x)^{-1}S(x)^T > 0.$$

We will make use of this result whenever we deal with the algebraic Riccati inequalities that arise in the system analysis and controller synthesis problems.

2.5 Switched Systems

Systems described by continuous and discrete dynamics are called hybrid systems. While the study of continuous and discrete dynamics separately is well documented, hybrid systems have attracted attention until relatively recently. Most of the material in this subsection can be found in [vdSS99], [Lib03], and their bibliographies.

The continuous dynamics may be represented by a nonlinear state-space system or any of its special cases. The discrete dynamics may be represented by a state-space model too, but instead of the state being in $\mathbb{R}^n$, it lies in a finite or countable set $\{q_1, q_2, \ldots\}$.

Switched systems are a subset of hybrid systems (switched systems differ from hybrid control in the level of analysis of the discrete dynamics), and consist of continuous-time systems with isolated discrete switching events. They have received renewed attention recently and become a very active area of research as illustrated by [BL99] and [DBPL00], both of which appear in special issues on hybrid systems,[LA09], [HaPH10], [SWM$^+$07], the textbook [Lib03], and references therein. Concretely, they consist of two main ingredients:

- A family of indexed dynamical systems:

$$\dot{x} = f_p(x),\ p \in \mathcal{P} \tag{2.12}$$

- A switching signal (piecewise constant function of t):

$$\sigma : [0, \infty) \to \mathcal{P} \tag{2.13}$$

These two ingredients are combined into the ODE

$$\dot{x} = f_\sigma(x). \tag{2.14}$$

to obtain a switched system. In addition, the initial condition of each indexed dynamical system is given by the reset map. The reset map may generate discontinuous system trajectories in the state-space, and if it does, these jumps are called impulse effects. In case that the reset map is the identity, the initial condition of the p^{th} system is equal to the value of x of the system which was previously active. Figure 2.1 illustrates a scalar system with an impulse effect at $t = t_1$ and without at $t = t_2$. In this investigation we only consider the identity reset map. Finally, the switching signal is typically characterized as:

- Autonomous: The location of switching surfaces in the state-space of x or rules on the switching signal are predetermined.
- Controlled: Chosen by the designer to achieve a desired system behavior.

More details on the switching signal that we consider in this investigation will be presented in the next chapter. The previous concepts are shown schematically in Figure 2.1 to illustrate the main features of a switched system.

To provide some context to our method, we now present a few results on stability of switched systems. Although there are several approaches to prove stability of switched

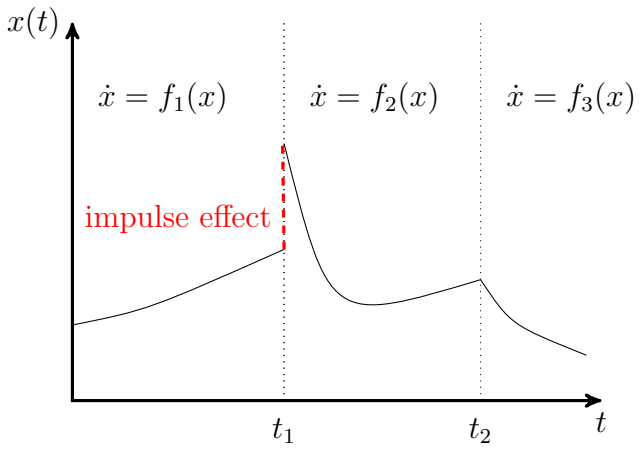

Figure 2.1: A scalar switched system

systems which include commutation relations [DLM99] and dwell time concepts [Mor93], the results we present in this dissertation are based on Lyapunov arguments.

For studying uniform stability (with respect to $\sigma(t)$) of the switched system, Theorem 2.2.1 may be extended to take the following form.

Theorem 2.5.1 (Stability theorem for switched systems)**.** *If there exists a positive definite function $W : \mathbb{R}^n \to \mathbb{R}$ and a positive definite function, $V : \mathbb{R}^n \to \mathbb{R}$, whose derivative along solutions of all systems in the family (2.12) satisfies*

$$\dot{V} = \frac{\partial V}{\partial x} f_p(x) \leq -W(x) \;\; \forall x, \; \forall p \in \mathcal{P} \tag{2.15}$$

then the switched system (2.14) is globally uniformly asymptotically stable.

If a common Lyapunov function cannot be found, it is still possible to prove stability of the switched system using several Lyapunov functions. However, stability properties of the switched system generally depend on the switching signal σ. There are many results in this direction but we leave them out as they are outside the scope of this dissertation.

Chapter 3
Linear Feedback Stabilization for Classes of Nonlinear Systems

In this chapter we propose an approach for the design of feedback controllers for two classes of nonlinear systems: Autonomous sector-bounded nonlinear systems and quadratic nonlinear systems. We refer to the design methods by:

1. Generalized sector-bound

2. Polytope

Both design methods are intended for feedback stabilization to an equilibrium point. In the first method, our approach consists in modeling the sector-bounded nonlinearities as time-varying uncertainties. The second method exploits the form of the Lyapunov inequality obtained when the Lyapunov function is quadratic, and the system involves quadratic nonlinearities. While both methods rely on quadratic forms for Lyapunov function candidates, we will see through a simulation result that the conservativeness of the results differs.

In addition to the regional controller design, we propose a scheduling or switching approach for regional stabilization. This solution is inspired by the success of gain scheduling as an effective method for the control of nonlinear systems. However, classical gain scheduling doesn't satisfactorily address the stability of the closed loop system when the state is far away from the equilibrium point. To address this shortcoming, we combine the insight from absolute stability theory with the gain scheduling method. As mentioned in Section 2.5, both switching and hybrid control are regarded as viable control strategies for a variety of systems. In our specific design, when the initial state of the nonlinear system is outside the estimated RoA of the desired equilibrium point, the notion of centered-ϵ-cover is proposed and assumed. This notion will be made explicit later, but in general terms the assumption is that the RoAs of different equilibrium points overlap one another. An equilibria path

lying in this centered-ϵ-cover will then be programmed and a sequence of linear controllers can then be designed to steer each initial state to the desired operating point along the equilibria path, thereby regionally stabilizing the nonlinear state-space system. Roughly speaking, in the context of switched systems, the ϵ-cover condition effectively determines the switching signal, and the stability of the switched system (which is equivalent to the nonlinear system in this region) may be established by the theorems in Section 3.1.2.

3.1 Generalized Sector-bound Method

With this method, the error residue resulting from linearization is treated as unmodeled nonlinear dynamics, and an $\mathcal{H}_\infty$ robust controller is synthesized to not only stabilize the linearized state-space system, but also enlarge the estimated RoA quantified by an ϵ-distance. However, caution needs to be taken not to treat the unmodeled nonlinear dynamics as exogenous uncertainties. In fact, the uncertainty induced by the regionally bounded modeling error is dependent on the state of the linearized system. A formula to compute the ϵ-distance is derived under both state feedback and output feedback control.

3.1.1 Stability Analysis

Consider the autonomous nonlinear system

$$\dot{x} = f(x), \quad x(0) = x_0, \tag{3.1}$$

Without loss of generality the equilibrium point is assumed at the origin, i.e., $f(0) = 0$. To analyze the asymptotic stability of the equilibrium point $x_\mathrm{e} = 0$, we rewrite the nonlinear system (3.1) as

$$\dot{x}(t) = \left[A + B_1\Delta_t \left(I - D_{11}\Delta_t\right)^{-1} C_1\right] x(t), \quad x(0) = x_0, \tag{3.2}$$

for some admissible $\Delta_t = \Delta[x(t)]$ that is continuous and satisfies $\Delta(0) = 0$ by an abuse of notation. The set of admissible Δ_t will be made precise in the development of this section.

The dynamics $\dot{x}(t) = Ax(t)$ with $A \in \mathbb{R}^{n\times n}$ represents the linearized system at $x_e = 0$. The dimensions of B_1, C_1, and D_{11} are $n \times m_1$, $p_1 \times n$, and $p_1 \times m_1$, respectively. Although Δ_t is a nonlinear map: $\mathbb{R}^n \mapsto \mathbb{R}^{m_1\times p_1}$, it can be treated as a time-varying gain dependent on the state $x(t)$.

Asymptotic stability for nonlinear systems specified in (3.1) has had a long history for which Lyapunov theory has provided the foundation. If A is a stability matrix, then the solution $x(t)$ to (3.1) approaches zero asymptotically provided that x_0 is in the RoA of the origin. However, local asymptotic stability does not allude to the size of the RoA. That is, local asymptotic stability provides no estimate for the region of the initial condition x_0 that ensures asymptotic convergence of the solution $x(t)$ to the equilibrium point $x_e = 0$. The difficulty may lie in the notion of asymptotic stability which is typically difficult to quantify. For this reason we consider the notion of quadratic stability stated earlier in Definition 6.

Definition 8 (Quadratic Stability)**.** *The system* (3.2) *is said to be quadratically stable if there exists a* $P > 0$ *and a constant* $\alpha > 0$ *such that for each admissible* Δ_t*, the Lyapunov derivative of the Lyapunov function* $V(x) = x^T Px$ *satisfies*

$$\dot{V} = 2x^T P\left(A + B_1\Delta_t\left(I - D_{11}\Delta_t\right)^{-1} C_1\right) x \leq -\alpha \left\|x(t)\right\|^2 \tag{3.3}$$

for all state variables $x(t) \in \mathbb{R}^n$ *and* $t \in \mathbb{R}$*.*

The notion of region of quadratic attraction (RoQA) is also important.

Definition 9 (RoQA)**.** *The system* (3.2) *is said to admit* RoQA *of Q-weighted size* $\varepsilon_m > 0$ *at the equilibrium point* $x_e = 0$*, if there exist square matrices* $P > 0$ *and* $Q > 0$ *such that the Lyapunov derivative of the Lyapunov function* $V[x(t)] = \|x(t)\|_P^2 = x(t)^T Px(t)$ *satisfies* $\dot{V}(t) < 0$ *for all* $t \geq 0$ *and* $x_0 \in \mathcal{B}_Q(\varepsilon_m), x_0 \neq 0$*.*

The notion of quadratic stability is stronger, and thus more tractable, than that of asymptotic stability which helps to estimate the size of RoQA. Furthermore, the $\mathcal{H}_\infty$ norm

can be used to characterize quadratic stability as it was shown in [KPZ90]. For a given transfer matrix $T(s)$, recall that its $\mathcal{H}_\infty$-norm is defined by

$$\|T\|_{\mathcal{H}_\infty} := \sup_{\mathrm{Re}\{s\}>0} \overline{\sigma}[T(s)] \tag{3.4}$$

where $\overline{\sigma}(\cdot)$ is the maximum singular value. Denote

$$\mathbf{\Delta}(\delta) := \{\Delta_t \ : \ \overline{\sigma}(\Delta_t) \leq \delta, \ \Delta(0) = 0\}, \ \delta > 0 \tag{3.5}$$

as the set of admissible Δ_t. Consider the case when $T_1(s)$ is a real rational transfer matrix given by

$$T_1(s) := D_{11} + C_1(sI - A)^{-1}B_1. \tag{3.6}$$

The next lemma will be useful to streamline the arguments to be developed. It essentially establishes an $\mathcal{H}_\infty$-norm equivalence between proper and strictly proper transfer matrices in terms of an algebraic Riccati inequality (ARI).

Lemma 3.1.1. *Consider the transfer matrix $T_1(s)$ in* (3.6) *where A is a stability matrix and define $\delta_{\mathrm{m}} := \|T_1\|_{\mathcal{H}_\infty}^{-1}$. For each positive $\delta < \delta_{\mathrm{m}}$, $\delta\overline{\sigma}(D_{11}) < 1$ holds and*

$$\begin{aligned}\tilde{A} &= A + \delta^2 B_1 D_{11}^T (I - \delta^2 D_{11} D_{11}^T)^{-1} C_1, \tilde{B}_1 = B_1 (I - \delta^2 D_{11}^T D_{11})^{-1/2}, \\ \tilde{C}_1 &= (I - \delta^2 D_{11} D_{11}^T)^{-1/2} C_1,\end{aligned}$$

are well-defined. Denote $\tilde{T}_1(s) = \tilde{C}_1(sI - \tilde{A})^{-1}\tilde{B}_1$. Then $\|T_1\|_{\mathcal{H}_\infty} < \delta^{-1}$ if and only if $\|\tilde{T}_1\|_{\mathcal{H}_\infty} < \delta^{-1}$, which is equivalent to the existence of a solution $P_\delta > 0$ to the ARI

$$\tilde{A}^T P_\delta + P_\delta \tilde{A} + P_\delta \tilde{B}_1 \tilde{B}_1^T P_\delta + \delta^2 \tilde{C}_1^T \tilde{C}_1 < 0. \tag{3.7}$$

Proof. We prove by invoking Lemma 2.3.1 which establishes that $\|T_1\|_{\mathcal{H}_\infty} < \delta^{-1}$, if and

only if there exists a matrix $P_\delta > 0$ such that

$$\begin{bmatrix} A^T P_\delta + P_\delta A + \delta^2 C_1^T C_1 & P_\delta B_1 + \delta^2 C_1^T D_{11} \\ B_1^T P_\delta + \delta^2 D_{11}^T C_1 & \delta^2 D_{11}^T D_{11} - I \end{bmatrix} < 0. \tag{3.8}$$

By Schur complement the above is equivalent to the ARI

$$A^T P_\delta + P_\delta A + \delta^2 C_1^T C_1 + (P_\delta B_1 + \delta^2 C_1^T D_{11})(I - \delta^2 D_{11}^T D_{11})^{-1}(B_1^T P_\delta + \delta^2 D_{11}^T C_1) < 0.$$

Let $R = I - \delta^2 D_{11} D_{11}^T$. Then R^{-1} is well-defined by $\delta \overline{\sigma}(D_{11}) < 1$. We now rewrite the above ARI as

$$\begin{aligned} &P_\delta(A + \delta^2 B_1 D_{11}^T R^{-1} C_1) + (A + \delta^2 B_1 D_{11}^T R^{-1} C_1)^T P_\delta + P_\delta B_1 (I - \delta^2 D_{11}^T D_{11})^{-1} B_1^T P_\delta \\ &+ \delta^2 C_1^T (I + \delta^2 D_{11}(I - \delta^2 D_{11}^T D_{11})^{-1} D_{11}^T) C_1 < 0 \end{aligned}$$

By noting $I + \delta^2 D_{11}(I - \delta^2 D_{11}^T D_{11})^{-1} D_{11}^T = (I - \delta^2 D_{11} D_{11}^T)^{-1}$, there holds

$$P_\delta \tilde{A} + \tilde{A}^T P_\delta + P_\delta \tilde{B}_1 \tilde{B}_1^T P_\delta + \delta^2 \tilde{C}_1^T \tilde{C}_1 < 0$$

which is equivalent to $\|\tilde{T}_1\|_{\mathcal{H}_\infty} < \delta^{-1}$ by Lemma 2.3.1. □

We now connect the notions of quadratic stability and RoQA of the time varying system (3.2), with the nonlinear system (3.1).

Theorem 3.1.2. *Consider the nonlinear system* (3.1) *which admits a representation in* (3.2) *for some* $\Delta_t = \Delta[x(t)] \in \mathbf{\Delta}(\delta)$ *and some stability matrix* A. *Let* $T_1(s)$ *be given in* (3.6), $\tilde{T}_1(s) = \tilde{C}_1(sI - \tilde{A})^{-1}\tilde{B}_1$ *be the same as in* Lemma 3.1.1, *and* $P_\delta > 0$ *be the solution to the* ARI *in* (3.7) *where* $\delta_m = \|T_1\|_{\mathcal{H}_\infty} = \|\tilde{T}_1\|_{\mathcal{H}_\infty}$ *and* $\delta \in (0,\ \delta_m)$ *is a parameter. Define*

$$\varphi(\varepsilon) := \max\left\{\overline{\sigma}[\Delta(x)] : \quad x^T P_\delta x \le \varepsilon^2\right\}. \tag{3.9}$$

Then $\varphi(\varepsilon)$ is a continuous and monotonically increasing function of ε. If there exists a solution $\varepsilon > 0$ to $\delta = \varphi(\varepsilon)$ and a unique solution $\varepsilon_m > \varepsilon$ to $\delta_m = \varphi(\varepsilon_m)$, then $x_e = 0$ is regionally asymptotically stable with RoQA *of P-weighted size ε_m for some $P > 0$. If $\varphi(\varepsilon) < \delta_m$ for all $\varepsilon > 0$, then the nonlinear system in* (3.1) *is globally asymptotically stable.*

Proof. The continuity of $\varphi(\epsilon)$ follows from the continuity of $\Delta(\cdot)$ while the monotonicity of $\varphi(\epsilon)$ follows from the definition in (3.9). For convenience, denote

$$\begin{aligned} w(t) &= \Delta_t \left(I - D_{11}\Delta_t\right)^{-1} C_1 x(t), \\ z(t) &= C_1 x(t) + D_{11} w(t). \end{aligned} \tag{3.10}$$

Then $\dot{x}(t) = Ax(t) + B_1 w(t)$ by (3.2). Substituting the expression of $w(t)$ into that of $z(t)$ yields

$$\begin{aligned} z(t) &= \left(I + D_{11}\Delta_t \left(I - D_{11}\Delta_t\right)^{-1}\right) C_1 x \\ &= \left(\left(I - D_{11}\Delta_t\right)\left(I - D_{11}\Delta_t\right)^{-1} + D_{11}\Delta_t \left(I - D_{11}\Delta_t\right)^{-1}\right) C_1 x = \left(I - D_{11}\Delta_t\right)^{-1} C_1 x. \end{aligned}$$

As a result, there holds

$$w(t) = \Delta_t z(t). \tag{3.11}$$

The relationships derived above can be expresses as the feedback system in block diagram (a) of Figure 3.1. In light of Lemma 3.1.1, stability of A and the hypothesis on ARI (3.7) imply stability of $\tilde{A}$ and $\delta_m^{-1} = \|T_1\|_{\mathcal{H}_\infty} < \delta^{-1}$ which are equivalent to $I - \delta^2 D_{11} D_{11}^T > 0$ and $\|\tilde{T}_1\|_{\mathcal{H}_\infty} < \delta^{-1}$. More importantly there holds the following set equality [Che97]:

$$\begin{aligned} \mathcal{S} &:= \left\{ A + B_1\Delta_t \left(I - D_{11}\Delta_t\right)^{-1} C_1 : \ \ \overline{\sigma}(\Delta_t) \le \delta \right\} \\ &= \left\{ \tilde{A} + \tilde{B}_1\tilde{\Delta}_t\tilde{C}_1 : \ \ \overline{\sigma}(\tilde{\Delta}_t) \le \delta \right\} =: \tilde{\mathcal{S}}. \end{aligned} \tag{3.12}$$

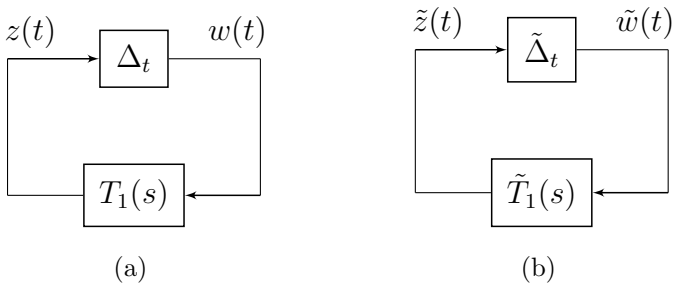

Figure 3.1: Equivalent feedback systems for stability analysis

The nonlinear system in (3.1) can thus be equivalently transformed to

$$\dot{x}(t) = \left[\tilde{A} + \tilde{B}_1\tilde{\Delta}_t\tilde{C}_1\right] x(t), \quad \tilde{\Delta}_t = \tilde{\Delta}[x(t)], \quad \tilde{\Delta}(0) = 0. \tag{3.13}$$

Let $\tilde{w}(t) = \tilde{\Delta}_t\tilde{z}(t)$ and $\tilde{z}(t) = \tilde{C}_1 x(t)$. Then $\dot{x}(t) = \tilde{A}x(t) + \tilde{B}_1\tilde{w}(t)$ that results in an equivalent feedback system in block diagram (b) on right of Fig. 1. Consequently, the local asymptotic stability of the nonlinear system in (3.1) with RoQA of P-weighted size ε is in turn equivalent to that of the nonlinear system in (b) of Figure 3.1 with RoQA of the same P-weighted size ε. Now set $\delta \in (0, \delta_m)$ as a parameter with $\delta_m^{-1} = \|\tilde{T}\|_\infty$. Assume that there exists a solution $\varepsilon > 0$ to $\delta = \varphi(\varepsilon)$, i.e., $\overline{\sigma}(\tilde{\Delta}_t) \leq \delta \ \forall \ x(t) \in \overline{\mathcal{B}}_{P_\delta}(\varepsilon)$ and that there exists a unique solution $\varepsilon_m > \varepsilon$ to $\delta_m = \varphi(\varepsilon_m)$, i.e., $\overline{\sigma}(\tilde{\Delta}_t) < \delta_m \ \forall \ x(t) \in \mathcal{B}_{P_\delta}(\varepsilon_m)$. Setting the Lyapunov function as $V(t) = \|x(t)\|_{P_\delta}^2$ with $P_\delta > 0$ the solution to the ARI in (3.7) leads to

$$\dot{V}(t) = x(t)^T \left[\tilde{A}^T P_\delta + P_\delta\tilde{A} + P_\delta(\tilde{B}_1\tilde{\Delta}_t\tilde{C}_1) + (\tilde{B}_1\tilde{\Delta}_t\tilde{C}_1)^T P_\delta\right] x(t). \tag{3.14}$$

Since for each pair of matrices (M_b, M_c) with compatible dimensions, there holds $M_bM_c + M_c^TM_b^T \leq M_bM_b^T + M_c^TM_c$. Taking $M_b = P_\delta\tilde{B}_1$ and $M_c = \tilde{\Delta}_t\tilde{C}_1$ yields

$$\dot{V}(t) \leq x(t)^T \left(\tilde{A}^T P_\delta + P_\delta\tilde{A} + P_\delta\tilde{B}_1\tilde{B}_1^T P_\delta + \tilde{C}_1^T\tilde{\Delta}_t^T\tilde{\Delta}_t\tilde{C}_1\right) x(t). \tag{3.15}$$

It follows that if $0 \neq x_0 = x(0) \in \overline{\mathcal{B}}_{P_\delta}(\varepsilon)$, then by the assumption that there exists a

solution $\varepsilon > 0$ to $\delta = \varphi(\varepsilon)$ and ARI (3.7), we have

$$\dot{V}(0) \leq x_0^T \left(\tilde{A}^T P_\delta + P_\delta \tilde{A} + P_\delta \tilde{B}_1 \tilde{B}_1^T P_\delta + \delta^2 \tilde{C}_1^T \tilde{C}_1 \right) x_0 < 0. \tag{3.16}$$

The condition $\overline{\sigma}(\tilde{\Delta}_t) \leq \delta \ \forall \ x(t) \in \overline{\mathcal{B}}_{P_\delta}(\varepsilon)$ implies that $\|f(x(t))\|$ is bounded over $x(t) \in \overline{\mathcal{B}}_{P_\delta}(\varepsilon)$. Consequently $\|\dot{x}\|$ is bounded for $x(t) \in \overline{\mathcal{B}}_{P_\delta}(\varepsilon)$. Since V is continuous and $\dot{V}(0) < 0$, $\exists \ t_1$ such that

$$V(x(t)) < V(x_0) \leq \varepsilon^2 < \varepsilon_m \tag{3.17}$$

for all $t \in [0, \ t_1]$. and hence $x(t_1) \in \overline{\mathcal{B}}_{P_\delta}(\varepsilon)$. Now consider the nonlinear system (3.1) for $t \geq t_1$ with the initial condition $x_1 = x(t_1) \in \overline{\mathcal{B}}_{P_\delta}(\varepsilon)$. The preceding process can be applied to conclude $x(t) \in \overline{\mathcal{B}}_{P_\delta}(\varepsilon)$ for $t \in [t_1, \ 2t_1]$ due to the independence of t for $f(\cdot)$. By induction, $x(t) \in \overline{\mathcal{B}}_{P_\delta}(\varepsilon)$ for all $t \geq 0$. The local asymptotic stability of the equilibrium point $x_e = 0$ follows which admits the RoQA of the P_δ-weighted size ε. Since $\delta \in (0, \ \delta_m)$ can be chosen arbitrarily close to δ_m, the size of the RoQA can be increased to arbitrarily close to ε_m. Finally if (3.9) holds for all $\varepsilon > 0$, then $\overline{\sigma}(\tilde{\Delta}_t) < \delta_m \ \forall x(t) \in \mathbb{R}^n$ by the fact $P_\delta > 0$. Hence $\varepsilon = \infty$ can be taken for which the global asymptotic stability holds. □

The strictly increasing $\delta(\varepsilon_1)$ in (3.9) is assumed for the simplicity of the proof. Indeed Theorem 3.1.2 holds even if this assumption is violated in which case ε_m can be taken as the minimum among all the solutions $\{\varepsilon_\kappa\}$ satisfying $\delta_m = \delta(\varepsilon_\kappa)$.

Remark 2. *Theorem 3.1.2 shows that the nonlinearity of the system (3.1) captured by Δ_t in (3.2) via linear fractional transformation (LFT) can be regarded as time-varying uncertainty for stability analysis. However, it is important to note that it cannot be treated as an exogenous uncertainty due to the dependence of Δ_t on the state vector $x(t)$. For this reason the estimate for the size of the RoQA in Theorem 3.1.2 is the largest possible in the best of our knowledge and in light of the existing results on quadratic stability for*

time-varying uncertain systems. It is interesting to observe the consistency between the equivalence of $\|T_1\|_{\mathcal{H}_\infty} < \delta^{-1}$ *and* $\|\tilde{T}_1\|_{\mathcal{H}_\infty} < \delta^{-1}$ *and the set equivalence (3.12) in the proof.*

Clearly for a given nonlinear system in (3.1), the representation in (3.2) is not unique. One way to search for such a representation is to set

$$f(x) = \left[A + E_1(I - E_2)^{-1}C_1\right] x$$

where E_1 and E_2 are both bounded functions of x according to

$$\begin{bmatrix} E_1(t) \\ E_2(t) \end{bmatrix} \begin{bmatrix} E_1(t)^T & E_2(t)^T \end{bmatrix} \leq \delta_m^2 \begin{bmatrix} B_1 \\ D_{11} \end{bmatrix} \begin{bmatrix} B_1^T & D_{11}^T \end{bmatrix}$$

$\forall\ x(t) \in \mathcal{B}_{P_\delta}(\varepsilon_m)$ and for some given B_1, D_{11}, and $P_\delta > 0$. The above can be simplified, if E_1 and E_2 are linear, i.e.,

$$E(t) = \begin{bmatrix} \Phi_1 x(t) & \Phi_2 x(t) & \cdots \Phi_n x(t) \end{bmatrix}$$

for some constant matrices $\{\Phi_i\}$. It follows that $\varepsilon_m = \sqrt{\lambda_{\min}(P_\delta)}\delta_m$ with (3.9) replaced by

$$\delta_m = \max\left\{\overline{\sigma}[\Delta(x)] : \quad x \in \mathbb{R}^n \ \ \& \ \ x^T P_\delta x \leq \varepsilon_m^2 = \lambda_{\min}(P_\delta)\delta_m^2\right\}, \tag{3.18}$$

because the strictly monotonicity holds.

The RoQA in Theorem 3.1.2 has an elliptical region. If a spherical region is preferred, then the following result will be useful in estimating the size of RoA.

Corollary 3.1.3. *Under the same hypotheses/conditions as in* Theorem 3.1.2*, the origin of the nonlinear system* (3.1) *is asymptotically stable with the spherical* RoA *of size* $\frac{\varepsilon_m}{\sqrt{\lambda_{\max}(P_\delta)}} \max\{1, \sqrt{\lambda_{\min}(P_\delta)}\}$.

Proof. In light of Theorem 3.1.2, $\mathcal{B}_{P_\delta}(\varepsilon_m)$ is the RoQA. Thus for the solution trajectory $x(t)$ to (3.1) with $x(0) = x_0 \in \mathcal{B}_{P_\delta}(\varepsilon_m)$, $V(t) = \|x(t)\|^2_{P_\delta} > 0$ and $\dot{V}(t) < 0$ for all $t > 0$ whenever $x(t) \neq 0$ where $P_\delta > 0$ satisfies the ARI (3.7) with δ arbitrarily close to δ_m. It follows that

$$V(t) = x(t)^T P_\delta x(t) < x_0^T P x_0 \leq \lambda_{\max}(P_\delta)\|x_0\|^2 < \varepsilon_m^2$$

for all $t > 0$, provided that $\|x_0\| < \varepsilon_m/\sqrt{\lambda_{\max}(P_\delta)}$. Consequently the set

$$\mathcal{B}\left(\varepsilon_m/\sqrt{\lambda_{\max}(P_\delta)}\right) \subseteq \mathcal{B}_{P_\delta}(\varepsilon) \tag{3.19}$$

that concludes the asymptotic stability of $x_e = 0$ with the spherical RoA of size $\varepsilon_m/\sqrt{\lambda_{\max}(P_\delta)}$. On the other hand, since $P > 0$, there exists a nonsingular matrix S such that $P = S^T S$. Denote $\tilde{x}(t) = Sx(t)$. Direct calculation shows that, by monotonic decreasing of $V(t) = \|\tilde{x}(t)\|^2$ to zero, there holds

$$\begin{aligned}\|x(t)\|^2 = x(t)^T x(t) = \tilde{x}(t)^T P_\delta^{-1} \tilde{x}(t) &\leq \lambda_{\max}(P_\delta^{-1})\|\tilde{x}(t)\|^2 \\ &< \|\tilde{x}(0)\|^2/\lambda_{\min}(P_\delta) \\ &\leq \|x_0\|^2 \lambda_{\min}(P_\delta)/\lambda_{\max}(P_\delta) \leq \varepsilon_m^2,\end{aligned}$$

provided that $\|x_0\| < \varepsilon_m\sqrt{\lambda_{\min}(P_\delta)}/\sqrt{\lambda_{\max}(P_\delta)}$. As a result, the set

$$\mathcal{B}\left(\varepsilon_m\sqrt{\lambda_{\min}(P_\delta)}/\sqrt{\lambda_{\max}(P_\delta)}\right) \subseteq \mathcal{B}_{P_\delta}(\varepsilon). \tag{3.20}$$

Hence the solution trajectory $x(t)$ converges to zero asymptotically, if the initial condition x_0 belongs to either the set in (3.19) or the set in (3.20) by Theorem 3.1.2. □

Our results in this section have an intimate relation to the classical nonlinear stability results [Zam66a, Zam66b] by Zames, i.e., the small gain theorem. Indeed the stability results of Zames are established for static sector-bounded nonlinearities in the input-ouput

framework while our results in Theorem 3.1.2 and Corollary 3.1.3 are applicable to dynamic sector-bounded nonlinearities embedded in the state-space model. Although our results are more conservative due to the dependence of the sector-bounded nonlinearity on the state variables, they provide a feasible procedure to cope with more general type of nonlinearities involved in the state-space model.

3.1.2 Feedback Stabilization

The nonlinear system under consideration is described by the nonlinear state-space model $\mathcal{N}_S$:

$$\dot{x}(t) = f[x(t), u(t)], \quad y(t) = h[x(t), u(t)], \quad x(0) = x_0, \tag{3.21}$$

where $x(t) \in \mathbb{R}^n$ is the state vector, $u(t) \in \mathbb{R}^{m_2}$ is the control input, and $y(t) \in \mathbb{R}^{p_2}$ is the measured output. Without loss of generality the nonlinear control system in (3.21) assumes the origin as the equilibrium point, i.e., $f(0,0) = 0$. The problem of feedback stabilization aims at design of a state or output feedback controller such that the equilibrium point is asymptotically stable.

We start by rewriting the nonlinear state-space model in (3.21) as

$$\begin{bmatrix} \dot{x} \\ y \end{bmatrix} = \left(\begin{bmatrix} A & B_2 \\ C_2 & D_{22} \end{bmatrix} + \begin{bmatrix} B_1 \\ D_{21} \end{bmatrix} \Delta_t (I - D_{11}\Delta_t)^{-1} \begin{bmatrix} C_1 & D_{12} \end{bmatrix} \right) \begin{bmatrix} x \\ u \end{bmatrix}, \tag{3.22}$$

where $x(0) = x_0$ and $\Delta_t = \Delta[x(t), u(t)] \in \mathbf{\Delta}$ by an abuse of notation. Note that Δ_t also satisfies

$$\Delta_t|_{x(t)=0, u(t)=0} = \Delta(0,0) = 0. \tag{3.23}$$

Realization matrices (A, B_2, C_2, D_{22}) can be obtained via linearization as

$$A = \left.\frac{\partial f(x,u)}{\partial x}\right|_{x=0,u=0,} \qquad B_2 = \left.\frac{\partial f(x,u)}{\partial u}\right|_{x=0,u=0,}$$
$$C_2 = \left.\frac{\partial h(x,u)}{\partial x}\right|_{x=0,u=0,} \qquad D_{22} = \left.\frac{\partial h(x,u)}{\partial u}\right|_{x=0,u=0,}$$

with $A \in \mathbb{R}^{n\times n}, B_2 \in \mathbb{R}^{n\times m_2}, C_2 \in \mathbb{R}^{p_2\times n}$, and $D_{22} \in \mathbb{R}^{p_2\times m_2}$. The dimensions of B_1, C_1, and D_{11} are $n\times m_1$, $p_1\times n$, and $p_1\times m_1$, respectively, and those of D_{12} and D_{21} can be easily determined based on (3.22). The nonlinearities of (3.21) are captured by $\Delta_t = \Delta[x(t), u(t)]$ that is a nonlinear map: $\mathbb{R}^n \times \mathbb{R}^{m_2} \mapsto \mathbb{R}^{m_1\times p_1}$.

Our approach to nonlinear stabilization is again based on the notion of quadratic stability and by treating the nonlinear term $\Delta_t = \Delta[x(t), u(t)]$ as bounded time-varying uncertainty which is now dependent on both the state and control input. For convenience, denote

$$G(s) = \begin{bmatrix} D_{11} & D_{12} \\ D_{21} & D_{22} \end{bmatrix} + \begin{bmatrix} C_1 \\ C_2 \end{bmatrix} (sI - A)^{-1} \begin{bmatrix} B_1 & B_2 \end{bmatrix}. \tag{3.24}$$

It is assumed that (A, B_2) is stabilizable, (C_2, A) is detectable, and $D_{22} = 0$. Further assumptions on the plant data will depend on the computational method chosen to solve the $\mathcal{H}_\infty$ synthesis problems that follow, and generally there is a trade-off between computational complexity and restrictions on the plant data.

Our first result is concerned with stabilization of the nonlinear system in (3.21) under linear state feedback control as illustrated in block diagram (a) of Figure 3.2. We assume that $R = D_{12}^T D_{12} > 0$ and

$$\text{rank}\left\{\begin{bmatrix} A - j\omega I & B_2 \\ C_1 & D_{12} \end{bmatrix}\right\} = n + m_2 \;\forall\; \omega \in \mathbb{R}. \tag{3.25}$$

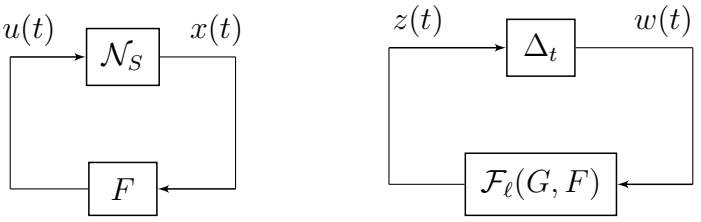

(a) (b)

Figure 3.2: (a) Nonlinear system with linear state feedback; (b) Equivalent loop

Theorem 3.1.4. *Consider the nonlinear system in* (3.21) *that admits the representation in* (3.22) *where* $D_{22} = 0$, $D_{21} = 0$ *and* $C_2 = I$. *Let* F *be the stabilizing state feedback gain and* $T_F(s) = D_{11} + (C_1 + D_{12}F)(sI - A - B_2F)^{-1}B_1$. *Then*

$$\delta_m := \left(\inf_F \|T_F\|_{\mathcal{H}_\infty}\right)^{-1} > 0 \tag{3.26}$$

exists. Let $(\tilde{A}, \tilde{B}_1, \tilde{C}_1)$ *be the same as in* Lemma 3.1.1 *and* $\tilde{D}_{12} = (I - \delta^2 D_{11}D_{11}^T)^{-1/2}D_{12}$ *for some parameter* $\delta \in (0,\ \delta_m)$ *arbitrarily close to* δ_m. *Then there exists an* $X > 0$ *to the following* ARI*:*

$$\tilde{A}_R^T X + X\tilde{A}_R - X(B_2R^{-1}B_2^T - \delta^{-2}\tilde{B}_1\tilde{B}_1^T)X + \tilde{C}_R^T\tilde{C}_R < 0 \tag{3.27}$$

where $\tilde{A}_R = \tilde{A} - B_2\tilde{R}^{-1}\tilde{D}_{12}^T\tilde{C}_1$, $\tilde{C}_R = (I - \tilde{D}_{12}\tilde{R}^{-1}\tilde{D}_{12}^T)\tilde{C}_1$, *and* $\tilde{R} = \tilde{D}_{12}^T\tilde{D}_{12}$. *Let*

$$u(t) = Fx(t), \quad F = -\tilde{R}^{-1}(\tilde{D}_{12}^T\tilde{C}_1 + B_2^T X), \tag{3.28}$$

be the state feedback control law. If there exists an $\varepsilon_m > 0$ *such that*

$$\overline{\sigma}[\Delta(x, Fx)] < \delta_m \quad \forall\ x \in \mathcal{B}_X(\varepsilon_m), \tag{3.29}$$

then the nonlinear system in (3.21) *under the state feedback control law* (3.28) *is regionally asymptotically stable with* RoQA *of* X*-weighted size* ε_m. *If* (3.29) *holds for all* $x \in \mathbb{R}^n$, *then the nonlinear system in* (3.21) *under the state feedback control law* (3.28) *is globally*

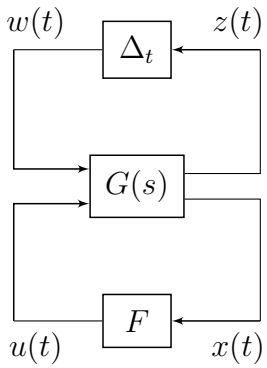

Figure 3.3: Equivalent LFT state feedback system

asymptotically stable.

Proof. The representation in (3.22) can be used to aid feedback stabilization. Denote

$$w(t) = \Delta_t(I - D_{11}\Delta_t)^{-1}[C_1x(t) + D_{12}u(t)], \tag{3.30}$$

$$z(t) = C_1x(t) + D_{11}w(t) + D_{12}u(t). \tag{3.31}$$

Then $w(t)$ is bounded for all $x(t) \in \mathcal{B}_X(\varepsilon_m)$, $\overline{\sigma}(D_{11}\Delta_t) \leq \overline{\sigma}(D_{11})\delta < 1$ in light of (3.29) and the fact that $\delta > 0$ can be made arbitrarily close to δ_m. Hence $w(t)$ can be rewritten as

$$w(t) = \Delta_t\left[C_1x(t) + D_{11}w(t) + D_{12}u(t)\right] = \Delta_t z(t). \tag{3.32}$$

The dynamic equations in (3.22) can now be described equivalently by

$$\dot{x}(t) = Ax(t) + B_1w(t) + B_2u(t), \tag{3.33}$$

$$z(t) = C_1x(t) + D_{11}w(t) + D_{12}u(t), \tag{3.34}$$

where $w(t) = \Delta_t z(t)$ and $y(t) = x(t)$ is the measured output. This gives rise to the block diagram in Figure 3.3 where $G(s)$ is the same as in (3.24) except that $D_{21} = 0$, $D_{22} = 0$, and $C_2 = I$.

Since $u(t) = Fx(t)$ is the state feedback control law, the block diagram in Figure 3.3 is

equivalent to the one in (b) of Figure 3.2 and thus

$$\mathcal{F}_\ell(G, F) = G_{11}(s) + G_{12}(s)F[I - G_{22}(s)F]^{-1}G_{21}(s). \tag{3.35}$$

As a result the dynamic equations in (3.33) are changed to

$$\dot{x}(t) = (A + B_2F)x(t) + B_1w(t), \tag{3.36}$$

$$z(t) = (C_1 + D_{12}F)x(t) + D_{11}w(t), \tag{3.37}$$

$$w(t) = \Delta_t z(t), \quad \Delta_t = \Delta[x(t), Fx(t)]. \tag{3.38}$$

Hence the closed-loop stability for the nonlinear feedback system in block diagram (b) of Figure 3.2 is identical to that in (a) of Figure 3.1 with $T_1(s)$ replaced by

$$T_F(s) = \mathcal{F}_\ell(G, F) = D_{11}+(C_1 + D_{12}F)(sI - A - B_2F)^{-1}B_1. \tag{3.39}$$

A similar method to the proof of Theorem 3.1.2 can be employed to eliminate $D_{11} \neq 0$ by noting the following set equality similar to (3.12):

$$\begin{aligned}
\mathcal{S}_F &:= \left\{A + B_2F + B_1\Delta_t \left(I - D_{11}\Delta_t\right)^{-1} (C_1 + D_{12}F) : \overline{\sigma}(\Delta_t) \leq \delta\right\} \\
&= \left\{\tilde{A} + B_2F + \tilde{B}_1\tilde{\Delta}_t(\tilde{C}_1 + \tilde{D}_{12}F) : \ \ \overline{\sigma}(\tilde{\Delta}_t) \leq \delta\right\} \\
&=: \tilde{\mathcal{S}}_F.
\end{aligned} \tag{3.40}$$

We thus have an equivalent feedback system in block diagram (b) of Figure 3.1 with $\tilde{T}_1(s)$ replaced by

$$\tilde{T}_F(s) = (\tilde{C}_1 + \tilde{D}_{12}F)(sI - \tilde{A} - B_2F)^{-1}\tilde{B}_1. \tag{3.41}$$

In light of the $\mathcal{H}_\infty$ control theory and Lemma 3.1.1, the existence of a solution $X > 0$ to the

ARI in (3.27) implies that $\|\tilde{T}_F\|_{\mathcal{H}_\infty} < \delta^{-1}$ that is equivalent to $\|T_F\|_{\mathcal{H}_\infty} = \|\mathcal{F}_\ell(G,F)\|_{\mathcal{H}_\infty} < \delta^{-1}$. Local asymptotic stability of the origin for the closed-loop system thus holds which admits RoQA of X-weighted size ε_m under the condition in (3.29) in light of Theorem 3.1.2 by setting $V(t) = \|x\|_X^2 = x(t)^T X x(t)$. Global asymptotic stability of the closed-loop system follows as well if the condition (3.29) holds for all $x \in \mathbb{R}^n$ that completes the proof. □

The result of Theorem 3.1.4 can be stated in terms of an algebraic Riccati equality (ARE), rather than ARI. However the ARI is more convenient to deal with the case when D_{12} does not have full row rank or even $D_{12} = 0$. For this reason, the LMI method is preferred [GA94, Gah96].

Similar to Theorem 3.1.2, ε_m can be obtained via the monotonically increasing function

$$\varphi(\varepsilon) = \max\left\{\overline{\sigma}[\Delta(x,Fx)] : \quad x^T X x \le \varepsilon^2\right\}. \tag{3.42}$$

If $\varphi(\varepsilon)$ is strictly increasing, then $\varphi(\varepsilon_m) = \delta_m$ has a unique solution ε_m for the given δ_m. Otherwise $\delta(\varepsilon_i) = \delta_m$ may admit more than one solution in which case ε_m can be chosen as the minimum of the solution set $\{\varepsilon_i\}$. How to pick a suitable value for ε_m depends on the form of Δ_t. The simplest case is when Δ_t is a linear function of $x(t)$ and $u(t)$ in the form of

$$\Delta_t = \begin{bmatrix} \Phi_1 x(t) + \Psi_1 u(t) & \cdots \Phi_n x(t) + \Psi_n u(t) \end{bmatrix}. \tag{3.43}$$

More complicated ones may involve high order terms or even transcendental functions of $x(t)$ and $u(t)$. For Δ_t in (3.43), it can be shown that a suitable value for ε_m is given by

$$\varepsilon_m = \delta_m \Big/ \sqrt{\lambda_{\max}\left(\begin{bmatrix} I \\ F \end{bmatrix} X^{-1} \begin{bmatrix} I & F^T \end{bmatrix}\right)}. \tag{3.44}$$

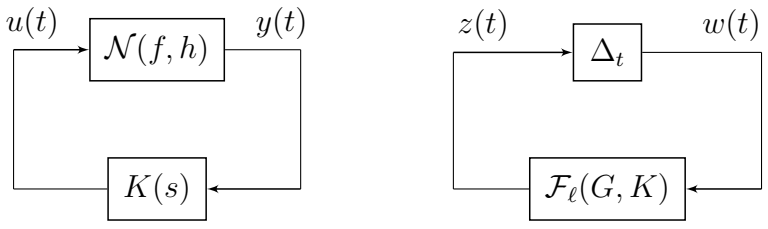

(a) (b)

Figure 3.4: (a) Nonlinear system with linear output feedback; (b) Equivalent loop

In the case when A is a stability matrix and $F = 0$, or $u(t) \equiv 0$, the above reduces to $\varepsilon_m = \delta_m \sqrt{\lambda_{\min}(X)}$ by $\lambda_{\max}(X^{-1}) = 1/\lambda_{\min}(X)$, that agrees with the result in Section 3.1.1. The following result provides the spherical size of the RoA. Its proof is skipped since it is similar to that of Corollary 3.1.3.

Corollary 3.1.5. *Under the same hypotheses/conditions as in* Theorem 3.1.4*, the origin of the nonlinear system* (3.1) *is asymptotically stable with the spherical* RoA *of size* $\frac{\varepsilon_m}{\sqrt{\lambda_{\max}(X)}} \max\{1, \sqrt{\lambda_{\min}(X)}\}$.

We now consider stabilization of the nonlinear system in (3.21) under output feedback control as illustrated in block diagram (a) of Figure 3.4.

While Lemma 3.1.1 served as a useful method to simplify stability analysis in Section 3.1.1 and state feedback synthesis, we prefer to invoke the loopshifting and scaling argument [SL88] for output feedback synthesis. Consequently we assume that $D_{11} = 0$,

$$D_{12}^T \begin{bmatrix} C_1 & D_{12} \end{bmatrix} = \begin{bmatrix} 0 & I_{m_2} \end{bmatrix}, \quad D_{21} \begin{bmatrix} B_1^T & D_{21}^T \end{bmatrix} = \begin{bmatrix} 0 & I_{p_2} \end{bmatrix}.$$

Let the strictly proper stabilizing controller $K(s)$ be described by

$$\dot{\hat{x}}(t) = A_K \hat{x}(t) + B_K y(t), \qquad u(t) = C_K \hat{x}(t). \tag{3.45}$$

Then the closed-loop transfer matrix $T_{OF}(s) = \mathcal{F}_\ell[G(s), K(s)]$ with $G(s)$ in (3.24) is given

by

$$T_{OF}(s) = \begin{bmatrix} C_1 & D_{12}C_K \end{bmatrix} \left(sI - \begin{bmatrix} A & B_2C_K \\ B_KC_2 & A_K \end{bmatrix} \right)^{-1} \begin{bmatrix} B_1 \\ B_KD_{21} \end{bmatrix}. \tag{3.46}$$

The significance of the transfer matrix $T_{OF}(s)$ will be made clear in Theorem 3.1.6. Define

$$\delta_m := \left(\inf_K \|T_{OF}\|_{\mathcal{H}_\infty} \right)^{-1} > 0 \tag{3.47}$$

that exists. By standard $\mathcal{H}_\infty$ theory, $\|T_{OF}\|_\infty < \delta^{-1}$ for some parameter $\delta \in (0, \delta_m)$, if and only if there exist $X > 0$ and $Y > 0$ to the following ARIs

$$AY + YA^T - (B_2B_2^T - \delta^2 B_1B_1^T) + YC_1^TC_1Y < 0, \tag{3.48}$$

$$A^TX + XA - (C_2^TC_2 - \delta^2 C_1^TC_1) + YB_1B_1^TY < 0, \tag{3.49}$$

respectively, which satisfy the coupling condition:

$$\begin{bmatrix} \delta^{-1}X & I \\ I & \delta^{-1}Y \end{bmatrix} \geq 0. \tag{3.50}$$

The stabilizing output feedback controller is given by

$$\begin{aligned} A_K &= -U^{-1}(A^T + \delta^{-2}X(A + LC_2 + B_2F)Y + XB_1B_1^T + C_1^TC_1Y)(V^T)^{-1}, \\ B_K &= \frac{1}{\delta}U^{-1}XL, \;\; C_K = \frac{1}{\delta}FY(V^T)^{-1}, \end{aligned} \tag{3.51}$$

where $VU^T = I - \delta^{-2}YX$, $F = -B_2^TY^{-1}$, and $L = -X^{-1}C_2^T$.

Theorem 3.1.6. *Consider the nonlinear system in* (3.21) *that admits the representation*

in (3.22). *If there exists an* $\varepsilon_m > 0$ *such that*

$$\overline{\sigma}[\Delta(x, C_K\hat{x})] < \delta_m \quad \forall \quad \begin{bmatrix} x \\ \hat{x} \end{bmatrix} \in \mathcal{B}_{\mathcal{P}}(\varepsilon_m) \tag{3.52}$$

with $\mathcal{P} = \begin{bmatrix} \frac{1}{\delta}X & U \\ U^T & X_2 \end{bmatrix}$, *then the nonlinear system in* (3.21) *under the output feedback controller* $K(s)$ *is regionally asymptotically stable with* RoQA *of* $\mathcal{P}$*-weighted size* ε_m. *If* (3.52) *holds for all* $x, \hat{x} \in \mathbb{R}^n$, *then the nonlinear system in* (3.21) *under the output feedback controller* $K(s)$ *is globally asymptotically stable.*

Proof. Similar to Theorem 3.1.4, the dynamic and measurement equations in (3.22) can be described equivalently by

$$\dot{x}(t) = Ax(t) + B_1 w(t) + B_2 u(t) \tag{3.53}$$

$$z(t) = C_1 x(t) + D_{12} u(t) \tag{3.54}$$

$$y(t) = C_2 x(t) + D_{21} w(t) + D_{22} u(t) \tag{3.55}$$

where $w(t) = \Delta_t z(t)$. This gives rise to the block diagram in Figure 3.5.

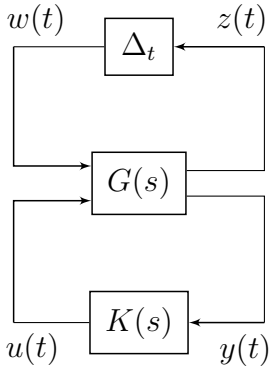

Figure 3.5: Equivalent LFT output feedback system

With the controller realization given in (3.45) and $G(s)$ in (3.24), the block diagram in

Figure 3.5 is equivalent to the one in (b) of Figure 3.4, and thus

$$\mathcal{F}_\ell(G, K) = G_{11} + G_{12}K[I - G_{22}K]^{-1}G_{21} \tag{3.56}$$

As a result the dynamic equations in (3.53) are changed to

$$\dot{x}(t) = Ax(t) + B_2C_K\hat{x}(t) + B_1w(t) \tag{3.57}$$

$$\dot{\hat{x}}(t) = B_KC_2x(t) + A_K\hat{x}(t) + B_KD_{21}w(t) \tag{3.58}$$

$$z(t) = C_1x(t) + D_{12}C_K\hat{x}(t) \tag{3.59}$$

Define augmented state matrices as

$$\mathcal{A} = \begin{bmatrix} A & B_2C_K \\ B_KC_2 & A_K \end{bmatrix},\ \mathcal{B} = \begin{bmatrix} B_1 \\ B_KD_{21} \end{bmatrix},$$
$$\mathcal{C} = \begin{bmatrix} C_1 & D_{12}C_K \end{bmatrix}. \tag{3.60}$$

Then is clear that

$$T_{\text{OF}}(s) = \mathcal{F}_\ell(G, K) = \mathcal{C}(sI - \mathcal{A})^{-1}\mathcal{B} \tag{3.61}$$

Hence the closed-loop stability for the nonlinear output feedback system in block diagram (b) of Figure 3.4 is identical to that in (a) of Fig. 3.1 with $T_1(s)$ replaced by $T_{\text{OF}}(s)$. In light of $\mathcal{H}_\infty$ control theory, the existence of a solution $\mathcal{P} > 0$ to

$$\mathcal{A}^T\mathcal{P} + \mathcal{P}\mathcal{A} + \delta\mathcal{P}\mathcal{B}\mathcal{B}^T\mathcal{P} + \delta\mathcal{C}^T\mathcal{C} < 0 \tag{3.62}$$

is equivalent to $\|T_{\text{OF}}\|_\infty < \delta^{-1}$. By standard $\mathcal{H}_\infty$ theory, we may restate (3.62) in terms of the two ARIs in (3.48) and (3.49), plus the coupling condition in (3.50) that simplifies

the computation of the RoQA and also allows us to compute the stabilizing controller. Partition $\mathcal{P} = \begin{bmatrix} \hat{X} & U \\ U^T & X_2 \end{bmatrix}$ and $\mathcal{P}^{-1} = \begin{bmatrix} \hat{Y} & V \\ V^T & Y_2 \end{bmatrix}$. Define $\mathcal{R} = \begin{bmatrix} \hat{X} & U \\ I & 0 \end{bmatrix}$ and $\mathcal{S} = \begin{bmatrix} I & 0 \\ \hat{Y} & V \end{bmatrix}$, then $\mathcal{SP} = \mathcal{R}$. Assume that the controller order is not smaller than n. Hence U has more columns than rows, which allows us to assume that U has full row rank. This implies that $\mathcal{R}$ has full row rank too. Due to $\mathcal{SP} = \mathcal{R}$, $\mathcal{S}$ also has full row rank. Now multiply (3.62) and $\mathcal{P} > 0$ by $\mathcal{S}$ on the left and $\mathcal{S}^T$ on the right to obtain

$$\mathcal{S}\mathcal{A}^T\mathcal{R}^T + \mathcal{R}\mathcal{A}\mathcal{S}^T + \delta\mathcal{R}\mathcal{B}\mathcal{B}^T\mathcal{R}^T + \delta\mathcal{S}\mathcal{C}^T\mathcal{C}\mathcal{S}^T < 0 \tag{3.63}$$

$$\mathcal{S}\mathcal{R}^T > 0 \tag{3.64}$$

Note that the inequalities (3.62) and $\mathcal{P} > 0$ are preserved since $\mathcal{S}$ has full row rank. After some algebra, recalling $\hat{Y}\hat{X} + VU^T = I$ and defining

$$L = \hat{X}^{-1}UB_K \tag{3.65}$$

$$F = C_K V^T \hat{Y}^{-1} \tag{3.66}$$

we conclude that (3.63) and (3.64) may be written as

$$\begin{bmatrix} (A+LC_2)^T\hat{X} + \hat{X}(A+LC) & A^T + \hat{X}(A+LC_2+B_2F)\hat{Y} + UA_KV^T \\ A + (\hat{X}(A+LC_2+B_2F)\hat{Y} + UA_KV^T)^T & (A+B_2F)\hat{Y} + \hat{Y}(A+B_2F)^T \end{bmatrix} +$$
$$\delta \begin{bmatrix} \hat{X}(B_1+LD_{21})(B_1+LD_{21})^T\hat{X} & \hat{X}(B_1+LD_{21})B_1^T \\ B_1(B_1+LD_{21})^T\hat{X} & B_1B_1^T \end{bmatrix} +$$
$$\delta \begin{bmatrix} C_1^TC_1 & C_1^T(C_1+D_{12}F)\hat{Y} \\ \hat{Y}(C_1+D_{12}F)^TC_1 & \hat{Y}(C_1+D_{12}F)^T(C_1+D_{12}F)\hat{Y} \end{bmatrix} < 0 \tag{3.67}$$

$$\begin{bmatrix} \hat{X} & I \\ I & \hat{Y} \end{bmatrix} > 0 \tag{3.68}$$

Now we use the fact that if $x^T \begin{bmatrix} M_{11} & M_{12} \\ M_{12}^T & M_{22} \end{bmatrix} x < 0 \; \forall \; x \in \mathbb{R}^n$ then

$$\begin{bmatrix} x_1 & 0 \end{bmatrix}^T \begin{bmatrix} M_{11} & M_{12} \\ M_{12}^T & M_{22} \end{bmatrix} \begin{bmatrix} x_1 \\ 0 \end{bmatrix} = x_1^T M_{11} x_1 < 0.$$

So $\begin{bmatrix} M_{11} & M_{12} \\ M_{12}^T & M_{22} \end{bmatrix} < 0$ implies $M_{11} < 0$, the same argument may be applied to obtain that $\begin{bmatrix} M_{11} & M_{12} \\ M_{12}^T & M_{22} \end{bmatrix} < 0$ implies $M_{22} < 0$. Therefore, (3.67) implies

$$(A + B_2F)\hat{Y} + \hat{Y}(A + B_2F)^T + \delta B_1 B_1^T + \delta \hat{Y}(C_1 + D_{12}F)^T(C_1 + D_{12}F)\hat{Y} < 0 \tag{3.69}$$

$$(A + LC_2)^T\hat{X} + \hat{X}(A + LC_2) + \delta \hat{X}(B_1 + LD_{21})(B_1 + LD_{21})^T\hat{X} + \delta C_1^T C_1 < 0 \tag{3.70}$$

Now multiply (3.69) and (3.70) by δ and define $Y = \delta\hat{Y}$ and $X = \delta\hat{X}$ to obtain

$$(A + B_2F)Y + Y(A + B_2F)^T + \delta^2 B_1 B_1^T + Y(C_1 + D_{12}F)^T(C_1 + D_{12}F)Y < 0 \tag{3.71}$$

$$(A + LC_2)^T X + X(A + LC_2) + X(B_1 + LD_{21})(B_1 + LD_{21})^T X + \delta^2 C_1^T C_1 < 0 \tag{3.72}$$

Next we use the well known fact that for any F,

$$\begin{aligned} &(A + B_2F)Y + Y(A + B_2F)^T + \delta^2 B_1 B_1^T + Y(C_1 + D_{12}F)^T(C_1 + D_{12}F)Y \geq \\ &AY + YA^T - (B_2B_2^T - \delta^2 B_1 B_1^T) + YC_1^T C_1 Y \end{aligned} \tag{3.73}$$

and a dual version of it to conclude that (3.70) and (3.69) imply

$$AY + YA^T - (B_2B_2^T - \delta^2 B_1B_1^T) + YC_1^TC_1Y < 0 \tag{3.74}$$

$$A^TX + XA - (C_2^TC_2 - \delta^2 C_1^TC_1) + YB_1B_1^TY < 0 \tag{3.75}$$

It is claimed that if X and Y satisfy (3.48), (3.49), and (3.50), then an output feedback controller can be synthesized. First we set $F = -B_2^TY^{-1}$ and $L = -X^{-1}C_2^T$. By the well known fact quoted above, if X and Y satisfy (3.48) and (3.49), then with our particular choice of F and L, (3.69) and (3.70) are also satisfied. Since $(I - \hat{Y}\hat{X})^{-1}$ exists, there exist U and V such that $VU^T = I - \hat{Y}\hat{X}$. A particular choice is $U = I$ and $V = I - \hat{Y}\hat{X}$. Now set $B_K = U^{-1}\hat{X}L$ and $C_K = F\hat{Y}V^{-T}$ which also satisfy (3.65) and (3.66). Now the diagonal blocks of (3.67) are negative definite and we only need to compute A_K. We choose A_K such that the off diagonal blocks are zero so that (3.67) holds. Hence

$$A_K = -U^{-1}(A^T + \hat{X}(A + LC_2 + B_2F)\hat{Y} + \delta\hat{X}(B_1 + LD_{21})B_1^T + \delta C_1^T(C_1 + D_{12}F)\hat{Y})V^{-T} \tag{3.76}$$

which simplifies by the assumptions on the plant realization. Specifically, $\mathcal{P} > 0$ is constructed as $\mathcal{P} = \begin{bmatrix} \delta^{-1}X & U \\ U^T & X_2 \end{bmatrix}$ where $X_2 = -\delta^{-1}U^TY(V^T)^{-1}$. Local asymptotic stability of the origin for the closed-loop system thus holds which admits RoQA of $\mathcal{P}$-weighted size ε_m under the condition in (3.52) in light of Theorem 3.1.2 by setting

$$V(t) = \left\| \begin{bmatrix} x^T & \hat{x}^T \end{bmatrix}^T \right\|_{\mathcal{P}}^2 = \begin{bmatrix} x^T & \hat{x}^T \end{bmatrix} \mathcal{P} \begin{bmatrix} x^T & \hat{x}^T \end{bmatrix}^T.$$

Global asymptotic stability of the closed-loop system follows as well if the condition (3.52) holds for all $x, \hat{x} \in \mathbb{R}^n$ that completes the proof. □

Remark 3. *As mentioned previously, the* LMI *approach to controller synthesis places the*

least amount of restrictions on plant data. In fact, it only requires that (A, B_2) *be stabilizable and* (C_2, A) *be detectable. The solvability conditions, (3.48), (3.49), and (3.50), too have an equivalent description in the ARE approach. We refer to [LH06, Gah96] for further reading.*

For Δ_t with the form in (3.43) with $u = C_K\hat{x}$, it can be shown that a suitable value for ε_m for the output feedback case is given by

$$\varepsilon_m = \delta_m \Bigg/ \sqrt{\lambda_{\max}\left(\begin{bmatrix} I & 0 \\ 0 & C_K \end{bmatrix} \mathcal{P}^{-1} \begin{bmatrix} I & 0 \\ 0 & C_K^T \end{bmatrix}\right)}. \tag{3.77}$$

The following result provides the spherical size of the RoA. Its proof is skipped since it is similar to that of Corollary 3.1.3.

Corollary 3.1.7. *Under the same hypotheses/conditions as in* Theorem 3.1.4, *the origin of the nonlinear system* (3.1) *is asymptotically stable with the spherical* RoA *of size* $\frac{\varepsilon_m}{\sqrt{\lambda_{\max}(\mathcal{P})}} \max\{1, \sqrt{\lambda_{\min}(\mathcal{P})}\}$.

3.2 Polytope Method

We consider quadratic nonlinear systems of the form

$$\dot{x}(t) = f(x, u) = Ax(t) + Bu(t) + Q[x(t), u(t)], \tag{3.78}$$

where $Q[\cdot, \cdot]$ is the quadratic term given by

$$Q[x, u] = \begin{bmatrix} x^T N_1 x \\ \vdots \\ x^T N_n x \end{bmatrix} + \begin{bmatrix} x^T M_1 \\ \vdots \\ x^T M_n \end{bmatrix} u + \begin{bmatrix} u^T K_1 u \\ \vdots \\ u^T K_n u \end{bmatrix}.$$

In this method, we exploit the well known fact that an affine function is negative definite over a polytope if it is negative definite on its vertices, see for example [HB76]. As pointed

out in [ACM07], this property of convex functions is useful for stability analysis of quadratic systems, since the Lyapunov derivative of a quadratic system is negative definite over a polytope if it is negative definite on the vertices of the polytope. For the controller design we will use the following two equivalent descriptions of the polytope, $\mathcal{P}$,

$$\mathcal{P} = \left\{x : a_j^T x \leq 1,\ j = 1, \ldots, q\right\} \tag{3.79}$$

$$= \text{conv}\left\{x^{(1)}, \ldots, x^{(p)}\right\} \tag{3.80}$$

where $x^{(i)}$ is the i^{th} vertex of $\mathcal{P}$, $\text{conv}\{C\}$ is the convex hull of the set C, and a_j^T is a row vector (not the j^{th} element of vector a^T). The first description corresponds to the solution of a set of linear inequalities while the second to the the convex hull of the finite set $\left\{x^{(1)}, \ldots, x^{(p)}\right\}$ [BV04]. For this method, it is difficult to explicitly provide an expression for $\Delta(t)$ as we did in (3.5) since the bounding set consists of an intersection of sets. We point out that a similar design procedure was presented in [AAA$^+$07]. However, the work in [AAA$^+$07] did not consider systems that are quadratic in the input, i.e., the term involving K_i in (3.78).

Theorem 3.2.1. *Let $\delta > 0$, and $\mathbf{\Delta} = \{x : x \in \mathcal{P}, Fx \leq \delta\}$. The system (3.78) is quadratically stable if there exist $Y = Y^T$ and Z s.t.*

$$Y > 0 \tag{3.81}$$

$$\text{sym}(\text{AY} + \text{BZ}) + \text{sym}\left(\begin{bmatrix} x^{(i)^T}\left(N_1 Y + M_1 Z\right) \\ \vdots \\ x^{(i)^T}\left(N_n Y + M_n Z\right) \end{bmatrix}\right) + \text{sym}\left(\begin{bmatrix} \delta K_1 \\ \vdots \\ \delta K_n \end{bmatrix} \text{Z}\right) < 0,\ i = 1, \ldots, p \tag{3.82}$$

$$a_j^T Y a_j \leq 1,\ j = 1, \ldots, q \tag{3.83}$$

$$\begin{bmatrix} -\delta^2 I & Z \\ Z^T & -Y \end{bmatrix} \leq 0 \tag{3.84}$$

with RoQA $\mathcal{B}_P(1)$, where $P = Y^{-1}$. The stabilizing gain is given by $F = ZY^{-1}$.

Proof. Let $V(x) = x^T P x$. The Lyapunov derivative of V is given by

$$\dot{V} = x^T \left(A_F^T P + P A_F + \text{sym} \left(P \begin{bmatrix} x^T \left(N_1 + M_1 F + F^T K_1 F \right) \\ \vdots \\ x^T \left(N_n + M_n F + F^T K_n F \right) \end{bmatrix} \right) \right) x. \tag{3.85}$$

Now we pre and post multiply

$$A_F^T P + P A_F + \text{sym} \left(P \begin{bmatrix} x^T \left(N_1 + M_1 F + F^T K_1 F \right) \\ \vdots \\ x^T \left(N_n + M_n F + F^T K_n F \right) \end{bmatrix} \right) < 0 \tag{3.86}$$

by P^{-1} and subsitute $Y = P^{-1}$ and $Z = FP^{-1}$ to obtain the equivalent expression

$$\text{sym} \left(AY + BZ + \begin{bmatrix} x^T \left(N_1 Y + M_1 Z \right) \\ \vdots \\ x^T \left(N_n Y + M_n Z \right) \end{bmatrix} \right) + \text{sym} \left(\begin{bmatrix} x^T F^T K_1 \\ \vdots \\ x^T F^T K_n \end{bmatrix} Z \right) < 0. \tag{3.87}$$

If there exists a polytope $\mathcal{P}$ with vertices $\left\{ x^{(1)}, \ldots, x^{(p)} \right\}$ such that

$$\text{sym} \left(AY + BZ + \begin{bmatrix} x^{(i)^T} \left(N_1 Y + M_1 Z \right) \\ \vdots \\ x^{(i)^T} \left(N_n Y + M_n Z \right) \end{bmatrix} \right) + \text{sym} \left(\delta \begin{bmatrix} K_1 \\ \vdots \\ K_n \end{bmatrix} Z \right) < 0,\ i = 1, \ldots, p \tag{3.88}$$

then $\dot{V} < 0 \; \forall \; x \in \mathbf{\Delta}$. The inequality $\dot{V} < 0 \; \forall \; x \in \mathbf{\Delta}$ under the hypothesis of (3.88) on the vertices of $\mathcal{P}$ is due to the fact that (3.87) is an affine function of x (see theorem 1 in [HB76] or [BV04] for more general results) and due to $Fx \leq \delta \; \forall \; x \in \mathbf{\Delta}$. Therefore, if (3.81) and (3.82) hold, then $\dot{V} < 0$. To determine the RoQA we need to ensure that $\mathcal{B}_P(1)$ is contained in $\mathbf{\Delta}$. Condition (3.83) guarantees that $\mathcal{B}_P(1) \subseteq \mathcal{P}$ (see Section 5.2.2 in [BGFB94]). In addition, $Fx \leq \delta \; \forall \; x \in \mathcal{B}_P(1)$ must hold. In order to guarantee that this is indeed the case, we require that

$$FP^{-1}F^T = FYF^T \leq \delta^2 \tag{3.89}$$

again, by the argument in Section 5.2.2 of [BGFB94]. Since $FYF^T = ZY^{-1}Z^T$, we can write (3.89) as an LMI by Schur complement to obtain (3.84). □

An obvious disadvantage of this method is that the number of vertices that describe a polytope grows at $O\left(2^n\right)$. Therefore $p = 2^n$. This means that this method is only tractable for systems with a rather small number of states.

3.3 Equilibrium Path Design

The methods for analysis and synthesis described in Sections 3.1 and 3.2 provide regional stability results. However, if the initial condition is outside the RoQA of the desired operating point then system stability and feedback stabilization cannot be claimed. For practical problems this is an important issue. We address it in this section.

Consider the nonlinear system (3.21). In light of Theorems 3.1.4 and 3.1.6, a feedback controller can be designed such that the operating point (x_e, u_e) is regionally stable. Now the problem is to determine when the nonlinear system (3.21) can be semi-globally stabilized, i.e., given each initial condition x_0, does the state vector $x(t) \to x_e$ as $t \to \infty$? Apparently it is not possible for us to use a single fixed linear feedback control law to achieve semi-global stabilization. Therefore, our approach is the use of switching control laws and the stability results from Section 3.1.2. This leads to the following definition.

Definition 10 (Centered-ϵ-Cover)**.** *The state-space associated with system* (3.21) *is said to have a centered-ϵ-cover, if the center of each* RoQA *is contained inside a neighboring* RoQA.

We exploit this idea in the following manner: If the system (3.21) has a centered-ϵ-cover, then each initial state x_0 can be attracted to the center of the next RoQA (that is closer to the origin or the desired operating point) by an appropriate state or output feedback control law. The requirement in this path is that the center of the i^{th} RoQA must be inside the domain of the $(i^{th}+1)$ RoQA. This is illustrated in Figure 3.6 for a path divided into two sections, one corresponding to ϵ_1 and another to ϵ_2.

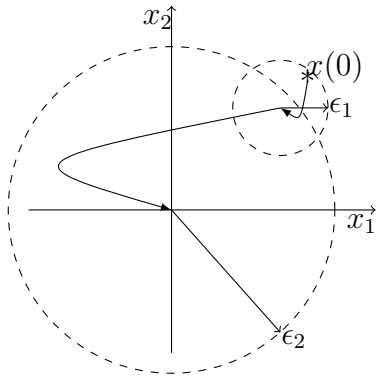

Figure 3.6: Equilibria path program example

Hence the following holds.

Theorem 3.3.1. *Suppose that the state-space associated with the system* (3.21) *admits a centered-ϵ-cover. Then there exists a linear time-varying state feedback control law such that the system is semi-globally stable for each initial condition x_0.*

It is important to emphasize a few key points in our proposed method related to the switched systems investigated in the literature and in our brief overview in Section 2.5. The family of indexed systems that we consider consists of the local description of the nonlinear system about the selected equilibrium point. Controller design is carried out based on the local linearization about the selected equilibrium point. The switching signal is most appropriately characterized as autonomous since switching depends on the location

of the state vector in the state-space. Therefore, roughly speaking, the ϵ-cover condition effectively determines the switching signal. In contrast to Theorem 2.5.1, we do not consider a single common Lyapunov function to prove stability of the switched system. Instead we establish the stability of the switched system by the Lyapunov arguments in Theorems 3.1.4 and 3.1.6 and the ϵ-cover condition. This allows us to use different Lyapunov functions (one per operating point) to prove stability. It is also interesting to note that the switched trajectory is continuous but may be non-differentiable at the switching instants.

3.4 An Illustrative Example

Consider a two spatial-dimension fluid convection problem with quadratic dynamics and linear measurement equation as it appears in [Bew99].

$$\begin{aligned}
\dot{\bar{x}}_1 &= \sigma(\bar{x}_2 - \bar{x}_1) \\
\dot{\bar{x}}_2 &= -\bar{x}_2 - \bar{x}_1\bar{x}_3 \\
\dot{\bar{x}}_3 &= -b\bar{x}_3 + \bar{x}_1\bar{x}_2 - b\bar{u} \\
y &= \bar{x}_2
\end{aligned} \tag{3.90}$$

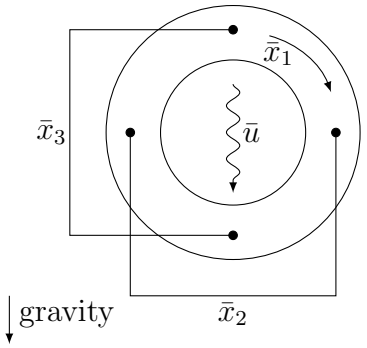

Figure 3.7: Fluid convection loop

Physically, $\bar{x}_1$ is proportional to the intensity of the fluid motion, $\bar{x}_2$ is proportional to the lateral temperature fluctuations in the fluid, and $\bar{x}_3$ is proportional to the vertical temperature fluctuations in the fluid. The control input is the loop Rayleigh number, $\bar{u}$, and is proportional to the heating rate at the bottom of the convective sys-

tem. Laboratory scale parameter values $\sigma = 4$, $b = 1$,and $\bar{u} = 48$ ensure the system operates in the chaotic regime as shown in Figure 3.8. We consider two unstable operating points $(\bar{x}_e^{(1)}, \bar{u}_e^{(1)}) = \left(\begin{bmatrix} \sqrt{b(r-1)} & \sqrt{b(r-1)} & -1 \end{bmatrix}^T, r \right)$ and $(\bar{x}_e^{(2)}, \bar{u}_e^{(2)}) = \left(\begin{bmatrix} \sqrt{b(\tilde{r}-1)} & \sqrt{b(\tilde{r}-1)} & -1 \end{bmatrix}^T, \tilde{r} \right)$ which physically correspond to the fluid moving with a constant clockwise velocity.

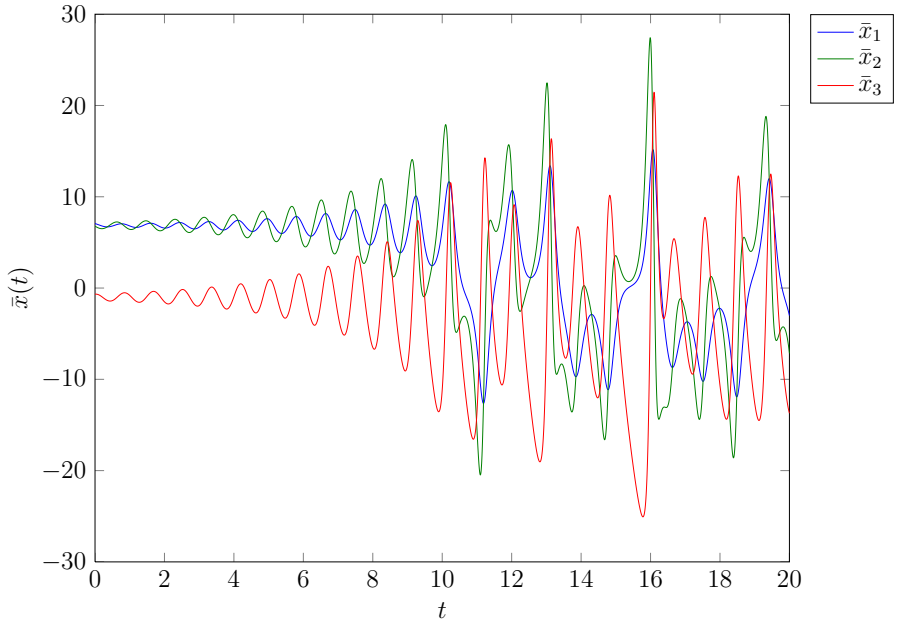

Figure 3.8: Convection loop in chaotic regime

We will design a state and output feedback controller using the sector-bounded nonlinearity method, and a state feedback controller using the polytope method. Before designing the controller we notice that $\bar{x}_1(t)$ is always stable and tracks $\bar{x}_2(t)$ asymptotically. This special structure of the dynamics suggests us to only consider stabilization of the $(\bar{x}_2, \bar{x}_3)$ subsystem. In addition, designing a controller only for this subsystem results in less conservative estimates of the RoQA for the sector-bounded method.

By defining $x = \bar{x} - \bar{x}_e$ and $u = \bar{u} - \bar{u}_e$, the nonlinear state-space model (3.90) at $\bar{x}_e$ is rewritten into

$$\dot{x} = \begin{bmatrix} -1 & -\bar{x}_{e_1} \\ \bar{x}_{e_1} & -b \end{bmatrix} x + E(t)x + \begin{bmatrix} 0 \\ -b \end{bmatrix} u$$

where $E(t) = \begin{bmatrix} 0 & -x_1 \\ x_1 & 0 \end{bmatrix}$. We compute the bound

$$E(t)'E(t) = x_1^2 \begin{bmatrix} 1 & 0 \\ 0 & 1 \end{bmatrix} \leq \delta^2 I \ \ \forall \ \ x_1(t) \in \overline{\mathcal{B}}(\delta) \tag{3.91}$$

and note that for this example, Δ_t is a linear function of $x(t)$. The control objective is to stabilize the system to $\bar{x}_e^{(1)} = \begin{bmatrix} 6.8557 & 6.8557 & -1 \end{bmatrix}^T$ and then to $\bar{x}_e^{(2)} = \begin{bmatrix} 7.1084 & 7.1084 & -1 \end{bmatrix}^T$. The state trajectory for the state and output feedback case is shown in Figures 3.9(a) and 3.9(b), respectively. The initial condition for both the state and output feedback case is $\begin{bmatrix} 8.61 & 6.43 & -1.11 \end{bmatrix}^T$.

We see from Figures 3.10(a) and 3.10(b) that the main difference between the state and output feedback controller is the transient performance and the more conservative RoQA for the output feedback controller. In the case of the latter this is clear from the equilibria path which requires more switches than the state feedback case. In fact, for output feedback we have only illustrated the first half of the equilibria path (from $\bar{x}_0$ to $\bar{x}_e^{(1)}$) in order to keep the figure clearer.

For both cases there is a tradeoff between δ_m and the RoQA of x_2 and x_3. If δ_m is chosen near its maximum, then the RoQA of x_2 and x_3 will shrink too much. We therefore chose a value roughly a third of the maximum for δ_m; this choice provided a good tradeoff for this example.

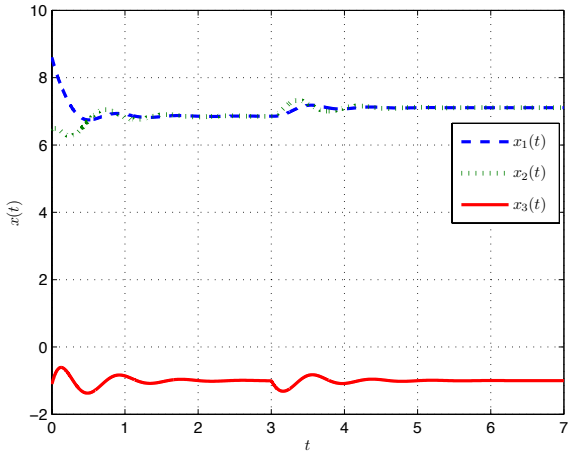

(a) State feedback

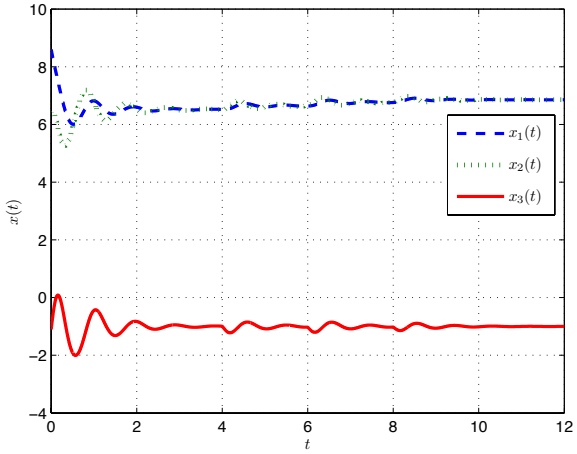

(b) Output feedback.

Figure 3.9: Closed loop equilibria path trajectory

We now design a state feedback controller via the polytope method. Although for the sector bounded approach we have to design the controller only for the $(\bar{x}_2, \bar{x}_3)$ subsystem mainly due to a vanishing RoQA, for the present method we consider the whole state vector. The initial condition is $\begin{bmatrix} 6.81 & 6.53 & -0.67 \end{bmatrix}^T$ and the state trajectory is shown in Figure 3.11.

From Figure 3.12 we can see that the controller only requires two switches to steer the state to $\bar{x}_e^{(2)}$. In addition, the initial condition of the third component of the state vector is farther away from the equilibrium value compared to the previous design method.

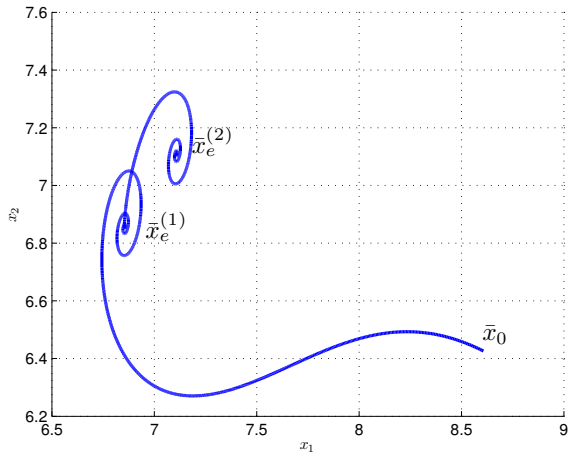

(a) State feedback

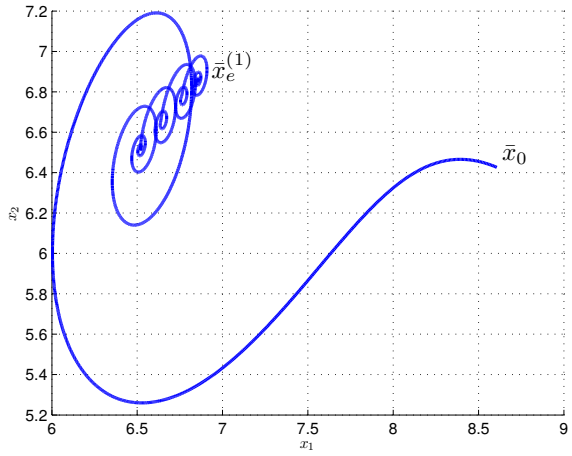

(b) Output feedback.

Figure 3.10: Closed loop equilibria path trajectory in state-space

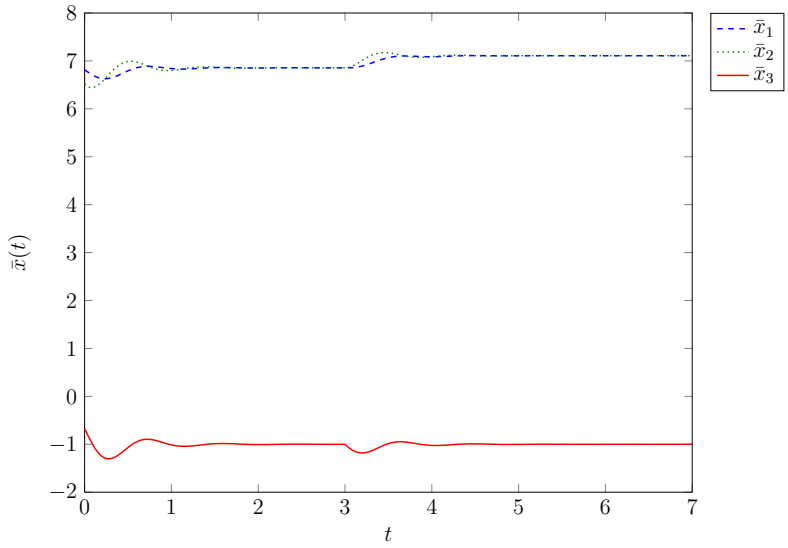

Figure 3.11: Equilibria path trajectory for state feedback controller

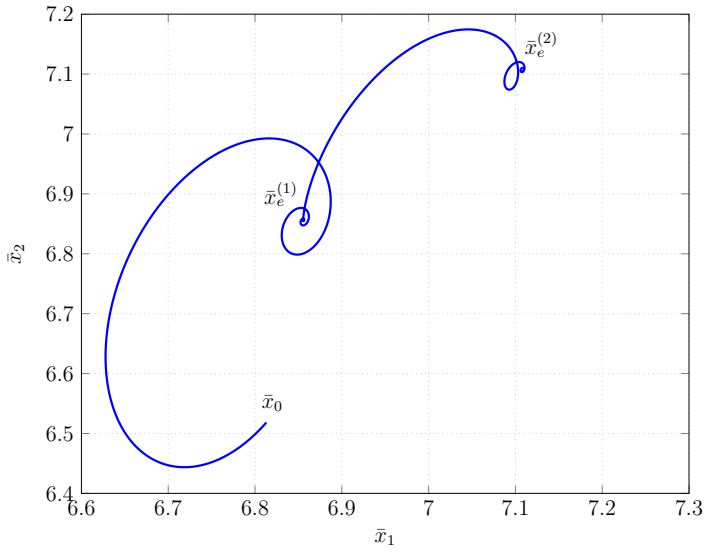

Figure 3.12: Equilibria path trajectory in state-space for state feedback controller

Chapter 4
Application: Fluid Flow Control

The efficiency of a gas turbine is closely related to the temperature at which it operates; essentially, efficiency is improved at a higher operating temperature as shown in Figure 4.1 [HDE00].

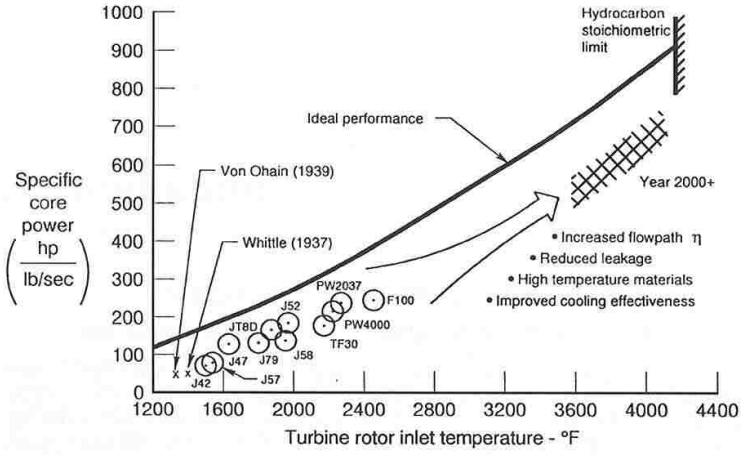

Figure 4.1: Increased turbine inlet temperature improves cycle power output

Usually the operating temperatures are in excess of 1600° F and it is not surprising that this situation poses a difficult challenge for the design of materials that are able to withstand these high temperatures. An alternative to material design is *film cooling*. Film cooling refers to the process of injecting cool air on the surface of components, we focus on the turbine blades, through small holes. If it is done right, a thin protective layer of cool air will form on the surface of the blades reducing heat transfer from the environment into the surface of the blade, allowing the turbine to operate at a high temperature without damaging the blades. A schematic of a typical blade with film cooling holes as it appears in [Lab06] is shown in Figure 4.2. A comprehensive overview of the technology can be found in [BT06].

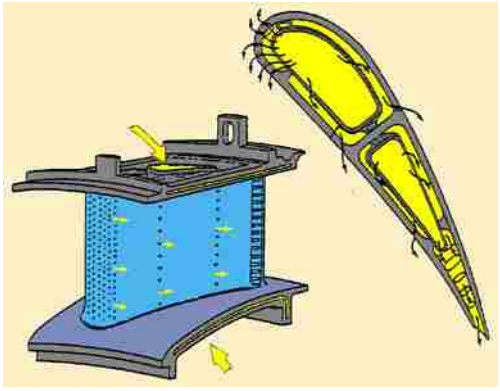

Figure 4.2: A typical blade with film cooling holes

Since we are trying to modify the natural flow of the gas turbine fluid, our problem falls into the category of *fluid flow control problems*. Fluid flow control problems are classified into two: *passive* and *active* [GeHPB98]. In a passive flow control problem, the flow field is modified through a control device that does not require external energy; for example, the roughness, shape, or curvature of a wall. In an active flow control problem, the flow is modified through a device that does require external energy; for example, suction/injection of fluid at a boundary. We focus on active flow control, in particular, feedback flow control.

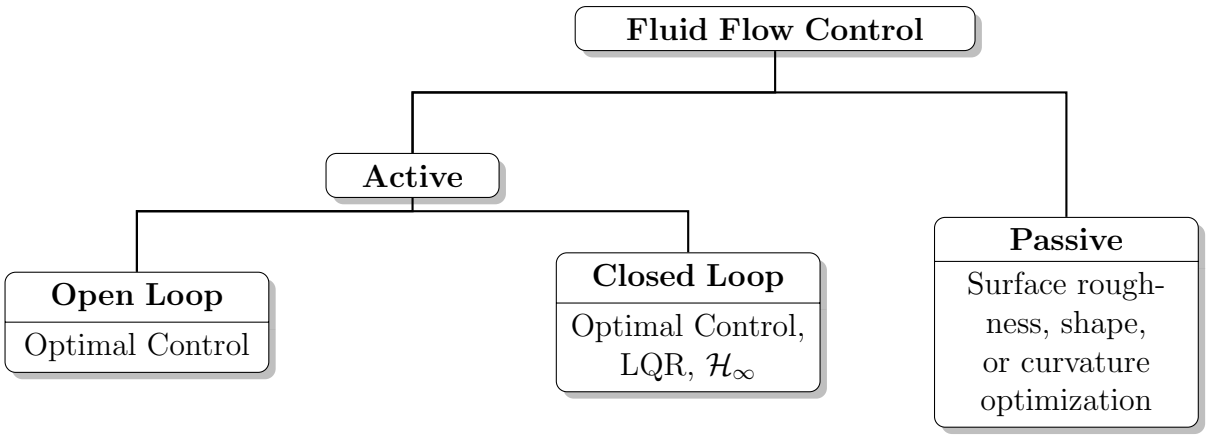

Figure 4.3: Fluid flow control classifications

There are several approaches to the film cooling problem. We approach it as a velocity tracking problem. The reason is that roughly speaking, we wish to prevent mixing of the coolant and combustion fluids so that the coolant remains close to the wall where it is injected. Although there is no consensus on what the best measure of mixing is, the kinetic energy of the flow seems to be a good choice (see chapter 5 in [AK03]). In general, as shown in [AKB01] for the Poiseuille flow problem, an increase in kinetic energy may serve as an indicator of increased mixing and vice-versa. If we can find some desired steady flow and design a controller that reduces the energy of the perturbation to this steady flow, then can expect that mixing will be reduced and that the coolant and combustion fluids will remain separate. A valid and obvious criticism is that we do not take into account the temperature dynamics of the flow. Indeed this is a valid criticism and in this investigation we design a feedback controller based only on the flow dynamics. However, at the end of this chapter we provide expressions for the mathematical form of the temperature dynamics and the difficulties they pose for control design. How to incorporate the temperature dynamics is part of a future research agenda.

In the literature there are many works concerned with stabilizing a perturbation of a flow to an equilibrium point. For example, [AR10] studies the linearized dynamics of flow past a flat plate and the stabilization of unstable steady states. The application is to regulate vortices in separated flows behind low aspect-ratio wings. The work [MIH12] analyzes the transition from steady to unsteady flow of a jet in cross-flow. It applies the tools of linear stability analysis to characterize the critical value of blowing ratio that destabilizes the flow from an equilibrium point. Investigating the growth of TS waves in the linearized Navier-Stokes equation, and their attenuation to a steady state using feedback control is considered in [OSH11]. In [BSS09], a feedback controller is designed for to stabilize a linearized open cavity flow to a steady flow. Global modes, POD, and balanced POD modes are used as expansion bases for model reduction and their performance is compared; the conclusion is that balanced POD modes provide the most effective approximation for

this problem. The article [Rav07] considers feedback stabilization of flow past an airfoil by POD/Galerkin model reduction. The feedback controller stabilizes the ROM solution but it stops short of implementing the controller in the DNS simulation.

This chapter presents the continued work in flow control based on the linearization method based on the ROM, which complements the existing work in the literature.

4.1 Modeling the Fluid Flow System

In this investigation we will consider a simplified geometry called a "jet in cross-flow" to model the film cooling setup. It consists of a computational box of dimensions $17D \times 10D \times 3D$ with a cross section in the xy plane along $z = 1.5D$ shown in Figure 4.4. The variables in this setup are shown in Table 4.1.

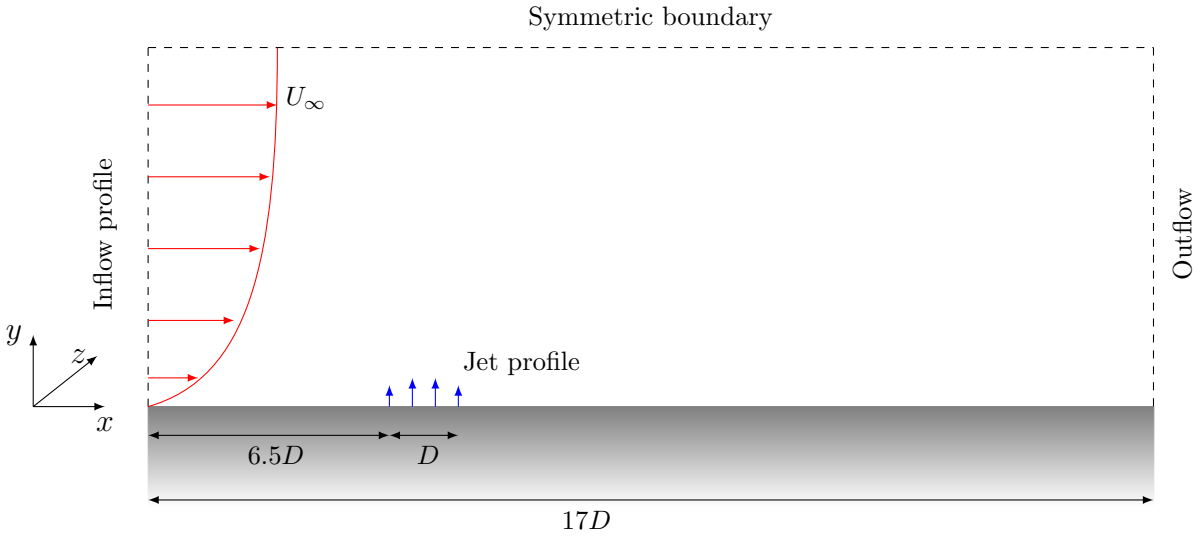

Figure 4.4: Jet in cross-flow setup

Table 4.1: Jet in cross-flow variables

Symbol	Variable
U_∞	Free stream cross-flow velocity
V	Peak inflow velocity of jet
D	Jet diameter
δ_0^*	Inflow boundary layer thickness
μ	Fluid viscosity
ρ	Fluid density
$\nu = \frac{\mu}{\rho}$	Kinematic viscosity

Fluid flow modeling is a well known subject so the following material is standard. Nevertheless we point out that we closely adhere to [AK03] in this section. We are interested in the behavior of a fluid contained in the spatial domain Ω, which in our case is associated with the geometry in Figure 4.4 in Cartesian coordinates. At every time instant $t > 0$, and to every point $p \in \Omega$ we assign a velocity to the fluid,

$$\mathbf{u} = \begin{bmatrix} u(x,y,z,t) & v(x,y,z,t) & w(x,y,z,t) \end{bmatrix}^T,$$

which is a vector valued function $\mathbf{u} : \Omega \times \mathbb{R}_+ \to \mathbb{R}^3$. We also associate a density to the fluid, $\rho : \Omega \times \mathbb{R}_+ \to \mathbb{R}$, and a pressure $P : \Omega \times \mathbb{R}_+ \to \mathbb{R}$; both are scalar valued functions. Since we are studying gas turbines that operate at a low Mach number (the ratio of the flow velocity to the local speed of sound), we may assume that ρ is constant. Furthermore, the fluids we deal with are Newtonian. Hence we consider the Navier-Stokes (N-S) and continuity equations for an incompressible Newtonian fluid as the fluid flow model. The N-S equation for three spatial dimensions is a set of three coupled, non-linear, partial differential equations that describe conservation of momentum:

$$\begin{aligned}
\frac{\partial u}{\partial t} + u\frac{\partial u}{\partial x} + v\frac{\partial u}{\partial y} + w\frac{\partial u}{\partial z} &= -\frac{1}{\rho}\frac{\partial P}{\partial x} + \frac{\mu}{\rho}\left(\frac{\partial^2 u}{\partial x^2} + \frac{\partial^2 u}{\partial y^2} + \frac{\partial^2 u}{\partial z^2}\right) \\
\frac{\partial v}{\partial t} + u\frac{\partial v}{\partial x} + v\frac{\partial v}{\partial y} + w\frac{\partial v}{\partial z} &= -\frac{1}{\rho}\frac{\partial P}{\partial y} + \frac{\mu}{\rho}\left(\frac{\partial^2 v}{\partial x^2} + \frac{\partial^2 v}{\partial y^2} + \frac{\partial^2 v}{\partial z^2}\right) \\
\frac{\partial w}{\partial t} + u\frac{\partial w}{\partial x} + v\frac{\partial w}{\partial y} + w\frac{\partial w}{\partial z} &= -\frac{1}{\rho}\frac{\partial P}{\partial z} + \frac{\mu}{\rho}\left(\frac{\partial^2 w}{\partial x^2} + \frac{\partial^2 w}{\partial y^2} + \frac{\partial^2 w}{\partial z^2}\right).
\end{aligned}$$

The continuity equation is an additional constraint that describes conservation of mass,

$$\frac{\partial u}{\partial x} + \frac{\partial v}{\partial y} + \frac{\partial w}{\partial z} = 0.$$

These four equations are written compactly as

$$\frac{\partial \mathbf{u}}{\partial t} + \mathbf{u} \cdot \nabla \mathbf{u} = -\frac{1}{\rho}\nabla P + \frac{\mu}{\rho}\nabla^2 \mathbf{u} \tag{4.1}$$

$$\nabla \cdot \mathbf{u} = 0. \tag{4.2}$$

Since there are 6 variables and 3 dimensions (length, time, and mass), the Buckingham π theorem can be invoked to characterize the jet in cross-flow with the 3 independent dimensionless parameters shown in Table 4.2.

Table 4.2: Jet in cross-flow dimensionless parameters

Symbol	**Dimensionless Parameter**
$Re = \frac{U_\infty D}{\nu}$	Free stream Reynolds number
$Re_{jet} = \frac{VD}{\nu}$	Jet Reynolds number
$R = \frac{V}{U_\infty}$	Velocity ratio

The equations can be non-dimensionalized by selecting a characteristic length scale l and a characteristic velocity scale U. We choose $l = D$ and $U = U_\infty$. By substituting the nondimensionalized variables denoted by

$$x' = \frac{x}{l},\ y' = \frac{y}{l},\ z' = \frac{z}{l},\ t' = \frac{tU}{l},\ u' = \frac{u}{U},\ v' = \frac{v}{U},\ w' = \frac{w}{U},\ P' = \frac{P}{\rho U^2},$$

into the N-S and continuity equations we obtain the nondimensionalized N-S and continuity equations

$$\frac{\partial \mathbf{u}'}{\partial t'} + \mathbf{u}' \cdot \nabla \mathbf{u}' = -\nabla P' + \frac{1}{Re}\nabla^2 \mathbf{u}' \tag{4.3}$$

$$\nabla \cdot \mathbf{u}' = 0 \tag{4.4}$$

where $\mathbf{u}' = \begin{bmatrix} u'(x', y', z', t') & v'(x', y', z', t') & w'(x', y', z', t') \end{bmatrix}^T$. *From now on we drop the prime notation ($'$) when referring to the nondimensionalized variables.*

4.1.1 Boundary Control

The boundary of Ω is denoted by Γ and is composed of $\Gamma^{(w)}$, $\Gamma^{(f)}$, and $\Gamma^{(c)}$. The boundary Γ_w includes walls, Γ_i is the inflow, and Γ_c is the boundary to which the control signal, $c_i(t)$, (or jet) is applied. Note that there may be more than one input, for instance, if we wish to consider jets in different parts of the spatial domain. Consequently we have Dirichlet boundary conditions of the type

$$\mathbf{u}(\mathbf{x},t) = \begin{cases} \tilde{c}_i(t)\tilde{\mathbf{h}}_i(\mathbf{x}), & \mathbf{x} \in \Gamma_i^{(c)}, t \in (0,T),\ i = 1,\ldots,m \\ \tilde{a}_0(t)\tilde{\mathbf{h}}_0(\mathbf{x}), & \mathbf{x} \in \Gamma^{(f)}, t \in (0,T) \\ 0, & \mathbf{x} \in \Gamma^{(w)}, t \in (0,T) \end{cases} \tag{4.5}$$

However, in this dissertation, we will only present results for one jet actuator, although the theory holds for multi-input systems.

4.2 Numerical Implementation

The question "Does the 3D incompressible Navier-Stokes equation possess a unique, continuously differentiable solution at high Reynolds number?" is presently not known [Doe09]. However, the fact that several numerical methods converge to an approximate solution has motivated the use of the direct numerical simulation (DNS) as an engineering tool. In addition, comparison between experimental results and numerical solutions suggests that DNS simulations are reliable models for studying flow dynamics. To solve the discretized N-S equation we use the hybrid staggered/semi-staggered finite difference algorithm described in [BA11]. This algorithm uses the fractional step method to advance the solution in time in two steps: 1) A semi-staggered grid structure is used to discretize the momentum equations and solve for an intermediate velocity with the pressure gradient term absent, and 2) A staggered grid is used to discretize the Poisson-Neumann equation that adds the pressure gradient to the projection step. This method combines the favorable features of the staggered grid and semi-staggered grid approaches. All the components of velocity are stored at the cell vertices and pressure is stored at the cell centers.

The momentum equations are discretized at cell vertices thus providing a consistent discretization of the diffusive and convective terms as the boundaries are approached. The projection method effectively evolves the discrete-time system of equations, while ensuring a divergence-free velocity field is obtained. The discrete divergence and gradient operators of the projection step are constructed on a staggered gird layout leading to the exact satisfaction of the discrete continuity equation. It is important to note that the solution of the Poisson-Neumann equation in the projection step is free of any spurious eigenmodes. The code has been validated through the following benchmark problems: Taylor-Green vortex problem, driven cavity, flow past cylinder, and flow in a 90° curved tube. In addition, it is capable of solving the discretized Navier-Stokes equation in a parallel computing environment.

A simple grid independence study (using the problem setup described in Section 4.5) was carried out using the grids illustrated in Table 4.3 and Figure 4.5.

Table 4.3: Grid sizes

Grid	**Size**
1. Coarse	623,322
2. Medium	971,152
3. Medium-Fine	1,240,512
4. Fine	1,479,072

Figure 4.6 shows the profile of the time averaged u component of velocity at $x = 4$ (downstream and not too far away from the jet). The data corresponds to a time average over a window of 60 time units after roughly 7 flow-throughs so that the results correspond to a statistically steady-state solution. We note that the numerical solutions obtained from grids 1-3 appear to converge to the solution obtained on the fine grid. Since there are not much computational savings between the medium-fine and fine grids, we choose to model the flow problem using the fine grid. In fact, using 8 Intel XeonE5620 2.4Ghz, 12M cache processors, it took about 8s to advance the solution one time-step.

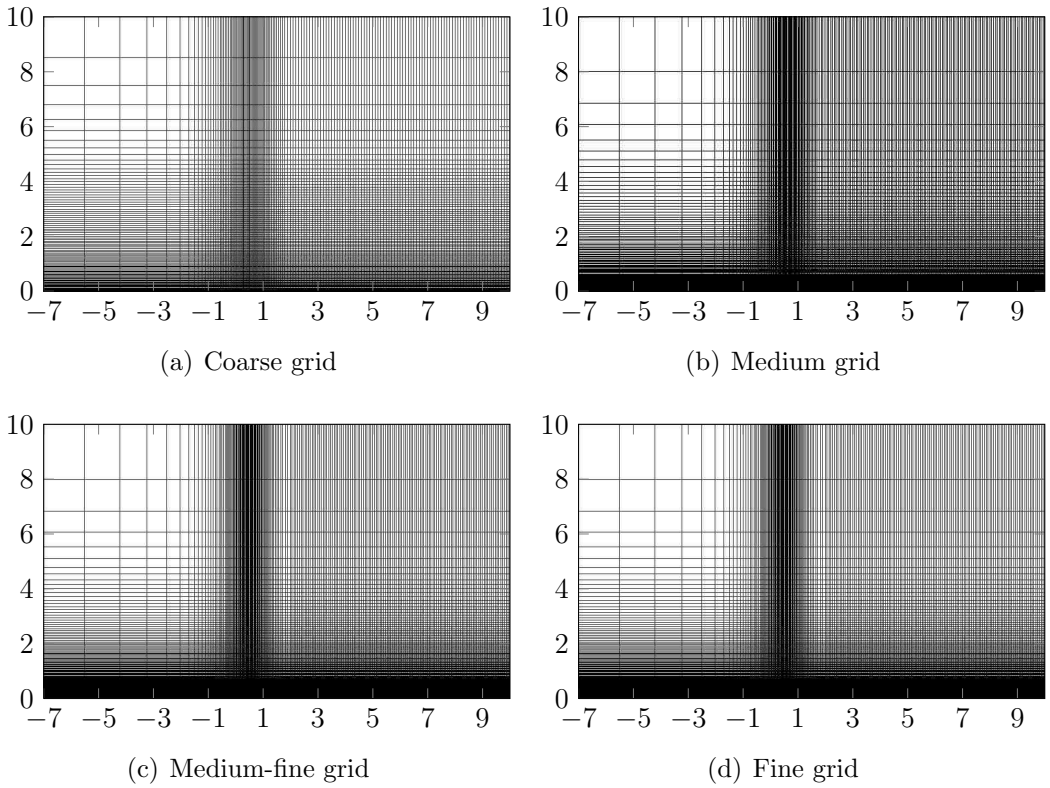

(a) Coarse grid

(b) Medium grid

(c) Medium-fine grid

(d) Fine grid

Figure 4.5: Grids used for grid-independence study

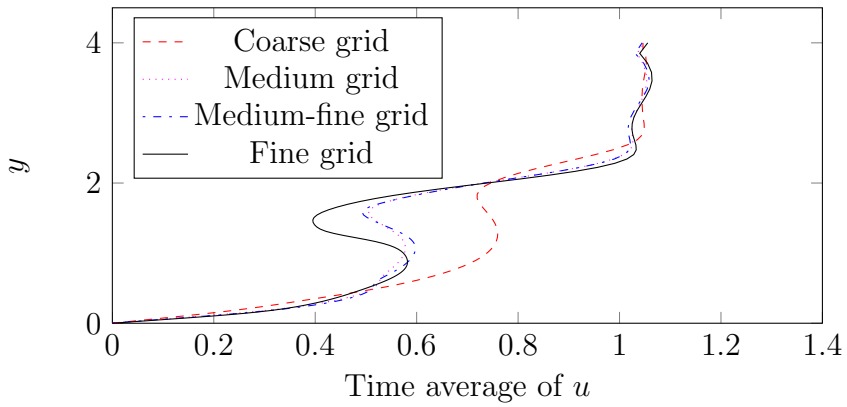

Figure 4.6: Time average of u component of velocity at $x = 4$ at midplane

4.3 Model Reduction for Fluids

Solving the discrete N-S equation provides us with valuable data, but does not give us too much insight into the dynamics of the system. It was this fact, as well as investigations

for a proper statistical framework in which to study turbulent flows, that motivated the search for mathematical techniques that would aid in the analysis of the dynamics of fluid flows. The proper orthogonal decomposition (POD) coupled with the Galerkin projection turned out to be a very useful model reduction tool. POD is also known as Karhunen-Loève expansion, principal component analysis, and total least squares estimation; for a detailed treatment of the Galerkin projection using POD see [HLB96, Kir00, Sir87] and the references therein. The key idea, as expressed in these references, in the model reduction framework for fluids is to adopt a dynamic systems approach similar to the Eulerian viewpoint of fluid dynamics. The state of the fluid at a given time is specified everywhere in the spatial domain of interest by a single point in a suitable phase space. This phase space turns out to be the reduced order model (ROM). As the dynamical system evolves, its solution describes a path or trajectory in this phase space, each point of which corresponds to a new velocity field in the physical domain. An explicit relation between physical space and phase space is provided by a modal decomposition such as

$$\mathbf{u}(\mathbf{x},t) = \sum_{i=1}^{\infty} a_i(t)\boldsymbol{\psi}_i(\mathbf{x}). \tag{4.6}$$

where $a_i(t)$ evolve in a phase space. A nice consequence of the ROM is that it also provides us with a method to construct models suitable for feedback control. It is important to point out that most of the results of this section are either known or easily derived from the known work. ROMs of various forms exist in the research literature.

4.3.1 Computing the POD Basis

In this subsection we closely follow [Fah00]. We assume that the flow field solution, $\mathbf{u}(\mathbf{x},t)$, belongs to the L^2 Hilbert space of square integrable functions, i.e.,

$$(\mathbf{u},\mathbf{u}) := \int_{\Omega\cup\Gamma} \mathbf{u}(\mathbf{x},t)\cdot\mathbf{u}(\mathbf{x},t)d\mathbf{x} < \infty. \tag{4.7}$$

We associate with the inner product $(\cdot,\cdot)$ the norm $\|\mathbf{u}\| = \sqrt{(\mathbf{u},\mathbf{u})}$; notice that the inner product is a function of t. Therefore we may express any flow field solution as a linear combination of basis functions

$$\mathbf{u}(\mathbf{x},t) = \sum_{i=1}^{\infty} a_i(t)\boldsymbol{\psi}_i(\mathbf{x}). \tag{4.8}$$

If, in addition $\boldsymbol{\psi}_i$ satisfy $(\boldsymbol{\psi}_i,\boldsymbol{\psi}_j) = \delta_{ij}$, where δ_{ij} is the Kronecker delta, then $a_i(t)$ may be determined by $a_i(t) = (\mathbf{u},\boldsymbol{\phi}_i)$. This means that we may write (4.8) as

$$\mathbf{u}(\mathbf{x},t) = \sum_{i=1}^{\infty} (\mathbf{u},\boldsymbol{\psi}_i)\,\boldsymbol{\psi}_i(\mathbf{x}) \tag{4.9}$$

At this point it is not clear how to choose the basis functions $\{\boldsymbol{\psi}_i\}_{i=1}^{\infty}$ although intuitively we would like them to be optimal in some sense. We delay the discussion on how to compute these basis functions to address an important issue that frequently arises in fluid flow problems.

Usually a transformation of the (x,y,z) coordinates to a new coordinate system given by (ξ_1,ξ_2,ξ_3) simplifies solving the N-S equations numerically. In our case, we must solve the N-S equation on a nonuniform (and potentially non-orthogonal depending on the geometry of the problem) grid given by (x,y,z), but instead of solving it on this grid, we transform (x,y,z) to (ξ_1,ξ_2,ξ_3), which is the coordinate system of a uniform/orthogonal grid. Such a transformation is represented by the multivariate function $c:\mathbb{R}^3\to\mathbb{R}^3$ and is written as

$$\begin{aligned}\xi_1 &= c_1(x,y,z)\\ \xi_2 &= c_2(x,y,z)\\ \xi_3 &= c_3(x,y,z).\end{aligned}$$

By applying the change of variables from multivariable calculus, it can be shown that

$$\int_{\Omega_\xi \cup \Gamma_\xi} \mathbf{u} \cdot \mathbf{u} d\boldsymbol{\xi} = \int_{\Omega \cup \Gamma} \mathbf{u} \cdot \mathbf{u} |J| d\mathbf{x}$$

where $|J| = \det(J_c)$ and $J_c = \begin{bmatrix} \frac{\partial c_1}{\partial x} & \frac{\partial c_1}{\partial y} & \frac{\partial c_1}{\partial z} \\ \frac{\partial c_2}{\partial x} & \frac{\partial c_2}{\partial y} & \frac{\partial c_2}{\partial z} \\ \frac{\partial c_3}{\partial x} & \frac{\partial c_3}{\partial y} & \frac{\partial c_3}{\partial z} \end{bmatrix}$ is the Jacobian matrix of the transformation c. By defining the J weighted inner product

$$(\mathbf{u}, \mathbf{u})_J := \int_{\Omega_\xi \cup \Gamma_\xi} \mathbf{u}(\boldsymbol{\xi}, t) \cdot \mathbf{u}(\boldsymbol{\xi}, t) |J|^{-1} d\boldsymbol{\xi}$$

we can see that $(\mathbf{u}, \mathbf{u}) = (\mathbf{u}, \mathbf{u})_J$ which is useful for computing these values numerically.

We now return to the question of computing the basis functions. We are looking for $\{\boldsymbol{\psi}_i\}_{i=1}^{\infty}$ that solve (4.10)

$$\min_{\{\boldsymbol{\psi}_k\}_{k=1}^{\infty}} \left\| \mathbf{u}(\mathbf{x}, t) - \sum_{j=1}^{\infty} (\mathbf{u}, \boldsymbol{\psi}_j) \boldsymbol{\psi}_j(\mathbf{x}) \right\|^2 \quad s.t. \quad (\boldsymbol{\psi}_i, \boldsymbol{\psi}_j) = \delta_{ij}. \tag{4.10}$$

Given our discussion on the coordinate transformation, we state an equivalent problem to (4.10) that is given by (4.11):

$$\min_{\{\boldsymbol{\psi}_k\}_{k=1}^{\infty}} \left\| \mathbf{u}(\mathbf{x}, t) - \sum_{j=1}^{\infty} (\mathbf{u}, \boldsymbol{\psi}_j)_J \boldsymbol{\psi}_j(\mathbf{x}) \right\|_J^2 \quad s.t. \quad (\boldsymbol{\psi}_i, \boldsymbol{\psi}_j)_J = \delta_{ij}. \tag{4.11}$$

However, we will only search for a finite number of basis functions, $\{\boldsymbol{\psi}_i\}_{i=1}^{n}$. We start our derivation with a given solution flow field ensemble $\mathcal{U} = \{\mathbf{u}_1, \ldots, \mathbf{u}_N\}$, where $\mathbf{u}_i := \mathbf{u}(\mathbf{x}, t_i)$, $\mathbf{x} \in \Omega \cup \Gamma$.

Definition 11 (POD problem)**.** *Given $\mathcal{U}$, find orthonormal basis functions $\{\boldsymbol{\psi}_i\}_{i=1}^n$ that solve*

$$\min_{\{\boldsymbol{\psi}_k\}_{k=1}^n} \sum_{i=1}^{N} \left\| \mathbf{u}_i - \sum_{j=1}^{n} (\mathbf{u}_i, \boldsymbol{\psi}_j)_J \boldsymbol{\psi}_j(\mathbf{x}) \right\|_J^2 \quad s.t. \quad (\boldsymbol{\psi}_i, \boldsymbol{\psi}_j)_J = \delta_{ij}. \tag{4.12}$$

Definition 12. *A solution $\{\boldsymbol{\phi}_1, \ldots, \boldsymbol{\phi}_n\}$ to (4.12) is a POD basis of order n and*

$$\mathcal{U}^{POD} = \{\boldsymbol{\phi}_1, \ldots, \boldsymbol{\phi}_n\} \tag{4.13}$$

Since the data $\mathcal{U}$ comes from DNS, instead of solving the POD problem, we will solve a discretized POD problem. First, define the finite dimensional state vector corresponding to the velocity field obtained by DNS

$$x^{(i)} := \begin{bmatrix} u^{(M)}(t_i) \\ v^{(M)}(t_i) \\ w^{(M)}(t_i) \end{bmatrix} \in \mathbb{R}^M \tag{4.14}$$

where M corresponds to the number of degrees of freedom in the the spatial variables. The notation $u^{(M)}(t_i)$ should be read as the finite dimensional column vector corresponding to u component of velocity obtained from a DNS simulation with M degrees of freedom (discrete spatial points) at i^{th} time. From now on we think of the solution flow field ensemble, $\mathcal{U}$, as the set of vectors $x^{(i)} \in \mathbb{R}^M,\ i = 1, \ldots, N$.

Definition 13. *Let the solution flow field ensemble $\mathcal{U} = \left\{x^{(i)}\right\}_{i=1}^N$ be given. We denote*

$$X = \begin{bmatrix} x^{(1)} & x^{(2)} & \cdots & x^{(N)} \end{bmatrix} \in \mathbb{R}^{M \times N} \tag{4.15}$$

as the snapshot data matrix of $\mathcal{U}$.

In order to state the solution of the discretized version of (4.12), we specify the discretized version of the inner product $(\mathbf{u}, \mathbf{u})_J$ as $\left\langle x^{(i)}, x^{(j)} \right\rangle_J = {x^{(j)}}^T J x^{(i)}$ and the norm $\left\| x^{(i)} \right\|_J = \sqrt{\left\langle \sqrt{J}x^{(i)}, \sqrt{J}x^{(i)} \right\rangle}$. The matrix J is $M \times M$ positive-definite diagonal (hence symmetric), where the entries on the diagonal represent the "volume" of each grid-cell in the (x, y, z) coordinate system.

Define $\phi^{(i)} \in \mathbb{R}^M$ and $x^{(i)} \in \mathbb{R}^M$ as the discretized version of $\boldsymbol{\phi}_i$ and $\mathbf{u}_i$ respectively. The discretized version of (4.12) is given by

$$\min_{\left\{\phi^{(i)}\right\}} \sum_{i=1}^{N} \left\| x^{(i)} - \sum_{j=1}^{n} \left\langle x^{(i)}, \phi^{(j)} \right\rangle_J \phi^{(j)} \right\|_J^2 \quad s.t. \quad \left\langle \phi^{(i)}, \phi^{(j)} \right\rangle_J = \delta_{ij}. \tag{4.16}$$

Using the fact that $\left\langle x^{(i)}, x^{(j)} \right\rangle_J = \left\langle x^{(i)}, Jx^{(j)} \right\rangle$, we rewrite (4.16) as

$$\min_{\left\{\phi^{(i)}\right\}} \sum_{i=1}^{N} \left\| \sqrt{J}x^{(i)} - \sqrt{J} \sum_{j=1}^{n} \left\langle x^{(i)}, J\phi^{(j)} \right\rangle \phi^{(j)} \right\|^2 \quad s.t. \quad \left\langle \phi^{(i)}, J\phi^{(j)} \right\rangle = \delta_{ij} \tag{4.17}$$

in order to formulate it in a matrix approximation context as in the following lemma.

Lemma 4.3.1. *Let $\mathcal{U}$ with snapshot data matrix X be given. Then (4.17) is equivalent to solving*

$$\min \left\| \sqrt{J}X - \sqrt{J}\Phi\Phi^T JX \right\|_F^2 \quad s.t. \quad \Phi^T J \Phi = I_n \tag{4.18}$$

where $\Phi := \begin{bmatrix} \phi^{(1)} & \phi^{(2)} & \dots & \phi^{(n)} \end{bmatrix}$ and $\|\cdot\|_F$ is the Frobenius norm.

Proof. First, note that

$$\begin{aligned} \Phi\Phi^T JX_{:,i} &= \left({\phi^{(1)}}^T J x^{(1)} \phi^{(1)} + {\phi^{(2)}}^T J x^{(1)} \phi^{(2)} + \cdots + {\phi^{(n)}}^T J x^{(1)} \phi^{(n)} \right) \\ &= \sum_{j=1}^{n} \left\langle x^{(i)}, J\phi^{(j)} \right\rangle \phi^{(j)} \end{aligned} \tag{4.19}$$

then we use the relation $\|X\|_F^2 = \sum_{i=1}^{N} \|X_{:,i}\|^2$ to show that the problems are equivalent. The notation $X_{:,i}$ denotes the i^{th} column of X. □

Problem (4.18) is a special case of the minimum rank approximation problem in linear algebra

$$\min_{Y \in \Re^{M \times N}} \|X - Y\|_F^2 \quad s.t. \;\; rank(Y) = n \tag{4.20}$$

which is solved by means of the singular value decomposition (SVD).

Theorem 4.3.2 (SVD for real matrices)**.** *For every real $M \times N$ matrix A, there exist orthogonal matrices $U \in \mathbb{R}^{M \times M}$ and $V \in \mathbb{R}^{N \times N}$ ($U^T U = I_M = UU^T$ and $V^T V = I_N = VV^T$) such that*

$$A = USV^T$$

where $S = \begin{bmatrix} S_1 & 0 \\ 0 & 0 \end{bmatrix} \in \mathbb{R}^{M \times N}$, $r = rank(A)$, $S_1 = diag(\sigma_i) \in \mathbb{R}^{r \times r}$, $i = 1, 2, \ldots, r$ *and* $\sigma_1 \geq \sigma_2 \geq \ldots \geq \sigma_r > 0$.

We call σ_i the ith singular value of A. The vectors u_i and v_j are the ith column of U and the jth column of V respectively and are referred to as the ith left singular vector and the jth right singular vector respectively. They are also often referred to as Schmidt pair. An important property of the SVD of a matrix is that it provides a dyadic decomposition for it,

$$A = \sum_{i=1}^{r} \sigma_i u_i v_i^T.$$

This decomposition provides a canonical description of a matrix (also called *reduced SVD*) as a sum of r rank-one matrices of decreasing importance as measured by the singular values. The dyadic decomposition is essential to the computation of the POD basis as we will see next.

Theorem 4.3.3. *Let $A = USV^T \in \mathbb{R}^{M\times N}$ and $k < r = rank(A)$, then*

$$\min_{rank(B)\leq k} \|A - B\|_F = \|A - A_k\|_F = \sqrt{\sum_{j=k+1}^{r} \sigma_j^2} \tag{4.21}$$

where $A_k = \sum_{i=1}^{k} \sigma_i u_i v_i^T$ is the dyadic decomposition of A.

Theorem 4.3.3 shows that the solution to (4.18) is given by a *truncated singular value decomposition* (TSVD). The next result provides the method for constructing the POD basis functions.

Theorem 4.3.4 (Computation of the POD basis)**.** *Let $\mathcal{U}$ with snapshot data matrix X be given. Compute SVD of $\sqrt{J}X$, $\sqrt{J}X = USV^T$. Then the POD basis Φ is given by*

$$\Phi = J^{-1/2}\begin{bmatrix} u_1 & u_2 & \cdots & u_n \end{bmatrix}. \tag{4.22}$$

Furthermore there holds the tail equality

$$\min_{\Phi} \left\| \sqrt{J}X - \sqrt{J}\Phi\Phi^T JX \right\|_F^2 = \sum_{j=n+1}^{N} \sigma_j^2 \tag{4.23}$$

where σ_j are the singular values of $\sqrt{J}X$.

Proof. By Theorem 4.3.3 we know that the solution to (4.18) is given by a TSVD of $\sqrt{J}X$ of order n, i.e., $\sqrt{J}X = U_n S_n V_n^T$. Now we just need to solve for Φ in

$$\sqrt{J}\Phi\Phi^T JX = \sqrt{J}\Phi(\sqrt{J}\Phi)^T\sqrt{J}X = U_n S_n V_n^T \tag{4.24}$$

which is the second term of (4.18) . Since $\sqrt{J}X = U_n S_n V_n^T$

$$\sqrt{J}\Phi(\sqrt{J}\Phi)^T = U_n U_n^T = I, \tag{4.25}$$

and $\Phi = J^{-1/2}\begin{bmatrix} u_1 & \cdots & u_n \end{bmatrix}$ satisfies (4.24). $\square$

Remark 4. *Depending on the spatial discretization and number of snapshots that have to be collected, the size of $\sqrt{J}X$ may become too large for the computation of its SVD. In this case we have to compute $\sqrt{J}X = USV^T$ indirectly, by the so called method of snapshots [Sir87]. The limiting dimension for the computation is N, i.e., as long as we can compute the SVD of an $N \times N$ matrix, the computation of the SVD of $\sqrt{J}X$ is possible. In addition, we suggest the following procedure to implement the method of snapshots: By taking "blocks" of data at a time, it is possible to compute SVDs of data sets that may not completely fit in computer memory.*

1. *Partition $\sqrt{J}X$ into b blocks*

$$\sqrt{J}X = \begin{bmatrix} \sqrt{J}X_1 & \sqrt{J}X_2 & \cdots & \sqrt{J}X_{b-1} & \sqrt{J}X_b \end{bmatrix}$$

   where the number of columns of each $\sqrt{J}X_i$ block should be chosen such that each $\sqrt{J}X_i$ fits in the computer memory.

2. *Compute the covariance matrix*

$$C = X^T J X = \begin{bmatrix} X_1^T J X_1 & \cdots & X_1^T J X_b \\ \vdots & \ddots & \vdots \\ X_b^T J X_1 & \cdots & X_b^T J X_b \end{bmatrix} \in \Re^{N \times N}$$

   one block at a time.

3. *Compute TSVD of C, i.e., $C = X^T J X = (USV^T)^T (USV^T) = VS^2V^T$. Note that $V \in \Re^{N \times n}$ and $S \in \Re^{n \times n}$.*

4. Compute Φ one block at a time.

$$\Phi = J^{-1/2} X V S^{-1} = J^{-1/2} \begin{bmatrix} X_1 & \cdots & X_b \end{bmatrix} \begin{bmatrix} V_1 \\ \vdots \\ V_b \end{bmatrix} S^{-1} = J^{-1/2} \left(X_1 V_1 + \cdots + X_b V_b \right) S^{-1}$$

A similar discussion applies to the construction of temperature POD modes. In fact, the POD modes for temperature may be viewed as a $d = 1$ 'flow field' ensemble.

4.4 Computing the Reduced Order Model

Computing the ROM will consist in performing a Galerkin projection on the N-S equation to derive a set of ODEs. Before computing the ROM though, we need to take care of how to include the boundary control terms. To achieve this we propose a modal expansion of the form

$$\mathbf{u}(\mathbf{x}, t) = \sum_{i=1}^{n} a_i(t) \boldsymbol{\phi}_i(\mathbf{x}) + \tilde{a}_0(t) \tilde{\mathbf{h}}_0(\mathbf{x}) + \sum_{i=1}^{m} \tilde{c}_i(t) \tilde{\mathbf{h}}_i(\mathbf{x}) \tag{4.26}$$

where $\boldsymbol{\phi}_i, i = 1, \ldots, n$ are homogeneous on the boundary POD basis functions and $\tilde{\mathbf{h}}_0$ and $\tilde{\mathbf{h}}_i, i = 1, \ldots, m$ are divergence-free extensions of the boundary conditions in (4.5) (i.e., they match boundary conditions on Γ and are divergence free in Ω). Since there is no danger of confusion, we refer to the boundary conditions and their divergence free extensions by the same symbol. While in the literature there are several methods on how to compute these extra modes, for example [NTM04a], [KSOE08], [NTM04b], [BGL06], and [Rav07], we take a slightly different route.

First, we call $\mathbf{u}_{unact}(\mathbf{x}, t)$ an *unactuated solution* when it is obtained with the boundary conditions $\tilde{c}_i(t) = 0 \; \forall \; i$ and $\tilde{a}_0(t) = a_0$. We call $\mathbf{u}_{act_i}(\mathbf{x}, t)$ an i^{th} *actuated solution* when it is obtained with the boundary conditions $\tilde{c}_i(t) = c_i$, $\tilde{c}_j(t) = 0 \; \forall \; j \neq i$ and $\tilde{a}_0(t) = a_0$. The term $\tilde{\mathbf{h}}_0(\mathbf{x})$ is taken as the time average of an unactuated solution and $\tilde{\mathbf{h}}_i(\mathbf{x})$ is taken as the time average of $\mathbf{u}_{act_i}(\mathbf{x}, t) - \mathbf{u}_{unact}(\mathbf{x}, t)$.

Second, while (4.26) is a useful expansion, we would prefer divergence-free extensions of the boundary that are orthonormal to the POD basis. We denote this orthonormal expansion as

$$\mathbf{u}(\mathbf{x},t) = \sum_{i=1}^{n} a_i(t)\boldsymbol{\phi}_i(\mathbf{x}) + a_0(t)\mathbf{h}_0(\mathbf{x}) + \sum_{i=1}^{m} c_i(t)\mathbf{h}_i(\mathbf{x}) \tag{4.27}$$

where $\mathbf{h}_0(\mathbf{x})$ is the *inflow boundary mode* and $\mathbf{h}_i(\mathbf{x})$ is the i^{th} *control mode*. We use the following procedure to compute the POD modes, inflow, and i^{th} control mode:

1. Let X denote a snapshot matrix corresponding to

$$\mathbf{u}(\mathbf{x},t) - \tilde{a}_0(t)\tilde{\mathbf{h}}_0(\mathbf{x}) - \sum_{i=1}^{m} \tilde{c}_i(t)\tilde{\mathbf{h}}_i(\mathbf{x}). \tag{4.28}$$

   Note that X is homogeneous on the boundary.

2. Obtain the POD basis functions corresponding to X by the method in Section 4.3.1, i.e., SVD factorization of X. The POD basis will be zero on the boundary by construction.

3. Compute $\mathbf{h}_0 = \frac{\tilde{\mathbf{h}}_0 - \sum_{i=1}^{n}\left(\tilde{\mathbf{h}}_0, \boldsymbol{\phi}_i\right)\boldsymbol{\phi}_i}{\|\tilde{\mathbf{h}}_0 - \sum_{j=1}^{n}\left(\tilde{\mathbf{h}}_0, \boldsymbol{\phi}_j\right)\boldsymbol{\phi}_j\|}$.

   Compute $\mathbf{h}_i = \frac{\tilde{\mathbf{h}}_i - \sum_{j=1}^{n}\left(\tilde{\mathbf{h}}_i, \boldsymbol{\phi}_j\right)\boldsymbol{\phi}_j - \sum_{j=1}^{m}\left(\tilde{\mathbf{h}}_i, \mathbf{h}_{j-1}\right)\mathbf{h}_{j-1}}{\|\tilde{\mathbf{h}}_i - \sum_{j=1}^{n}\left(\tilde{\mathbf{h}}_i, \boldsymbol{\phi}_j\right)\boldsymbol{\phi}_j - \sum_{j=1}^{m}\left(\tilde{\mathbf{h}}_i, \mathbf{h}_{j-1}\right)\mathbf{h}_{j-1}\|}$, $i = 1, \ldots, m$

Note that the inflow and control modes are orthogonal to the POD basis by the construction in step 3. A standard Galerkin projection with POD basis functions, inflow, and control modes can be carried out to derive the ROM. This is done by projecting the N-S equation to the i^{th} POD basis function using the inner product that we defined earlier

$$\int_{\Omega} \frac{\partial \mathbf{u}}{\partial t} \cdot \boldsymbol{\phi}_i d\mathbf{x} + \int_{\Omega} \mathbf{u} \cdot \nabla \mathbf{u} \cdot \boldsymbol{\phi}_i d\mathbf{x} = -\int_{\Omega} \nabla P \cdot \boldsymbol{\phi}_i d\mathbf{x} + \int_{\Omega} \frac{1}{Re} \nabla^2 \mathbf{u} \cdot \boldsymbol{\phi}_i d\mathbf{x}. \tag{4.29}$$

Using integration by parts on the term $\int_\Omega \frac{1}{Re}\nabla^2\mathbf{u}\cdot\boldsymbol{\phi}_i d\mathbf{x}$, i.e.,

$$\int_\Omega \frac{1}{Re}\nabla^2\mathbf{u}\cdot\boldsymbol{\phi}_i d\mathbf{x} = \frac{1}{Re}\left(\int_\Gamma \nabla\mathbf{u}\cdot\boldsymbol{\phi}_i d\mathbf{x} - \int_\Omega \nabla\mathbf{u}\cdot\nabla\boldsymbol{\phi}_i d\mathbf{x}\right)$$

and noting that the POD basis functions are divergence free and homogeneous on the boundary, i.e.,

$$\int_\Omega \nabla P\cdot\boldsymbol{\phi}_i d\mathbf{x} = -\int_\Omega P\nabla\cdot\boldsymbol{\phi}_i d\mathbf{x} + \int_\Gamma P\boldsymbol{\phi}_i\cdot\vec{n} d\mathbf{x} = 0$$

we obtain

$$\int_\Omega \frac{\partial\mathbf{u}}{\partial t}\cdot\boldsymbol{\phi}_i d\mathbf{x} + \int_\Omega \mathbf{u}\cdot\nabla\mathbf{u}\cdot\boldsymbol{\phi}_i d\mathbf{x} + \frac{1}{Re}\left(\int_\Omega \nabla\mathbf{u}\cdot\nabla\boldsymbol{\phi}_i d\mathbf{x} - \int_\Gamma \nabla\mathbf{u}\cdot\boldsymbol{\phi}_i d\mathbf{x}\right) = 0. \tag{4.30}$$

Since the POD basis functions are homogeneous on the boundary, $\int_\Gamma \nabla\mathbf{u}\cdot\boldsymbol{\phi}_i d\mathbf{x} = 0$. Finally, we substitute $\mathbf{u}$ with its truncated modal decomposition

$$\mathbf{u}_{ROM}(\mathbf{x},t) = \sum_{j=1}^{n} a_j(t)\boldsymbol{\phi}_j(\mathbf{x}) + a_0(t)\mathbf{h}_0(\mathbf{x}) + \sum_{i=1}^{m} c_i(t)\mathbf{h}_i(\mathbf{x}) \tag{4.31}$$

and insert it into (4.30) to obtain the following terms:

Time derivative

$$\begin{aligned}\int_\Omega \frac{\partial\mathbf{u}_{ROM}}{\partial t}\cdot\boldsymbol{\phi}_i d\mathbf{x} &= \sum_{j=1}^{n}\dot{a}_j(t)\left(\boldsymbol{\phi}_j,\boldsymbol{\phi}_i\right) + \dot{a}_0(t)\left(\mathbf{h}_0,\boldsymbol{\phi}_i\right) + \sum_{i=1}^{m}\dot{c}_i(t)\left(\mathbf{h}_i,\boldsymbol{\phi}_i\right)\\ &= \dot{a}_i(t)\end{aligned}$$

Convection

$$\begin{aligned}
\int_\Omega \mathbf{u}_{ROM}\cdot\nabla\mathbf{u}_{ROM}\cdot\boldsymbol{\phi}_i d\mathbf{x} &= \left(\sum_{j=1}^{n} a_j(t)\boldsymbol{\phi}_j\cdot\nabla\sum_{k=1}^{n} a_k(t)\boldsymbol{\phi}_k,\boldsymbol{\phi}_i\right)+\left(\sum_{j=1}^{n} a_j(t)\boldsymbol{\phi}_j\cdot\nabla a_0(t)\mathbf{h}_0,\boldsymbol{\phi}_i\right)\\
&+\left(\sum_{j=1}^{n} a_j(t)\boldsymbol{\phi}_j\cdot\nabla\sum_{k=1}^{m} c_k(t)\mathbf{h}_k,\boldsymbol{\phi}_i\right)+\left(a_0(t)\mathbf{h}_0\cdot\nabla\sum_{j=1}^{n} a_j(t)\boldsymbol{\phi}_j,\boldsymbol{\phi}_i\right)\\
&+\left(a_0(t)\mathbf{h}_0\cdot\nabla a_0(t)\mathbf{h}_0,\boldsymbol{\phi}_i\right)+\left(a_0(t)\mathbf{h}_0\cdot\nabla\sum_{j=1}^{m} c_j(t)\mathbf{h}_j,\boldsymbol{\phi}_i\right)\\
&+\left(\sum_{j=1}^{m} c_j(t)\mathbf{h}_j\cdot\nabla\sum_{k=1}^{n} a_k(t)\boldsymbol{\phi}_k,\boldsymbol{\phi}_i\right)+\left(\sum_{j=1}^{m} c_j(t)\mathbf{h}_j\cdot\nabla a_0(t)\mathbf{h}_0,\boldsymbol{\phi}_i\right)\\
&+\left(\sum_{j=1}^{m} c_j(t)\mathbf{h}_j\cdot\nabla\sum_{k=1}^{m} c_k(t)\mathbf{h}_k,\boldsymbol{\phi}_i\right)\\
&=\sum_{j=1}^{n} a_j(t)\sum_{k=1}^{n} a_k(t)\left(\boldsymbol{\phi}_j\cdot\nabla\boldsymbol{\phi}_k,\boldsymbol{\phi}_i\right)+a_0(t)\sum_{j=1}^{n} a_j(t)\left(\boldsymbol{\phi}_j\cdot\nabla\mathbf{h}_0,\boldsymbol{\phi}_i\right)\\
&+\sum_{j=1}^{n} a_j(t)\sum_{k=1}^{m} c_k(t)\left(\boldsymbol{\phi}_j\cdot\nabla\mathbf{h}_k,\boldsymbol{\phi}_i\right)+a_0(t)\sum_{j=1}^{n} a_j(t)\left(\mathbf{h}_0\cdot\nabla\boldsymbol{\phi}_j,\boldsymbol{\phi}_i\right)\\
&+a_0^2(t)\left(\mathbf{h}_0\cdot\nabla\mathbf{h}_0,\boldsymbol{\phi}_i\right)+a_0(t)\sum_{j=1}^{m} c_j(t)\left(\mathbf{h}_0\cdot\nabla\mathbf{h}_j,\boldsymbol{\phi}_i\right)\\
&+\sum_{j=1}^{m} c_j(t)\sum_{k=1}^{n} a_k(t)\left(\mathbf{h}_j\cdot\nabla\boldsymbol{\phi}_k,\boldsymbol{\phi}_i\right)+a_0(t)\sum_{j=1}^{m} c_j(t)\left(\mathbf{h}_j\cdot\nabla\mathbf{h}_0,\boldsymbol{\phi}_i\right)\\
&+\sum_{j=1}^{m} c_j(t)\sum_{k=1}^{m} c_k(t)\left(\mathbf{h}_j\cdot\nabla\mathbf{h}_k,\boldsymbol{\phi}_i\right)
\end{aligned}$$

Diffusion

$$\begin{aligned}
\int_\Omega \nabla\mathbf{u}_{ROM}\cdot\nabla\boldsymbol{\phi}_i d\mathbf{x} &= \left(\sum_{j=1}^{n} a_j(t)\nabla\boldsymbol{\phi}_j,\nabla\boldsymbol{\phi}_i\right)+\left(a_0(t)\nabla\mathbf{h}_0,\nabla\boldsymbol{\phi}_i\right)+\left(\sum_{j=1}^{m} c_j(t)\nabla\mathbf{h}_j,\nabla\boldsymbol{\phi}_i\right)\\
&=\sum_{j=1}^{n} a_j(t)\left(\nabla\boldsymbol{\phi}_j,\nabla\boldsymbol{\phi}_i\right)+a_0(t)\left(\nabla\mathbf{h}_0,\nabla\boldsymbol{\phi}_i\right)+\sum_{j=1}^{m} c_j(t)\left(\nabla\mathbf{h}_j,\nabla\boldsymbol{\phi}_i\right)
\end{aligned}$$

Finally we obtain the nonlinear state-space model:

$$\dot{\bar{\chi}} = \bar{A}\bar{\chi} + \bar{B}\bar{u} + \begin{bmatrix} \bar{\chi}^T \bar{N}_1 \bar{\chi} \\ \vdots \\ \bar{\chi}^T \bar{N}_n \bar{\chi} \end{bmatrix} + \begin{bmatrix} \bar{\chi}^T \bar{M}_1 \bar{u} \\ \vdots \\ \bar{\chi}^T \bar{M}_n \bar{u} \end{bmatrix} + \begin{bmatrix} \bar{u}^T \bar{K}_1 \bar{u} \\ \vdots \\ \bar{u}^T \bar{K}_n \bar{u} \end{bmatrix} + a_0 \bar{D}_1 \bar{\chi} + a_0 \bar{D}_2 \bar{u} + \bar{D}_3 a_0 + \bar{D}_4 a_0^2 \tag{4.32}$$

where

$$\begin{aligned}
\bar{A}_{ij} &= -\frac{1}{Re}\left(\nabla \boldsymbol{\phi}_j, \nabla \boldsymbol{\phi}_i\right), \bar{B}_{ij} = -\frac{1}{Re}\left(\nabla \mathbf{h}_j, \nabla \boldsymbol{\phi}_i\right), \\
\bar{N}_{i_{jk}} &= -\left(\boldsymbol{\phi}_j \cdot \nabla \boldsymbol{\phi}_k, \boldsymbol{\phi}_i\right), \bar{M}_{i_{jk}} = -\left(\boldsymbol{\phi}_j \cdot \nabla \mathbf{h}_k, \boldsymbol{\phi}_i\right) - \left(\mathbf{h}_k \cdot \nabla \boldsymbol{\phi}_j, \boldsymbol{\phi}_i\right), \\
\bar{K}_{i_{jk}} &= -\left(\mathbf{h}_j \cdot \nabla \mathbf{h}_k, \boldsymbol{\phi}_i\right), \bar{D}_{1_{ij}} = -\left(\mathbf{h}_0 \cdot \nabla \boldsymbol{\phi}_j, \boldsymbol{\phi}_i\right) - \left(\boldsymbol{\phi}_j \cdot \nabla \mathbf{h}_0, \boldsymbol{\phi}_i\right), \\
\bar{D}_{2_{ij}} &= -\left(\mathbf{h}_0 \cdot \nabla \mathbf{h}_j, \boldsymbol{\phi}_i\right) - \left(\mathbf{h}_j \cdot \nabla \mathbf{h}_0, \boldsymbol{\phi}_i\right), \tilde{D}_{3_i} = -\frac{1}{Re}\left(\nabla \mathbf{h}_0, \nabla \boldsymbol{\phi}_i\right), \\
\tilde{D}_{4_i} &= -\left(\mathbf{h}_0 \cdot \nabla \mathbf{h}_0, \boldsymbol{\phi}_i\right),
\end{aligned}$$

It is clear that $\bar{\chi}(t) \in \mathbb{R}^n$ is the state vector consisting of $\{a_i(t)\}_{i=1}^n$ as its elements, and $\bar{u}(t) \in \mathbb{R}^m$ is the input vector consisting of $\{c_i(t)\}_{i=1}^m$ as its elements. Recall that the boundary and control modes are orthogonal to the POD basis, thus canceling the corresponding terms in $\int_\Omega \frac{\partial \mathbf{u}_{ROM}}{\partial t} \cdot \boldsymbol{\phi}^{(i)} d\mathbf{x}$. For this investigation $a_0(t)$ will always be constant as it corresponds to a time-invariant inflow.

Regarding the output equation, we assume that the output measurements only have access to the velocity field information at a few points, say at p points, in the domain. Therefore for $i = 1, 2, \cdots, p$, using the POD expansion, we have

$$\begin{aligned}
\mathbf{u}(\mathbf{x}_i, t) &= \sum_{j=1}^{n} a_j(t)\boldsymbol{\phi}_j(\mathbf{x}_i) + a_0(t)\mathbf{h}_0(\mathbf{x}_i) + \sum_{j=1}^{m} c_j(t)\mathbf{h}_j(\mathbf{x}_i) \\
&= \begin{bmatrix} \boldsymbol{\phi}_1(\mathbf{x}_i) & \cdots & \boldsymbol{\phi}_n(\mathbf{x}_i) \end{bmatrix} \bar{\chi} + \mathbf{h}_0(\mathbf{x}_i) a_0 + \begin{bmatrix} \mathbf{h}_1(\mathbf{x}_i) & \cdots \mathbf{h}_m(\mathbf{x}_i) \end{bmatrix} \bar{u}
\end{aligned}$$

With

$$C_1 = \begin{bmatrix} \boldsymbol{\phi}_1(\mathbf{x}_1) & \cdots & \boldsymbol{\phi}_n(\mathbf{x}_1) \\ \vdots & \ddots & \vdots \\ \boldsymbol{\phi}_1(\mathbf{x}_p) & \cdots & \boldsymbol{\phi}_n(\mathbf{x}_p) \end{bmatrix}, \; C_2 = \begin{bmatrix} \mathbf{h}_0(\mathbf{x}_1) \\ \vdots \\ \mathbf{h}_0(\mathbf{x}_p) \end{bmatrix}, \text{ and } C_3 = \begin{bmatrix} \mathbf{h}_1(\mathbf{x}_1) & \cdots & \mathbf{h}_m(\mathbf{x}_1) \\ \vdots & \ddots & \vdots \\ \mathbf{h}_1(\mathbf{x}_p) & \cdots & \mathbf{h}_m(\mathbf{x}_p) \end{bmatrix},$$

the output equation then has the form

$$y = C_1\bar{\chi} + C_2 a_0 + C_3\bar{u}.$$

4.4.1 ROM Error Analysis

The relative error difference between the DNS and ROM solution that we focus on is the same one that we consider for the POD problem, i.e.,

$$E_{\mathbf{u}} = \frac{1}{N}\left(\frac{\sum_{i=1}^{N}\int \|\mathbf{u}_{DNS}(t_i) - \mathbf{u}_{ROM}(t_i)\|^2 \, d\mathbf{x}}{\sum_{i=1}^{N}\int \|\mathbf{u}_{DNS}(t_i)\|^2 \, d\mathbf{x}}\right) \tag{4.33}$$

It is important to note that due to the inclusion of the inflow and control modes, the modal expansion in (4.31) is not optimal in the POD sense. To see this, remember that $\{\boldsymbol{\phi}_k\}_{k=1}^n$ solves the problem

$$\min_{\{\boldsymbol{\phi}_k\}_{k=1}^n} \sum_{i=1}^{N} \left\| \left(\mathbf{u}_i - \tilde{a}_0(t)\tilde{\mathbf{h}}_0(\mathbf{x}) - \sum_{i=1}^{m} \tilde{c}_i(t)\tilde{\mathbf{h}}_i(\mathbf{x}) \right) - \sum_{j=1}^{n} a_j(t)\boldsymbol{\phi}_j(\mathbf{x}) \right\|_J^2 \tag{4.34}$$

but not

$$\min_{\{\boldsymbol{\phi}_k\}_{k=1}^n} \sum_{i=1}^{N} \left\| \left(\mathbf{u}_i - a_0(t)\mathbf{h}_0(\mathbf{x}) - \sum_{i=1}^{m} c_i(t)\mathbf{h}_i(\mathbf{x}) \right) - \sum_{j=1}^{n} a_j(t)\boldsymbol{\phi}_j(\mathbf{x}) \right\|_J^2 \tag{4.35}$$

which is the expansion we finally use, i.e., $\mathbf{u}_{ROM}$.

However, as seen from the simulation results presented in this section, the error between the DNS and ROM solution is small enough to proceed with the controller design.

4.5 Fluid Flow System in Open Loop

We now show DNS and ROM simulation results for the system in open loop. The simulation results correspond to $Re = 650$ and $R = 1$ ($\bar{u} = 1, \bar{a}_0 = 1$). The inflow boundary condition is given by the Blasius solution and the jet inflow by

$$v(r) = R\left(1 - r^2\right) e^{-\left(\frac{r}{0.7}\right)^4}$$

where r is the distance from the jet center. This expression is intended to model the parabolic velocity profile of pipe Poiseuille flow and is used in several studies, including [BSSH09] and [MIH12].

After about 7 flow-throughs, snapshots were collected and the POD and control modes were computed using Theorem 4.3.4 and the method outlined in Section 4.4. A total of 180 snapshots with a sampling period of $\Delta t = 0.0665$ were collected to compute the POD basis; this spans about 3.5 shedding cycles. The energy distribution in the POD modes is shown in Figure 4.7. We note that the singular values appear in pairs, a characteristic of flow systems with traveling structures [DKKO91].

Although most of the energy is contained in the first 8 modes as shown in Table 4.4, we investigate POD expansions of 16 and 32 modes. It is important to recall that here we are reporting the % energy captured by the POD modes with respect to the homogeneous on the boundary snapshots. Shortly we will consider the more appropriate error as defined in (4.33).

In Figures 4.8, 4.9, and 4.10 we plot the λ_2-criterion as defined in [JH95] and [CBA05] of the first 16 POD modes and the inflow and control modes. The λ_2-criterion is a measure

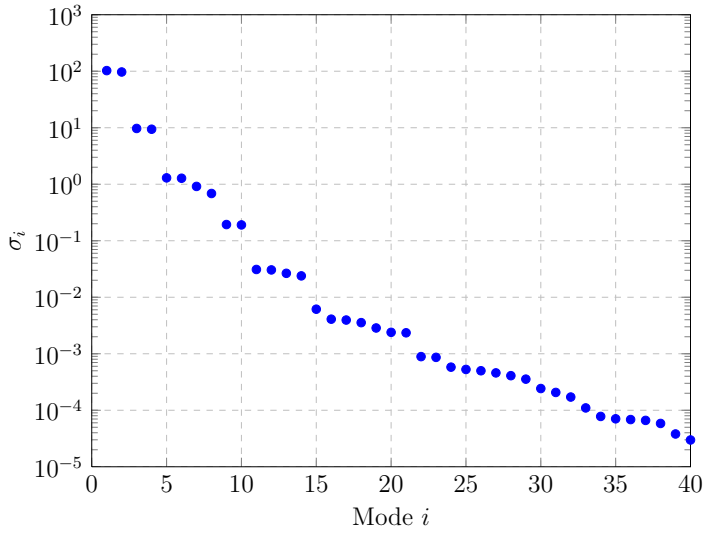

Figure 4.7: Energy in σ_i

Table 4.4: Energy captured by POD expansion

n	**% Energy**
2	61.4
4	80.4
8	92.9
16	98.1
32	99.7
64	100

used to identify vortices and is defined as the second eigenvalue of $S^2 + \Omega^2$ where

$$S = \frac{1}{2}\left(\nabla \mathbf{u} + \nabla \mathbf{u}^T\right)$$
$$Q = \frac{1}{2}\left(\nabla \mathbf{u} - \nabla \mathbf{u}^T\right).$$

From the figures we can see the features of the coherent structures of the jet in cross-flow such as the horseshoe vortex, jet shear-layer vortices, and wake vortices.

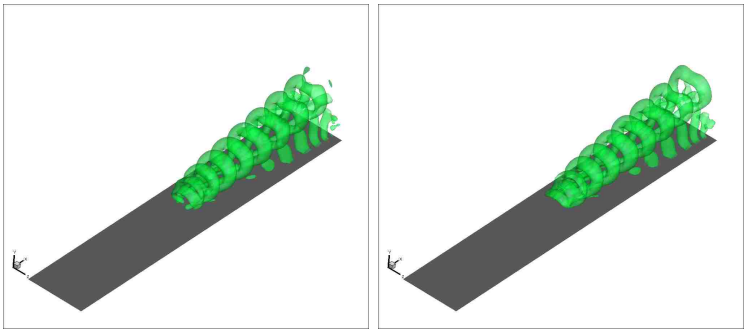

(a) $\boldsymbol{\phi}_1$

(b) $\boldsymbol{\phi}_2$

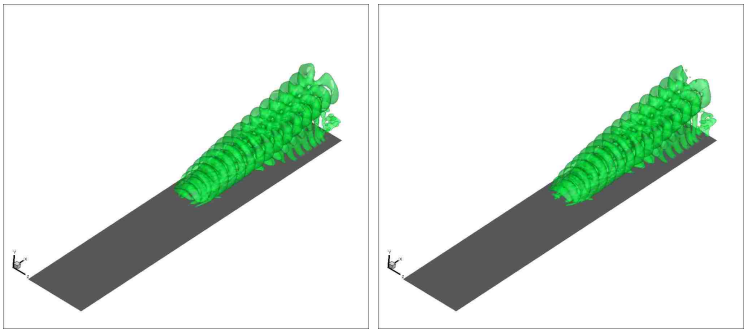

(c) $\boldsymbol{\phi}_3$

(d) $\boldsymbol{\phi}_4$

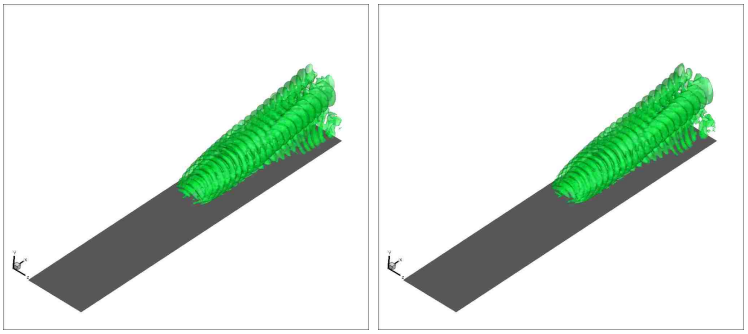

(e) $\boldsymbol{\phi}_5$

(f) $\boldsymbol{\phi}_6$

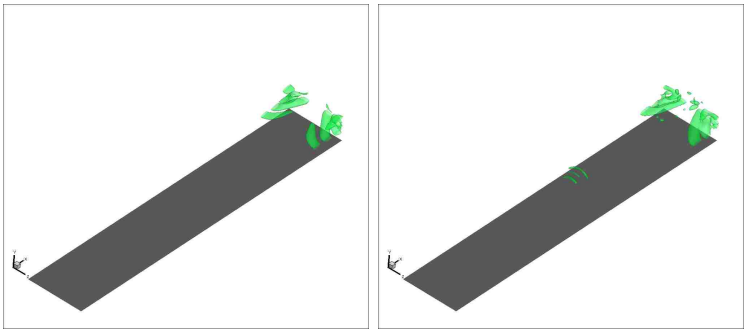

(g) $\boldsymbol{\phi}_7$

(h) $\boldsymbol{\phi}_8$

Figure 4.8: λ_2-criterion of POD modes ($\lambda_2 = -0.06$)

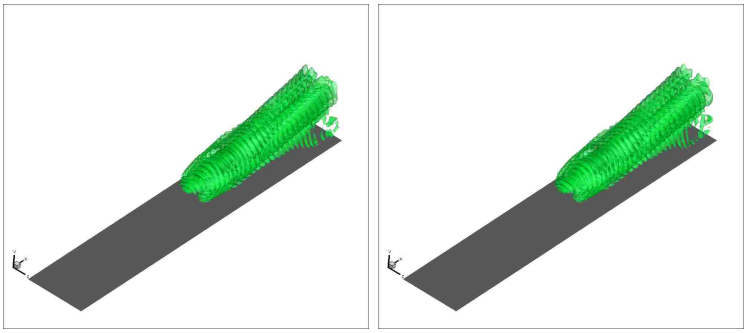

(a) $\boldsymbol{\phi}_9$ (b) $\boldsymbol{\phi}_{10}$

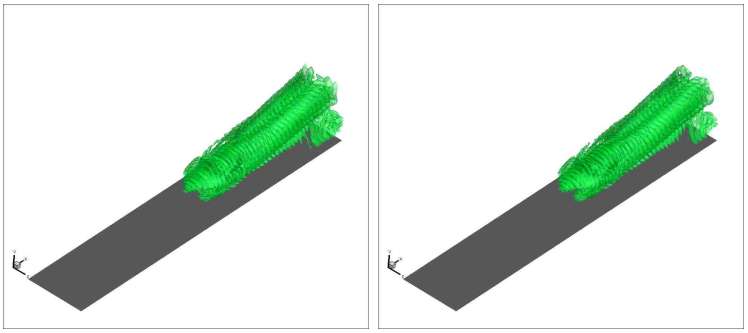

(c) $\boldsymbol{\phi}_{11}$ (d) $\boldsymbol{\phi}_{12}$

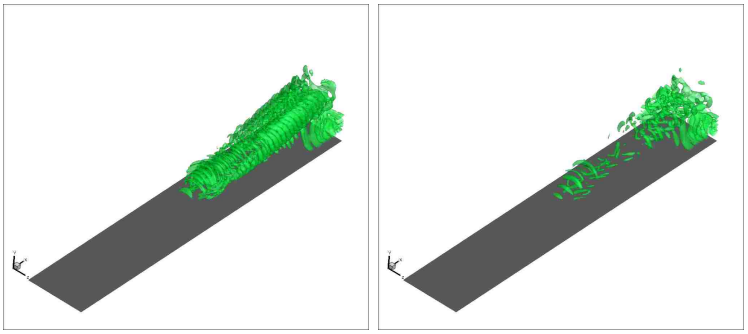

(e) $\boldsymbol{\phi}_{13}$ (f) $\boldsymbol{\phi}_{14}$

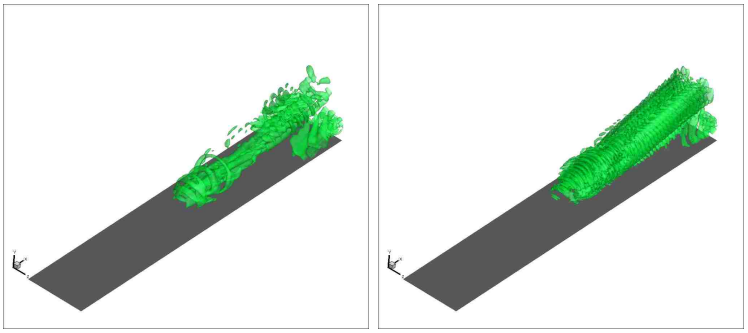

(g) $\boldsymbol{\phi}_{15}$ (h) $\boldsymbol{\phi}_{16}$

Figure 4.9: λ_2-criterion of POD modes ($\lambda_2 = -0.06$)

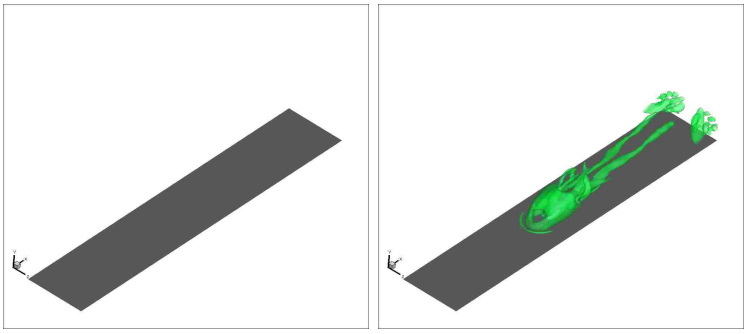

(a) $\mathbf{h}_0$ (b) $\mathbf{h}_1$

Figure 4.10: λ_2-criterion of control modes ($\lambda_2 = -0.06$)

Figures 4.11 and 4.12 show the x and y component of velocity at different time instants. A quick look at the figures confirms that for the considered time period there is a good match between the ROM solution ($n = 32$) and the DNS solution. However, high frequency features start to appear around $t = 3$ and become more pronounced as time advances. As expected, the same behavior is noted for the $n = 16$ ROM.

It is important to note that the fidelity of the ROM solution tends to decay as time advances. This becomes evident when the time history of $\bar{\chi}(t)$, or POD coefficients are visualized. Figures 4.13 and 4.14 show the time history of $\bar{\chi}(t)$ as well as the projection of the DNS data to the POD coefficients $\{a_i(t)\}_{i=1}^{32}$. First, we notice that the ROM and DNS solutions match well at the beginning, and the time at which the DNS and ROM solutions start to diverge depends on the mode number. For example, the 7^{th} mode matches well up until $t = 5$, while the 1^{st} mode starts to diverge around $t = 1$. The figures also show that the amplitude of the higher modes grows in the ROM solution, while they stay 'small' in the projected DNS data. This behavior helps to explain the appearance of high frequency features in the flow in both Figures 4.11 and 4.12. We also plot the same data for $n = 16$ in Figure 4.15 and note the same kind of behavior. It is well known that ROMs usually diverge to a limit cycle not present in the original data as time advances, this has been reported in [CWRM04], [MK02], and chapter 5 in [Row02], among many others.

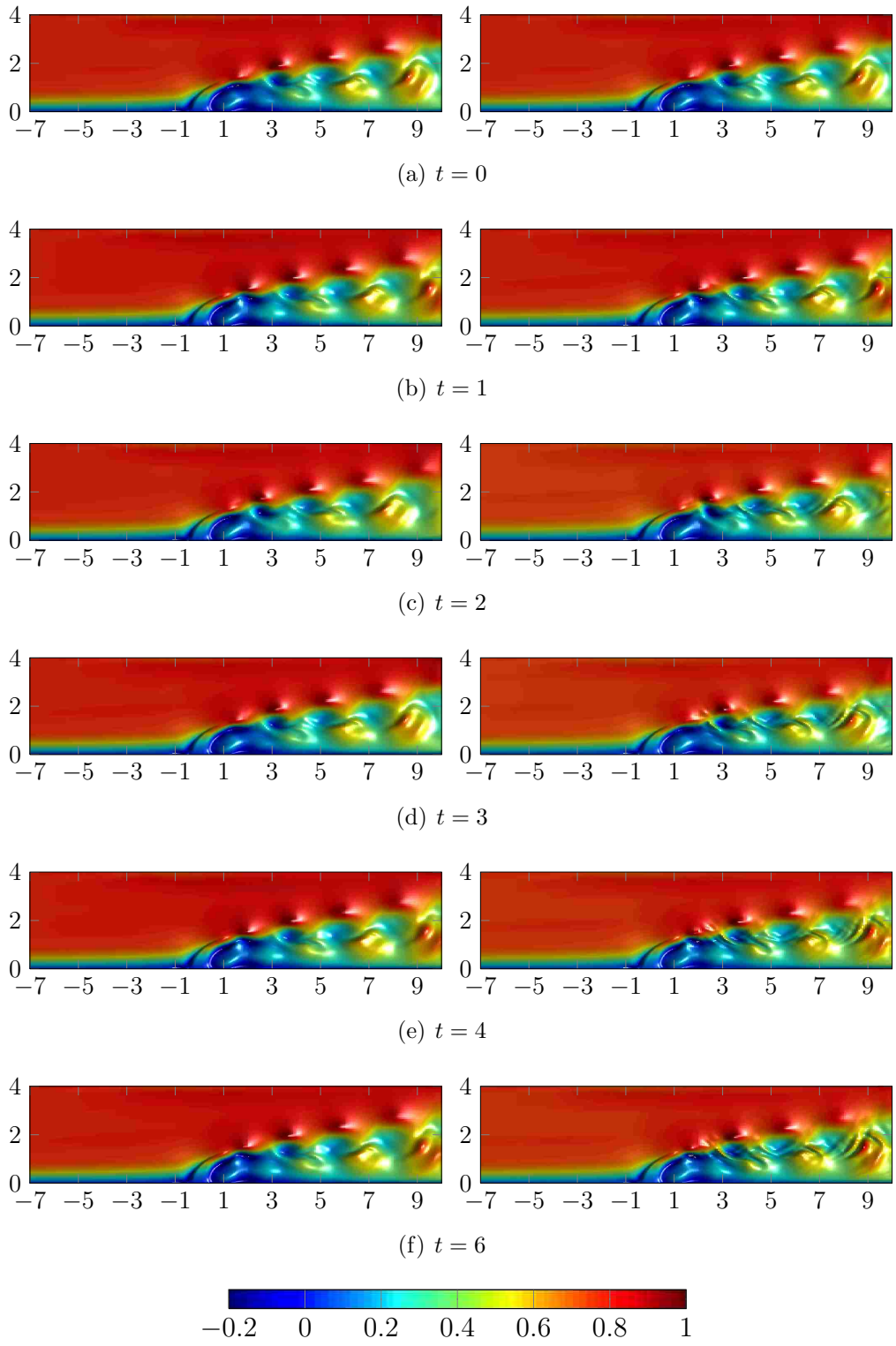

Figure 4.11: x-component of velocity. Left: DNS. Right: ROM.

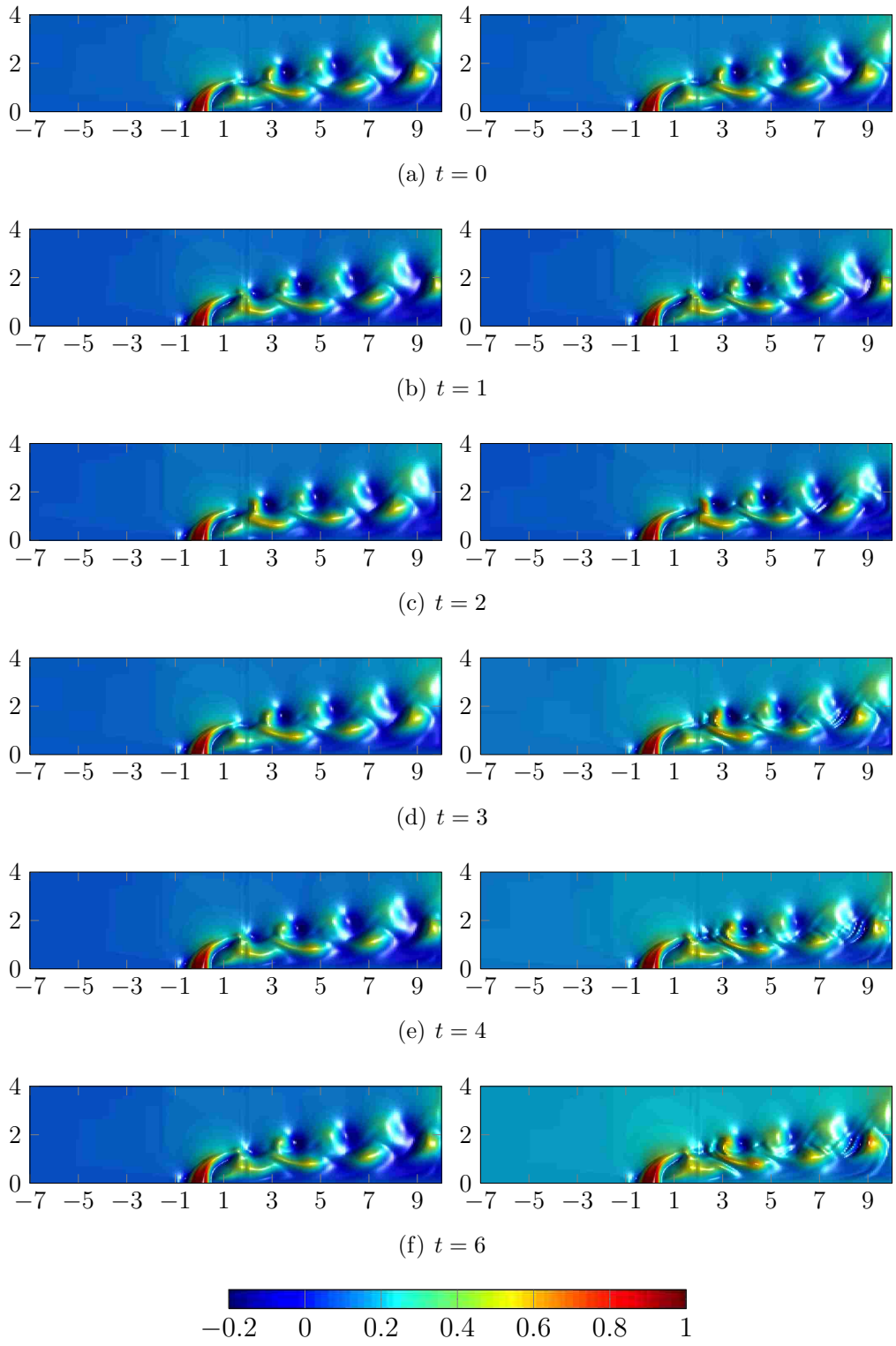

Figure 4.12: y-component of velocity. Left: DNS. Right: ROM.

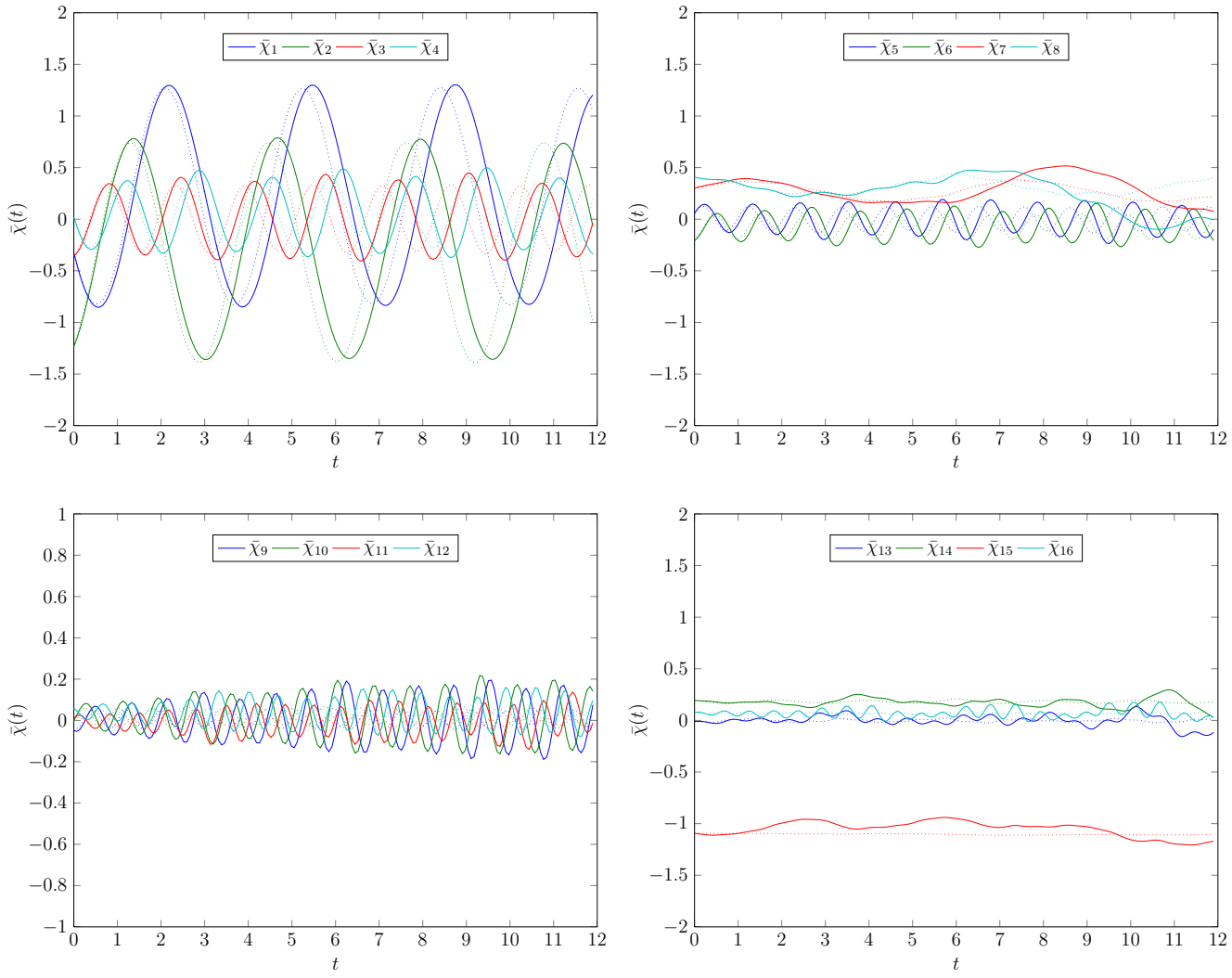

Figure 4.13: ROM (solid) and DNS (dotted) solution, $n = 32$

The error for the $n = 16$ model, as calculated in (4.33), is $E_{\mathbf{u}} = 1.99 \times 10^{-4}$ and the error for the $n = 32$ model is $E_{\mathbf{u}} = 1.95 \times 10^{-4}$. In addition, we plot the error in (4.33) as a function of time (i.e., the sequence) in Figure 4.16. Two observations that we obtain from that plot are that the difference in energy captured between a 16 and 32 order model is not significant and that the difference is larger for low values of t. As time increases the error seems to converge to the same values for both $n = 16$ and $n = 32$.

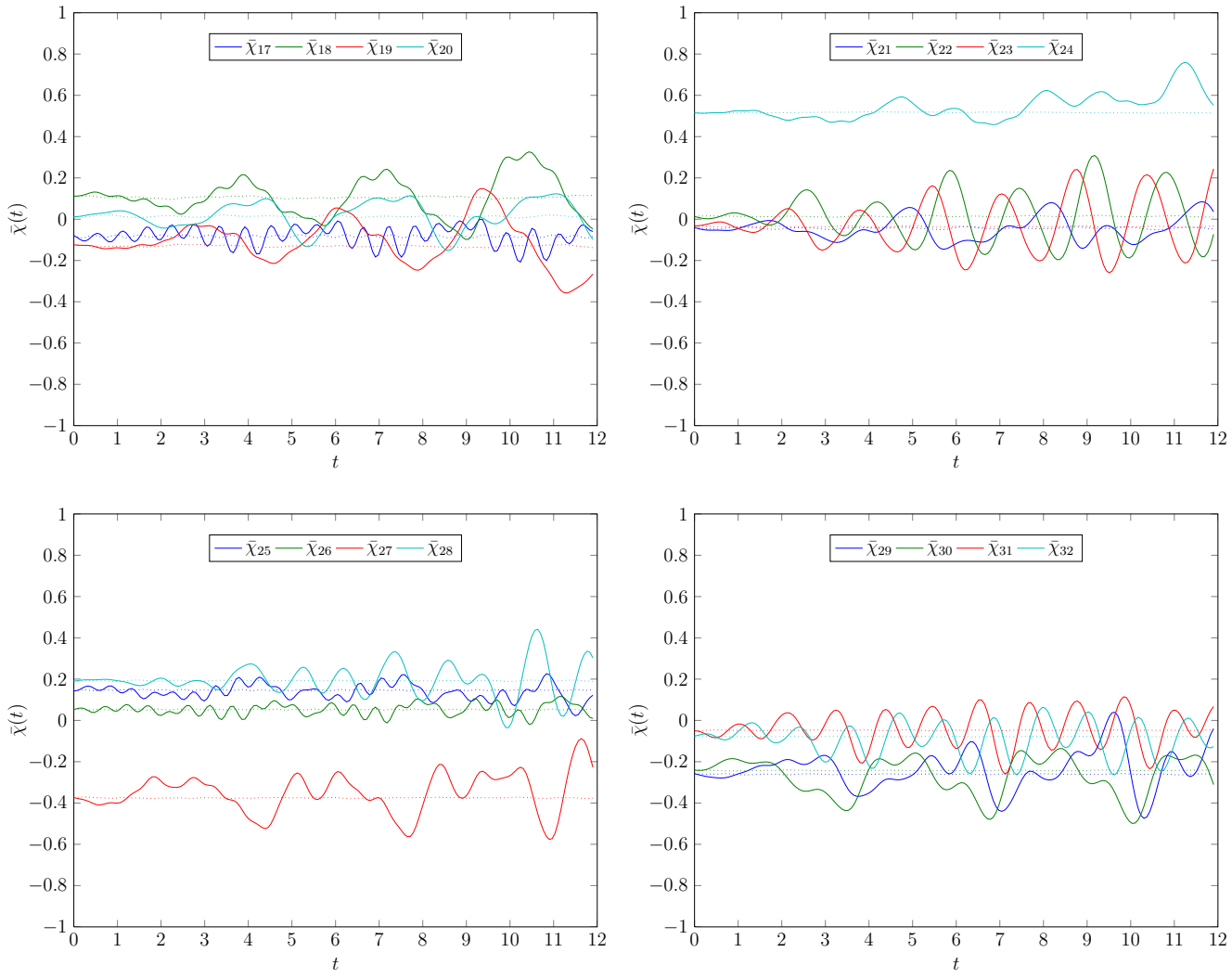

Figure 4.14: ROM (solid) and DNS (dotted) solution, $n = 32$

An additional property that we verify is the behavior of the correlation matrix

$$R = \begin{bmatrix} \int_0^T a_1(t)a_1(t)dt & \int_0^T a_1(t)a_2(t)dt & \cdots & \int_0^T a_1(t)a_n(t)dt \\ \int_0^T a_2(t)a_1(t)dt & \int_0^T a_2(t)a_2(t)dt & \cdots & \int_0^T a_2(t)a_n(t)dt \\ \vdots & \vdots & \ddots & \vdots \\ \int_0^T a_n(t)a_1(t)dt & \int_0^T a_n(t)a_2(t)dt & \cdots & \int_0^T a_n(t)a_n(t)dt \end{bmatrix} \tag{4.36}$$

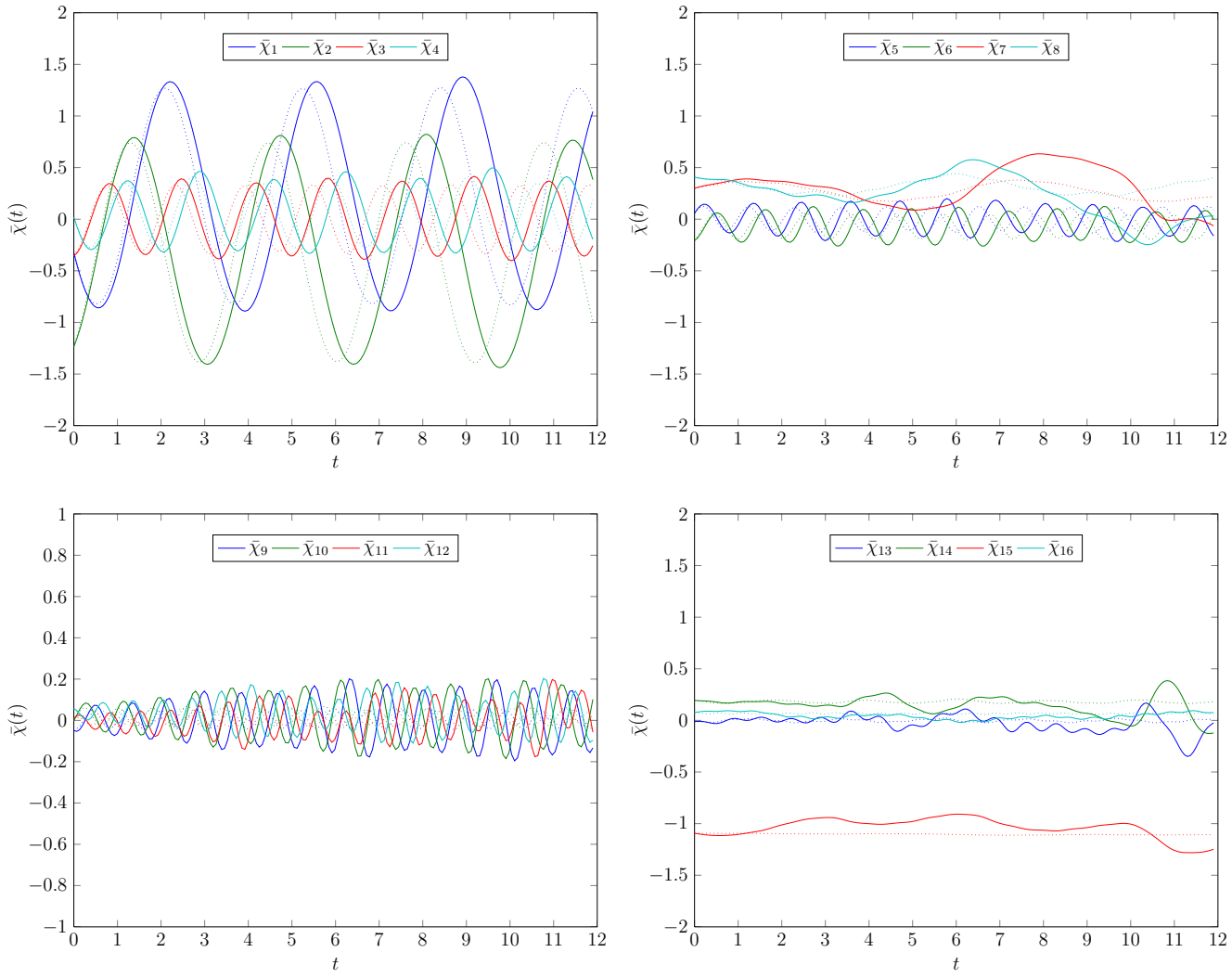

Figure 4.15: ROM (solid) and DNS (dotted) solution, $n = 16$

Figure 4.17 shows the structure of R for the DNS simulation projection with $n = 16$, and Figure 4.18 shows the structure of R for the ROM with $n = 16$. It is evident that the coefficients are not uncorrelated. The reason is that the inclusion of the inflow and control modes modifies the properties of the POD decomposition. As noted earlier, the inflow and boundary modes are computed after the SVD of $\sqrt{J}X$ is computed, and so, appending the inflow and boundary modes to the POD modes matrix Φ modifies the properties of the SVD expansion.

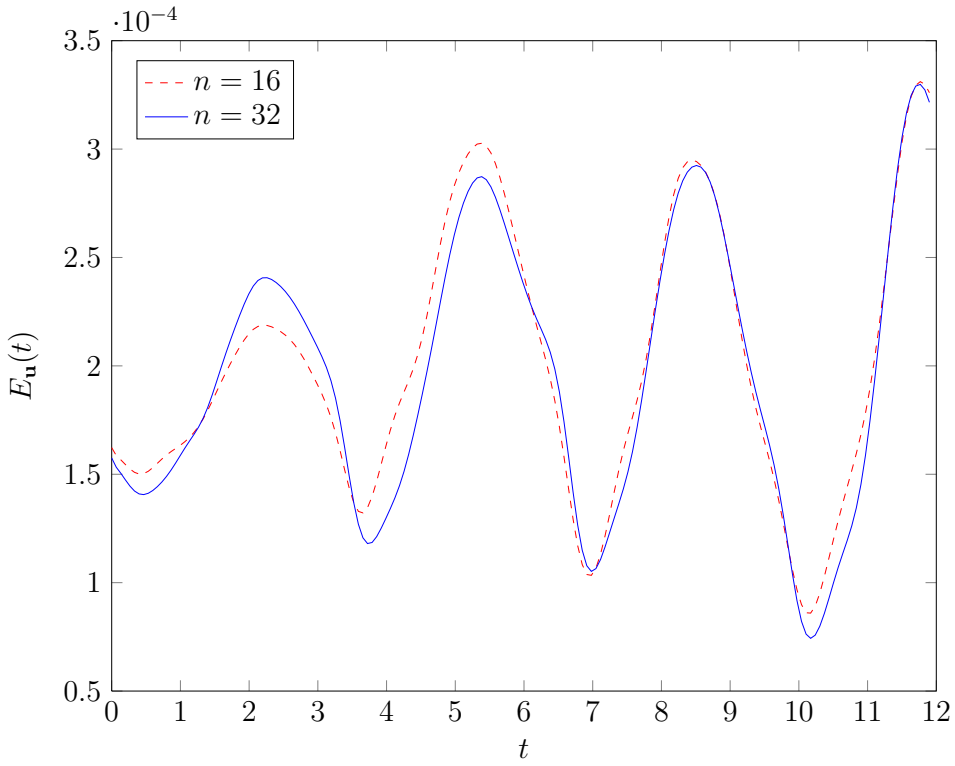

Figure 4.16: Error between DNS and ROM solution

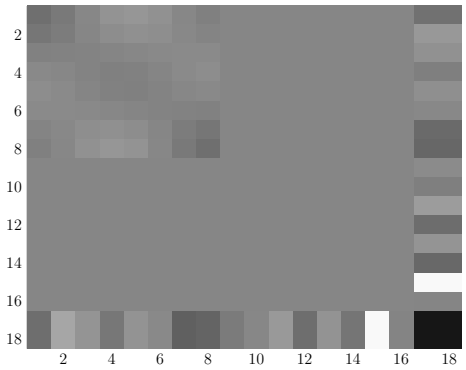

Figure 4.17: Correlation matrix R, DNS, $n = 16$

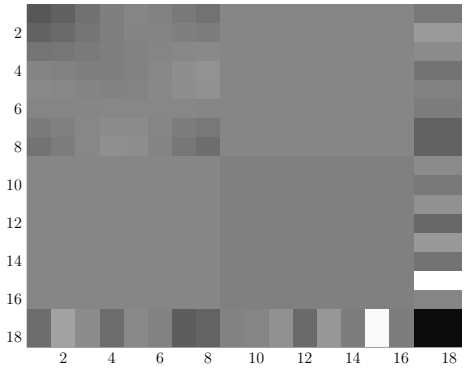

Figure 4.18: Correlation matrix R, ROM, $n = 16$

4.6 Feedback Control of Fluid Flow System

Following the discussion in the first section of this chapter, we approach the film cooling problem from a feedback control point of view and as a velocity tracking problem. Specifically, we are interested in stabilizing the flow to a certain desired operating point, $(\bar{\chi}_d, \bar{u}_d)$. As we will see, this operating point may not be stable, especially for high enough values of velocity ratio, R.

The first step in the design process is to define a new system, called the perturbation system, with $(\bar{\chi}_d, \bar{u}_d)$ as its origin. Let $\chi = \bar{\chi} - \bar{\chi}_d$ and $u = \bar{u} - \bar{u}_d$. Then we have

$$\begin{aligned}
\dot{\chi}(t) &= \dot{\bar{\chi}} - \dot{\bar{\chi}}_d \\
&= \bar{A}\bar{\chi} + \bar{B}\bar{u} + \begin{bmatrix} \bar{\chi}^T \bar{N}_1 \bar{\chi} \\ \vdots \\ \bar{\chi}^T \bar{N}_n \bar{\chi} \end{bmatrix} + \begin{bmatrix} \bar{\chi}^T \bar{M}_1 \bar{u} \\ \vdots \\ \bar{\chi}^T \bar{M}_n \bar{u} \end{bmatrix} + \begin{bmatrix} \bar{u}^T \bar{K}_1 \bar{u} \\ \vdots \\ \bar{u}^T \bar{K}_n \bar{u} \end{bmatrix} + a_0 \bar{D}_1 \bar{\chi} + a_0 \bar{D}_2 \bar{u} + \bar{D}_3 a_0 + \bar{D}_4 a_0^2 \\
&- \left(\bar{A}\bar{\chi}_d + \bar{B}\bar{u}_d + \begin{bmatrix} \bar{\chi}_d^T \bar{N}_1 \bar{\chi}_d \\ \vdots \\ \bar{\chi}_d^T \bar{N}_n \bar{\chi}_d \end{bmatrix} + \begin{bmatrix} \bar{\chi}_d^T \bar{M}_1 \bar{u}_d \\ \vdots \\ \bar{\chi}_d^T \bar{M}_n \bar{u}_d \end{bmatrix} + \begin{bmatrix} \bar{u}_d^T \bar{K}_1 \bar{u}_d \\ \vdots \\ \bar{u}_d^T \bar{K}_n \bar{u}_d \end{bmatrix} + a_0 \bar{D}_1 \bar{\chi}_d + a_0 \bar{D}_2 \bar{u}_d + \bar{D}_3 a_0 + \bar{D}_4 a_0^2 \right)
\end{aligned}$$

$$= \left(\bar{A} + a_0 \bar{D}_1 + \begin{bmatrix} \bar{\chi}_d^T N_1 \\ \vdots \\ \bar{\chi}_d^T N_n \end{bmatrix} + \begin{bmatrix} \bar{u}_d^T \bar{M}_1^T \\ \vdots \\ \bar{u}_d^T \bar{M}_n^T \end{bmatrix} \right) \chi$$
$$+ \left(\bar{B} + a_0 \bar{D}_2 + \begin{bmatrix} \bar{\chi}_d^T \bar{M}_1 \\ \vdots \\ \bar{\chi}_d^T \bar{M}_n \end{bmatrix} + \begin{bmatrix} \bar{u}_d^T K_1 \\ \vdots \\ \bar{u}_d^T K_n \end{bmatrix} \right) u + \begin{bmatrix} \chi^T \bar{N}_1 \chi \\ \vdots \\ \chi^T \bar{N}_n \chi \end{bmatrix} + \begin{bmatrix} \chi^T \bar{M}_1 u \\ \vdots \\ \chi^T \bar{M}_n u \end{bmatrix} + \begin{bmatrix} u^T \bar{K}_1 u \\ \vdots \\ u^T \bar{K}_n u \end{bmatrix} \quad (4.37)$$

where $N_i = \bar{N}_i^T + \bar{N}_i$ and $K_i = \bar{K}_i^T + \bar{K}_i$. We finally obtain the system

$$\dot{\chi}(t) = f(\chi, u) = A(\bar{\chi}_d, \bar{u}_d)\chi(t) + B(\bar{\chi}_d, \bar{u}_d)u(t) + Q[\chi(t), u(t)] \quad (4.38)$$

where

$$A = \bar{A} + a_0 \bar{D}_1 + \begin{bmatrix} \bar{\chi}_d^T N_1 \\ \vdots \\ \bar{\chi}_d^T N_n \end{bmatrix} + \begin{bmatrix} \bar{u}_d^T \bar{M}_1^T \\ \vdots \\ \bar{u}_d^T \bar{M}_n^T \end{bmatrix}, \; B = \bar{B} + a_0 \bar{D}_2 + \begin{bmatrix} \bar{\chi}_d^T \bar{M}_1 \\ \vdots \\ \bar{\chi}_d^T \bar{M}_n \end{bmatrix} + \begin{bmatrix} \bar{u}_d^T K_1 \\ \vdots \\ \bar{u}_d^T K_n \end{bmatrix},$$

and $Q[\cdot, \cdot]$ is the quadratic term given by

$$Q[\chi, u] = \begin{bmatrix} \chi^T \bar{N}_1 \chi \\ \vdots \\ \chi^T \bar{N}_n \chi \end{bmatrix} + \begin{bmatrix} \chi^T \bar{M}_1 u \\ \vdots \\ \chi^T \bar{M}_n u \end{bmatrix} + \begin{bmatrix} u^T \bar{K}_1 u \\ \vdots \\ u^T \bar{K}_n u \end{bmatrix}.$$

Note that $\bar{\chi}_d$ and $\bar{u}_d$ are constant, hence $A(\cdot)$ and $B(\cdot)$ are time invariant. We could also consider stabilization to a trajectory, $\bar{\chi}_d(t)$ and $\bar{u}_d(t)$, in which case $A(\cdot)$ and $B(\cdot)$ will be time varying.

We may now apply the stabilization and equilibria path programming results from the previous chapter to the perturbation system in (4.38). The first issue we deal with is which

operating point to pick. Using the MATLAB function `fsolve` we numerically solve

$$f(\bar{\chi}, \bar{u}, a_0) = 0$$

in (4.32) with $\bar{u} = 1$ and $a_0 = 1$ to obtain the desired operating point $\bar{\chi}_d^{(1)}$. To obtain the second operating point, $\bar{\chi}_d^{(2)}$, we set $\bar{u} = 1.0010$ and $a_0 = 1$. The values of the states for both operating points are shown in Tables 4.5 and 4.6.

Table 4.5: Operating point $\bar{\chi}_d^{(1)}$

State	Value		State	Value
$\bar{\chi}_{d_1}^{(1)}$	0.1804		$\bar{\chi}_{d_9}^{(1)}$	0.0112
$\bar{\chi}_{d_2}^{(1)}$	-0.2973		$\bar{\chi}_{d_{10}}^{(1)}$	0.0201
$\bar{\chi}_{d_3}^{(1)}$	-0.0015		$\bar{\chi}_{d_{11}}^{(1)}$	-0.0013
$\bar{\chi}_{d_4}^{(1)}$	0.0420		$\bar{\chi}_{d_{12}}^{(1)}$	0.0289
$\bar{\chi}_{d_5}^{(1)}$	0.0219		$\bar{\chi}_{d_{13}}^{(1)}$	0.0177
$\bar{\chi}_{d_6}^{(1)}$	-0.0690		$\bar{\chi}_{d_{14}}^{(1)}$	0.2212
$\bar{\chi}_{d_7}^{(1)}$	0.2815		$\bar{\chi}_{d_{15}}^{(1)}$	-0.4283
$\bar{\chi}_{d_8}^{(1)}$	0.3764		$\bar{\chi}_{d_{16}}^{(1)}$	-0.1707

Table 4.6: Operating point $\bar{\chi}_d^{(2)}$

State	Value		State	Value
$\bar{\chi}_{d_1}^{(1)}$	0.1804		$\bar{\chi}_{d_9}^{(1)}$	0.0112
$\bar{\chi}_{d_2}^{(1)}$	-0.2973		$\bar{\chi}_{d_{10}}^{(1)}$	0.0201
$\bar{\chi}_{d_3}^{(1)}$	-0.0015		$\bar{\chi}_{d_{11}}^{(1)}$	-0.0013
$\bar{\chi}_{d_4}^{(1)}$	0.0420		$\bar{\chi}_{d_{12}}^{(1)}$	0.0289
$\bar{\chi}_{d_5}^{(1)}$	0.0220		$\bar{\chi}_{d_{13}}^{(1)}$	0.0177
$\bar{\chi}_{d_6}^{(1)}$	-0.0691		$\bar{\chi}_{d_{14}}^{(1)}$	0.2215
$\bar{\chi}_{d_7}^{(1)}$	0.2816		$\bar{\chi}_{d_{15}}^{(1)}$	-0.4271
$\bar{\chi}_{d_8}^{(1)}$	0.3767		$\bar{\chi}_{d_{16}}^{(1)}$	-0.1713

With an operating point identified, we now study the stability of the operating point. Figures 4.19 and 4.20 clearly show that if the ROM is solved with a small perturbation to $\bar{\chi}(0) = \bar{\chi}_d^{(1)}$ or $\bar{\chi}(0) = \bar{\chi}_d^{(2)}$, then the resulting solution eventually leaves the operating point and so this shows that both operating points are unstable.

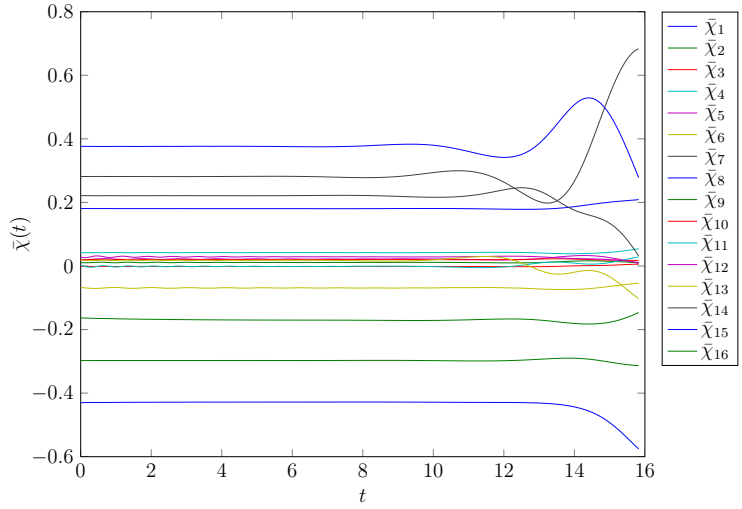

Figure 4.19: ROM solution with $\bar{\chi}_0 = \bar{\chi}_d^{(1)}$

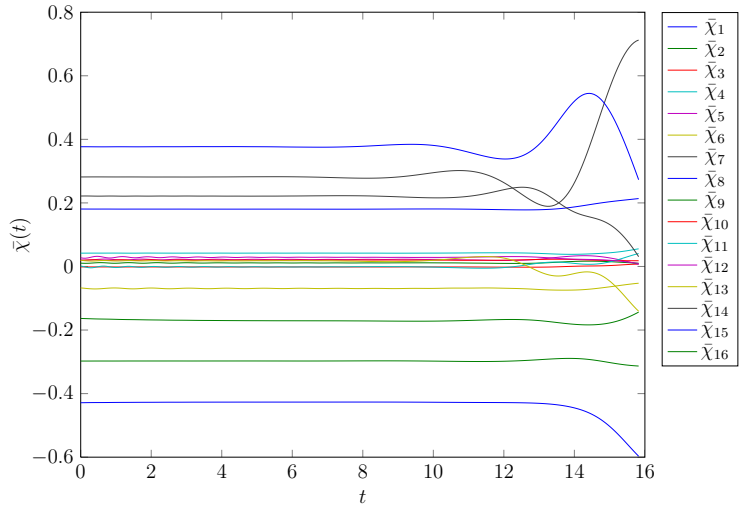

Figure 4.20: ROM solution with $\bar{\chi}_0 = \bar{\chi}_d^{(2)}$

We also note that both solutions are very similar since $\bar{\chi}_d^{(1)}$ and $\bar{\chi}_d^{(2)}$ are very near each other. To verify our intuition, Figures 4.21 and 4.22 show the eigenvalues of the matrix A of the perturbation system at $\bar{\chi}_d^{(1)}$ and $\bar{\chi}_d^{(2)}$, respectively. The two pairs of eigenvalues on the right hand side of the imaginary axis reveal that the selected operating point is indeed unstable. The role of the feedback controller then is to shift the unstable eigenvalues to the left hand side of the imaginary axis and to enlarge the RoQA of the perturbation system. Figures 4.23 and 4.24 show the location of the eigenvalues of the matrix $A + BF$ of the perturbation system at $\bar{\chi}_d^{(1)}$ and $\bar{\chi}_d^{(2)}$, respectively. The feedback gain F is designed using

the method in Section 3.1. The ROM solution of the perturbation system clearly depicts the stabilizing effect of the controller as shown in Figures 4.25 and 4.26.

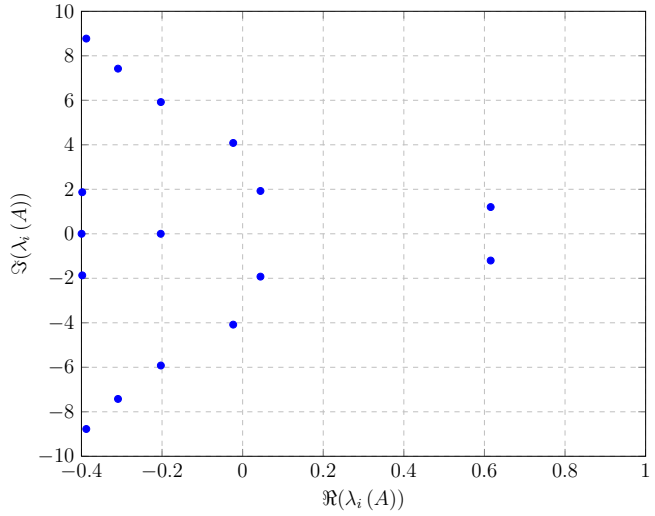

Figure 4.21: Eigenvalues of A (perturbation at $\bar{\chi}_d^{(1)}$)

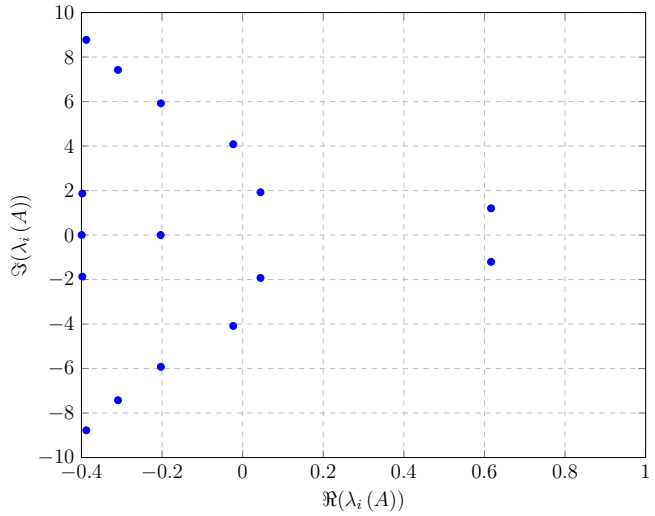

Figure 4.22: Eigenvalues of A (perturbation at $\bar{\chi}_d^{(2)}$)

We can see from Figures 4.25 or 4.26 that the RoQA is fairly small. This means that to stabilize the ROM, a fairly large number of switches will be required if the initial condition is far away from $\bar{\chi}_d$. However, this method provides us with an estimate of the RoQA while a simpler linearization study only provides asymptotic results, i.e., the RoQA may be vanishingly small.

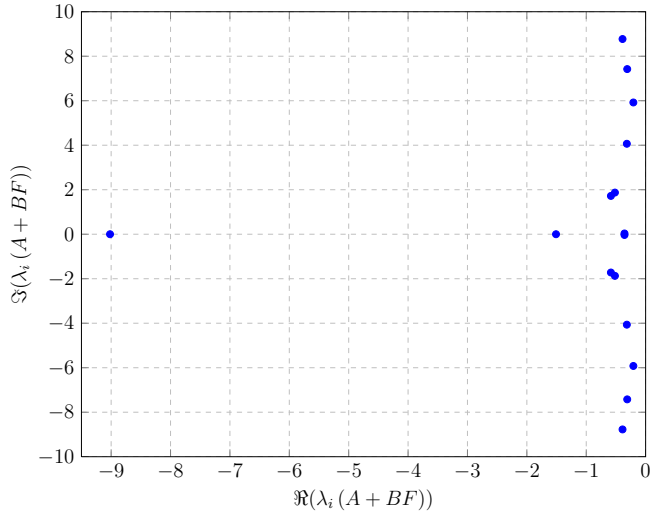

Figure 4.23: Eigenvalues of A+BF (perturbation at $\bar{\chi}_d^{(1)}$)

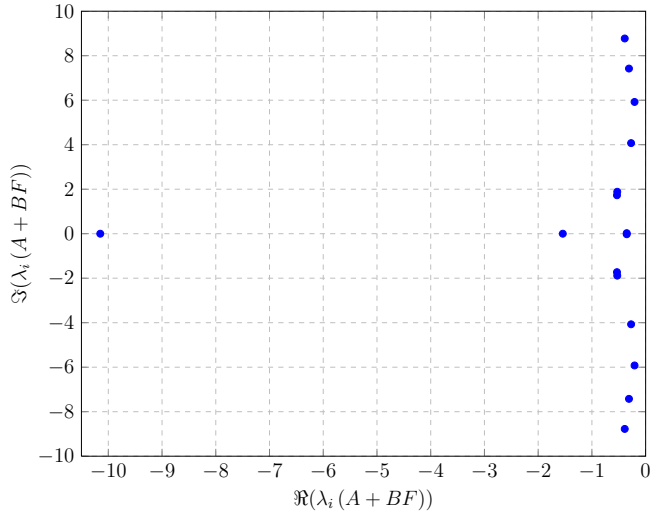

Figure 4.24: Eigenvalues of A+BF (perturbation at $\bar{\chi}_d^{(2)}$)

Figure 4.28 shows a two stage equilibria path simulation, from $\bar{\chi}_0$ to $\bar{\chi}_d^{(1)}$ and settling at $\bar{\chi}_d^{(2)}$. The initial condition for the simulation is shown in Table 4.7 is computed via our controller design method and lies in the maximized RoQA. The location of $\bar{\chi}_d^{(2)}$ is chosen such that $\bar{\chi}_d^{(1)}$ lies in the RoQA of $\bar{\chi}_d^{(2)}$. The switch occurs at $t = 12$ and appears clearly in the plot of the control signal.

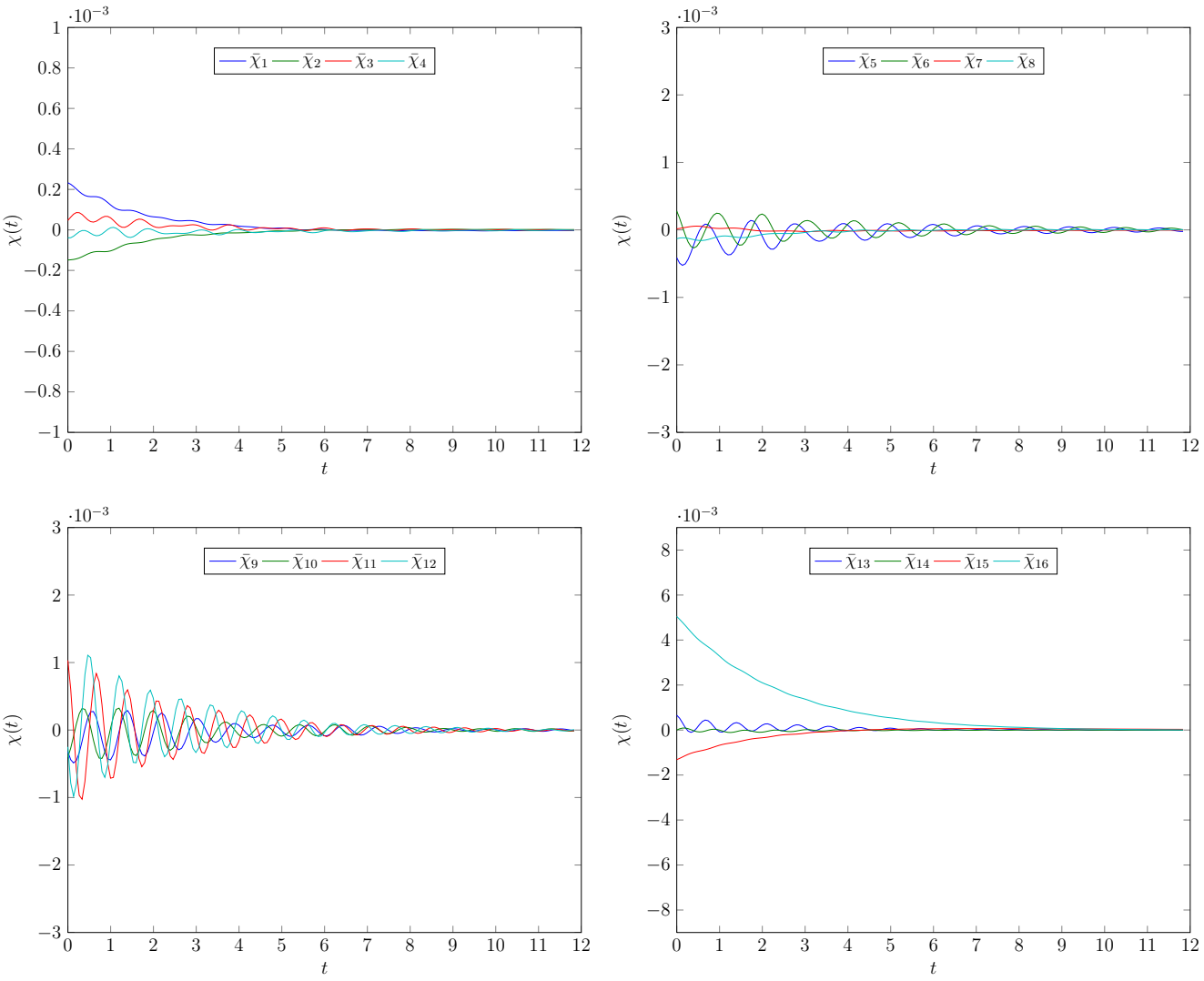

Figure 4.25: ROM solution in closed loop (perturbation at $\bar{\chi}_d^{(1)}$)

Table 4.7: Initial condition for switched system simulation, $\bar{\chi}_0$

State	Value		State	Value		State	Value		State	Value
$\bar{\chi}_1$	0.1807		$\bar{\chi}_5$	0.0215		$\bar{\chi}_9$	0.0108		$\bar{\chi}_{13}$	0.0183
$\bar{\chi}_2$	-0.2974		$\bar{\chi}_6$	-0.0688		$\bar{\chi}_{10}$	0.0197		$\bar{\chi}_{14}$	0.2212
$\bar{\chi}_3$	-0.0015		$\bar{\chi}_7$	0.2815		$\bar{\chi}_{11}$	-0.0003		$\bar{\chi}_{15}$	-0.4296
$\bar{\chi}_4$	0.0419		$\bar{\chi}_8$	0.3763		$\bar{\chi}_{12}$	0.0286		$\bar{\chi}_{16}$	-0.1657

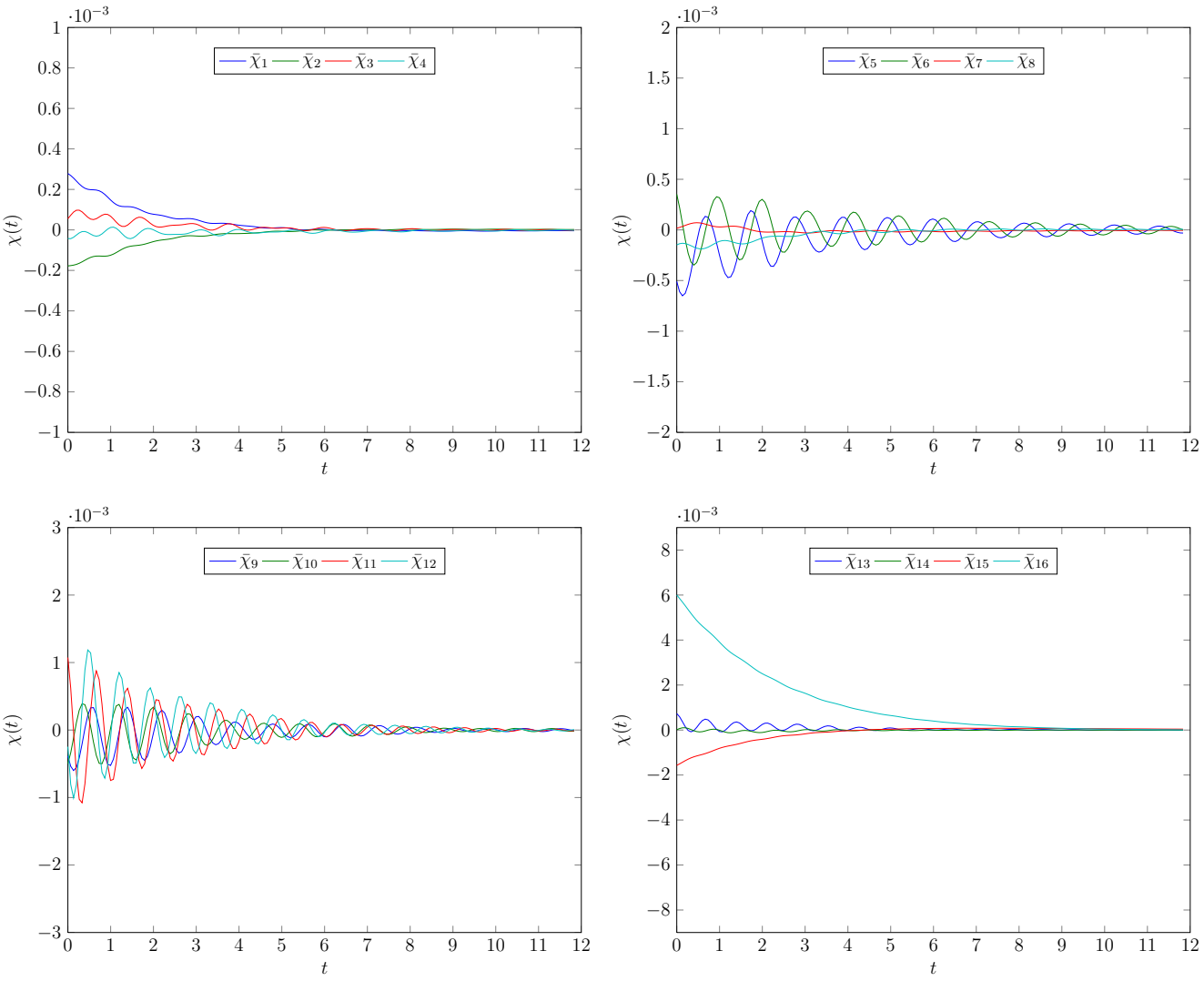

Figure 4.26: ROM solution in closed loop (perturbation at $\bar{\chi}_d^{(2)}$)

The result presented in Figure 4.28 corresponds to the setup shown in Figure 4.27 (a). Once a state feedback F has been designed, it is inserted into a DNS simulation as shown in Figure 4.27 (b) and (c).

The jet inlflow boundary condition is implemented as

$$v(r,t) = \bar{u}(t)\left(1 - r^2\right) e^{-\left(\frac{r}{0.7}\right)^4}.$$

The results of the ROM and DNS in closed loop (implementation 1) are shown in Figures 4.29 and 4.30. There is a noticeable difference between the ROM and DNS solution starting

at around $t = 2$ and from then onwards the DNS solution leaves the operating condition. In this sense, the behavior between the ROM and DNS solution is the same as in open loop, eventually the ROM solution loses fidelity. The solution using DNS implementation 2 behaves similarly in the first few units of time, but the control signal calculated in this setup diverges from the signal $c_1(t)$ of Figure 4.27 (a) . After about $t = 2$ the control signal behaves erratically which illustrates the difficulty in implementing the control signal from the ROM to the DNS simulation.

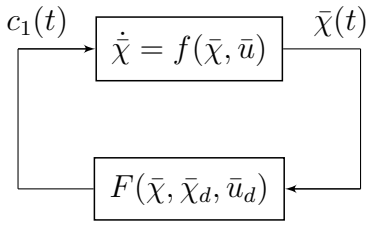

(a) ROM in closed loop

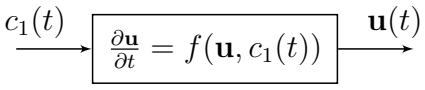

(b) DNS closed loop implementation 1

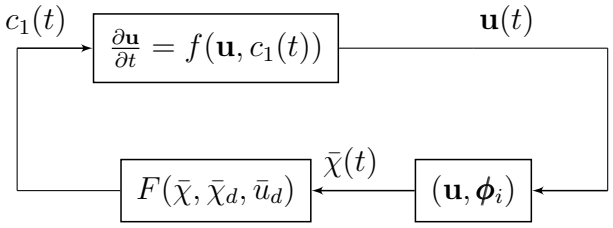

(c) DNS closed loop implementation 2

Figure 4.27: DNS closed loop implementations

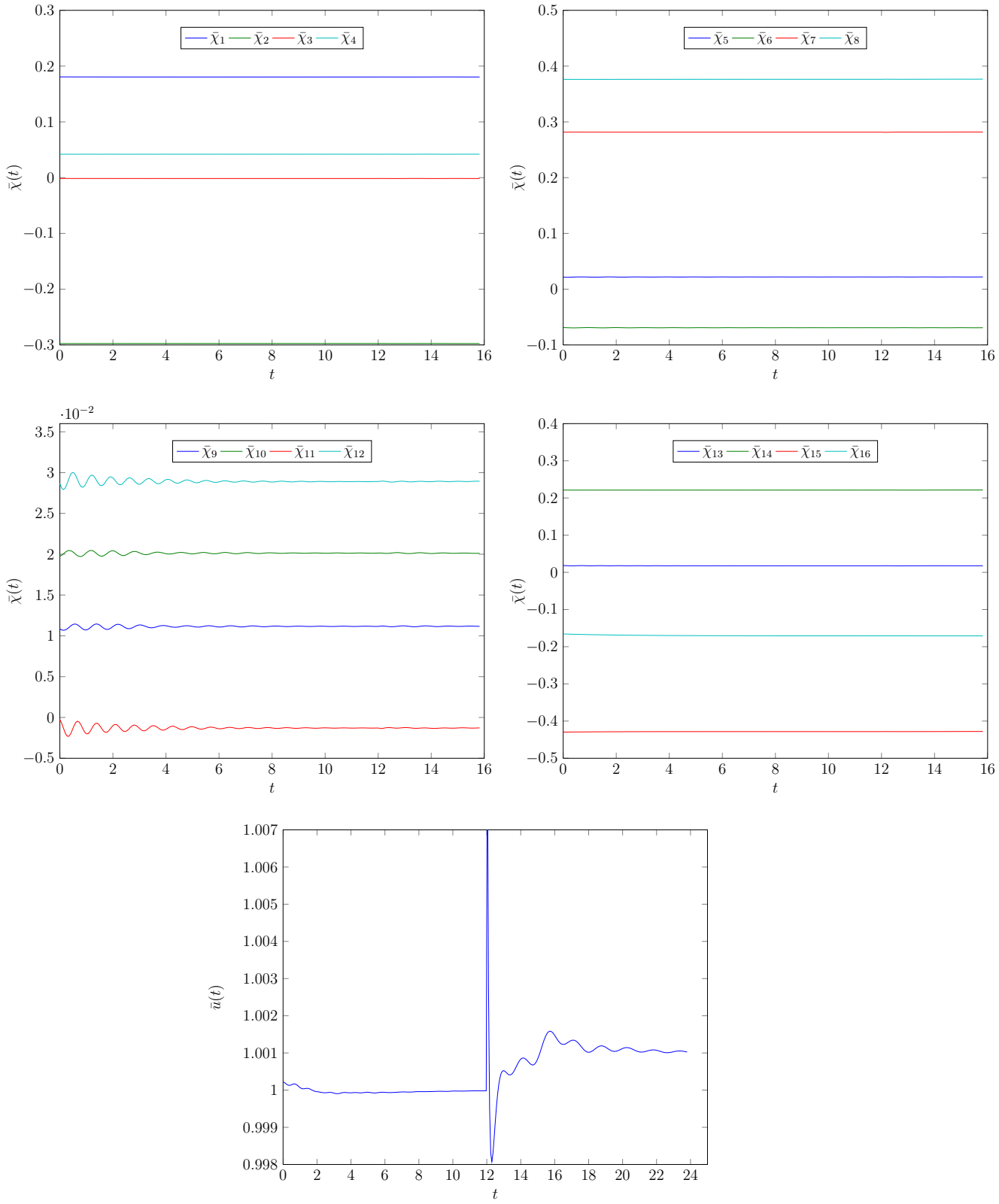

Figure 4.28: ROM solution in closed loop and input signal

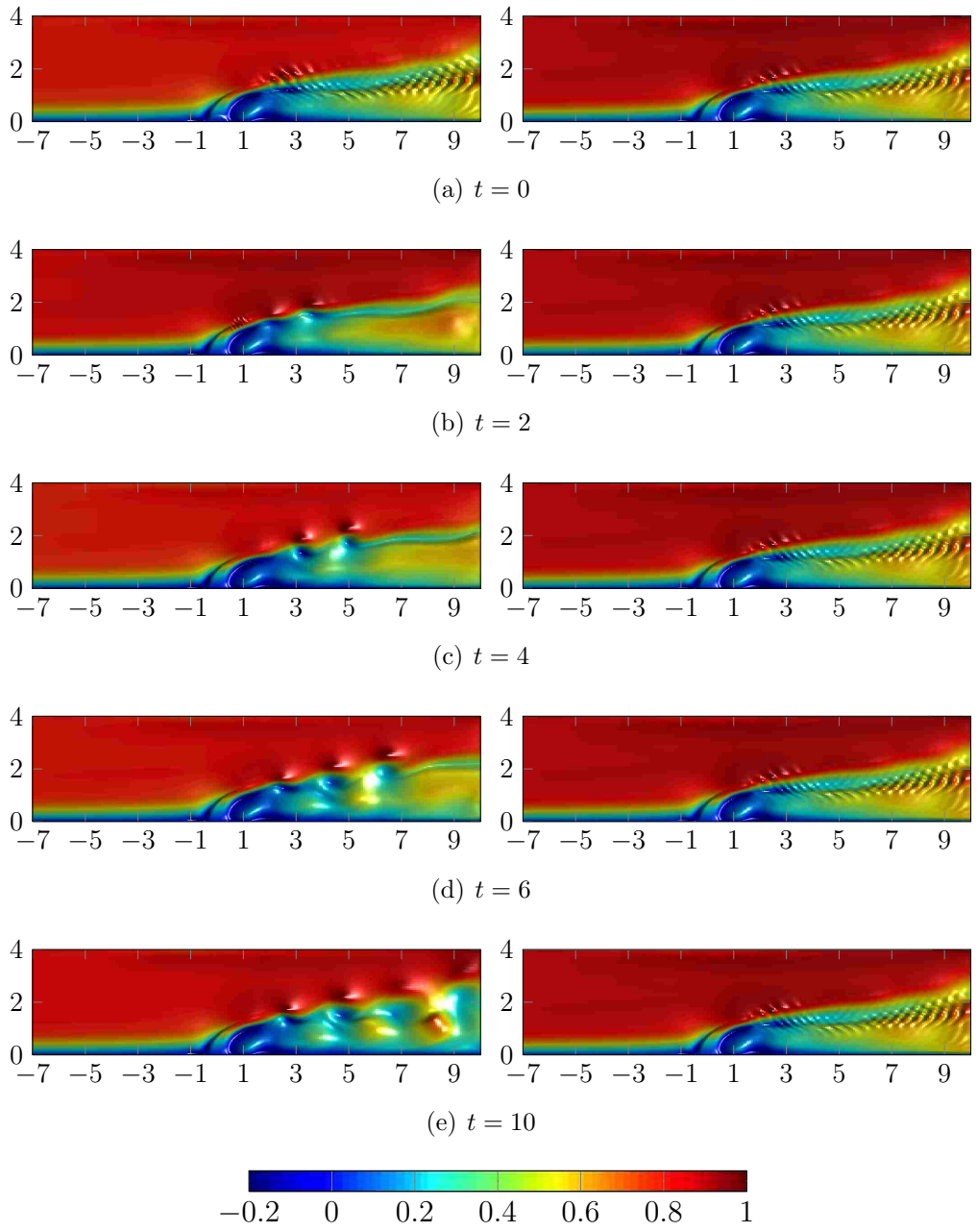

Figure 4.29: x-component of velocity in closed loop. Left: DNS. Right: ROM.

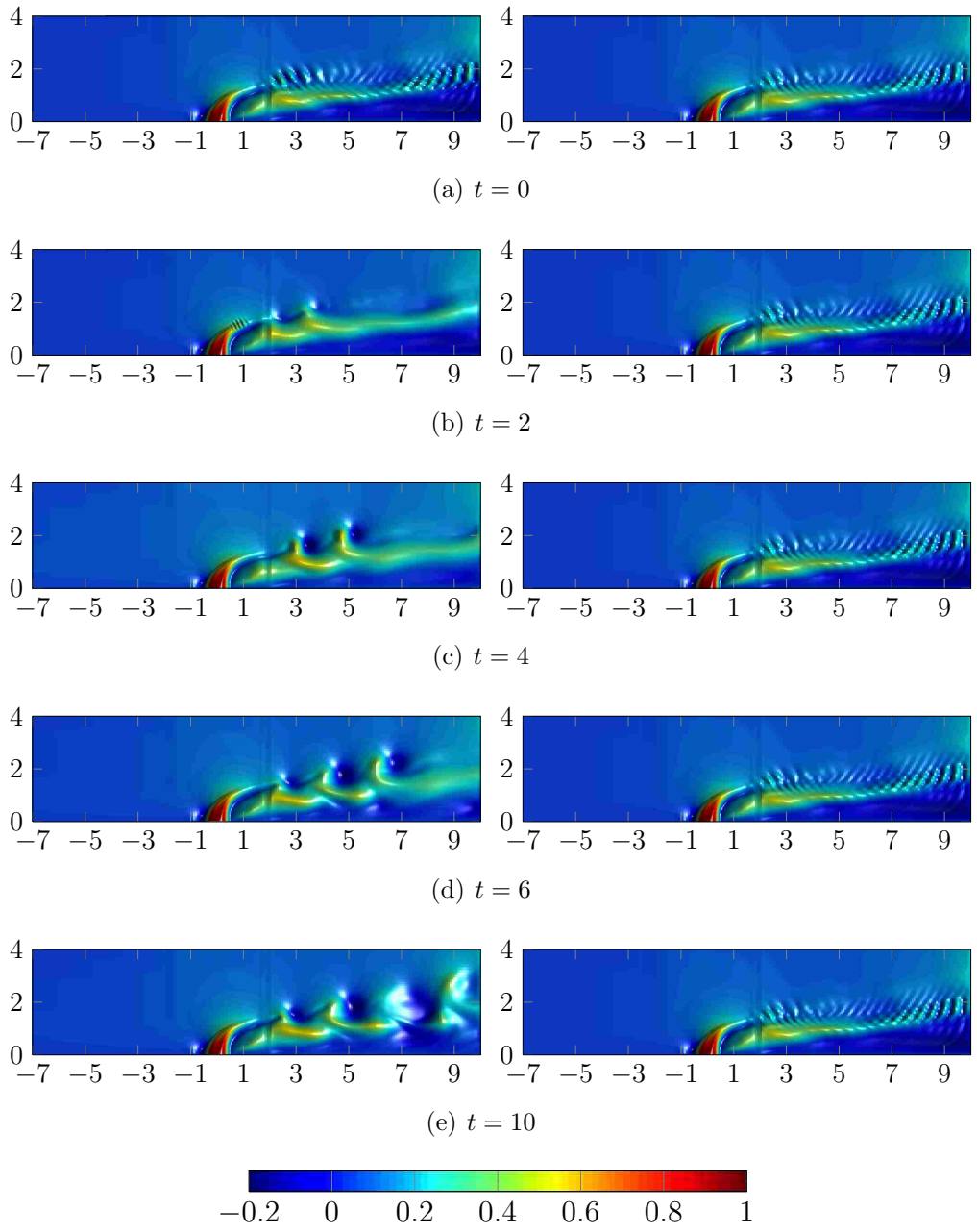

Figure 4.30: y-component of velocity in closed loop. Left: DNS. Right: ROM.

4.6.1 Temperature Dynamics

In this section we give a brief introduction to a future research direction that incorporates temperature dynamics for controller design. The temperature of the fluid is modeled as a passive scalar field, $T(\mathbf{x}, t)$, and it satisfies the scalar "one-way-coupled" non-dimensional equation

$$\frac{\partial T}{\partial t} + \left(u\frac{\partial T}{\partial x} + v\frac{\partial T}{\partial y} + w\frac{\partial T}{\partial z} \right) = \frac{1}{RePr}\left(\frac{\partial^2 T}{\partial x^2} + \frac{\partial^2 T}{\partial y^2} + \frac{\partial^2 T}{\partial z^2} \right). \tag{4.39}$$

where Pr is the Prandtl number. In a similar manner to the computation of the velocity POD basis functions, we compute the temperature POD basis functions $\{\mathrm{T}_j\}_{j=1}^{n}$, where n is not necessarily the number of velocity POD basis functions. The following truncated modal decomposition is used to represent the temperature

$$T_{ROM}(\mathbf{x}, t) = \sum_{j=1}^{n} b_j(t)\mathrm{T}_j(\mathbf{x}). \tag{4.40}$$

We note that there are no control modes since the controlled variable is the boundary velocity, not the temperature of the fluid. We then carry out a Galerkin projection by inserting (4.40) into (4.39) to obtain the following equations:

$$\int_\Omega \frac{\partial T_{ROM}}{\partial t}\mathrm{T}_i d\mathbf{x} = \sum_{j=1}^{n_T} \dot{b}_j(t)\left(\mathrm{T}_j, \mathrm{T}_i\right) = \dot{b}_i(t),$$

$$\begin{aligned}\int_\Omega u_{ROM}\frac{\partial T_{ROM}}{\partial x}\mathrm{T}_i d\mathbf{x} = &\sum_{j=1}^{n} a_j(t)\sum_{k=1}^{n_T} b_k(t)\left(\phi_{u_j}\frac{\partial \mathrm{T}_k}{\partial x}, \mathrm{T}_i\right) + a_0\sum_{k=1}^{n_T} b_k(t)\left(h_{u_0}\frac{\partial \mathrm{T}_k}{\partial x}, \mathrm{T}_i\right) \\ &+ \sum_{j=1}^{m} c_j(t)\sum_{k=1}^{n_T} b_k(t)\left(h_{u_j}\frac{\partial \mathrm{T}_k}{\partial x}, \mathrm{T}_i\right),\end{aligned}$$

$$\int_\Omega v_{ROM}\frac{\partial T_{ROM}}{\partial y}\mathrm{T}_i d\mathbf{x} = \sum_{j=1}^{n} a_j(t)\sum_{k=1}^{n_T} b_k(t)\left(\phi_{v_j}\frac{\partial \mathrm{T}_k}{\partial y},\mathrm{T}_i\right) + a_0\sum_{k=1}^{n_T} b_k(t)\left(h_{v_0}\frac{\partial \mathrm{T}_k}{\partial y},\mathrm{T}_i\right) + \sum_{j=1}^{m} c_j(t)\sum_{k=1}^{n_T} b_k(t)\left(h_{v_j}\frac{\partial \mathrm{T}_k}{\partial y},\mathrm{T}_i\right),$$

$$\int_\Omega w_{ROM}\frac{\partial T_{ROM}}{\partial z}\mathrm{T}_i d\mathbf{x} = \sum_{j=1}^{n} a_j(t)\sum_{k=1}^{n_T} b_k(t)\left(\phi_{w_j}\frac{\partial \mathrm{T}_k}{\partial z},\mathrm{T}_i\right) + a_0\sum_{k=1}^{n_T} b_k(t)\left(h_{w_0}\frac{\partial \mathrm{T}_k}{\partial z},\mathrm{T}_i\right) + \sum_{j=1}^{m} c_j(t)\sum_{k=1}^{n_T} b_k(t)\left(h_{w_j}\frac{\partial \mathrm{T}_k}{\partial z},\mathrm{T}_i\right),$$

and

$$\int_\Omega \left(\frac{\partial^2 T_{ROM}}{\partial x^2}+\frac{\partial^2 T_{ROM}}{\partial y^2}+\frac{\partial^2 T_{ROM}}{\partial z^2}\right)\mathrm{T}_i d\mathbf{x} = \sum_{j=1}^{n_T} b_j(t)\left(\frac{\partial^2 \mathrm{T}_j}{\partial x^2}+\frac{\partial^2 \mathrm{T}_j}{\partial y^2}+\frac{\partial^2 \mathrm{T}_j}{\partial z^2},\mathrm{T}_i\right).$$

Finally we obtain the nonlinear state-space model for the temperature dynamics:

$$\dot{b} = Lb + \begin{bmatrix}\bar{\chi}^T J_1\\ \vdots \\ \bar{\chi}^T J_{n_T}\end{bmatrix} b + \begin{bmatrix}\bar{u}^T H_1\\ \vdots \\ \bar{u}^T \bar{H}_{n_T}\end{bmatrix} b + a_0 I b \tag{4.41}$$

where

$$L_{ij} = \frac{k}{\rho c V l}\left(\frac{\partial^2 \mathrm{T}_j}{\partial x^2}+\frac{\partial^2 \mathrm{T}_j}{\partial y^2}+\frac{\partial^2 \mathrm{T}_j}{\partial z^2},\mathrm{T}_i\right), J_{i_{jk}} = \left(\phi_{u_j}\frac{\partial \mathrm{T}_k}{\partial x}+\phi_{v_j}\frac{\partial \mathrm{T}_k}{\partial y}+\phi_{w_j}\frac{\partial \mathrm{T}_k}{\partial z},\mathrm{T}_i\right),$$
$$H_{i_{jk}} = \left(h_{u_j}\frac{\partial \mathrm{T}_k}{\partial x}+h_{v_j}\frac{\partial \mathrm{T}_k}{\partial y}+h_{w_j}\frac{\partial \mathrm{T}_k}{\partial z},\mathrm{T}_i\right), \text{ and } I_{ij} = \left(h_{u_0}\frac{\partial \mathrm{T}_j}{\partial x}+h_{v_0}\frac{\partial \mathrm{T}_j}{\partial y}+h_{w_0}\frac{\partial \mathrm{T}_j}{\partial z},\mathrm{T}_i\right),$$

and $b(t) \in \mathbb{R}^{n_T}$ is the temperature state vector consisting of $\{b_i(t)\}_{i=1}^{n_T}$ as its elements. The structure of (4.41) complicates the design of a feedback controller since the control input enters as a coefficient of the state.

Chapter 5
Conclusion and Future Work

We have developed a design methodology for state and output feedback stabilization of nonlinear sector-bounded control systems in state-space form. In the tradition of the absolute stability problem, we have represented the nonlinear system with an LFT of the linearized part and the nonlinear error dynamics. This LFT representation enables the use of $\mathcal{H}_\infty$-based robust control to stabilize the nonlinear system and to maximize the estimated RoQA. Each operating point of the original nonlinear system is regionally stabilized by a linear controller that has been designed to solve a $\mathcal{H}_\infty$-norm problem and this strategy maximizes the estimate of the RoA of each stabilized operating point. The overall design consists of a sequence of linear controllers implemented in a switching strategy that regionally stabilize the desired equilibrium under the assumption that the system admits a centered-ϵ-cover. If this assumption is satisfied, then the switching controller will achieve semi-global stabilization of the nonlinear system. A formula to compute the ϵ-distance was derived under both state feedback and output feedback control. Roughly speaking, this provides a quantifiable region where the linearized representation of the system's dynamics is valid.

We then applied the control strategy to a ROM of the Navier-Stokes equation. We designed a two path switching controller that successfully stabilizes the ROM to an operating point and then implemented it in DNS. The controller that was designed based on the ROM was able to stabilize the flow to the selected operating point in DNS for a short time period until the DNS solution diverged to another operating condition. This highlights the difficulties encountered when a controller is designed for a ROM and then implemented on the full system.

Future work

Perhaps the most pressing issue is to obtain a better model than the current ROM, especially if it will be used for controller design. From the results obtained in Section 4.6, the current ROM provides useful physical information, but is not sufficient for controller design. It is clear that a feedback controller design based on the ROM does not perform as well as expected in DNS. For linear models, the balanced POD method has provided promising results and a nonlinear version of this method has been investigated in [LMG02] which may provide a path to obtaining better models for control design.

Closely related to the modeling problem, is incorporating the temperature dynamics for control design. We have sketched out the form of the ROM that includes the temperature variable and have pointed out the difficulty in designing a controller since the input enters the state equation as a coefficient of the state. Investigating this issue would undertake a considerable amount of effort but would provide more natural results since the controller design is based on temperature too, which is ultimately the main concern of film cooling.

Another future research problem is to consider switching at non-equilibrium points. The main idea is to construct linearized models at arbitrary points in the state space. This would probably relax the ϵ-cover condition and allow the designer to apply the controller design to more general classes of systems. A gain scheduling approach that explores this idea is the so called "velocity-based linarization" described in [LL98].

In addition, a more complete control strategy should consider performance issues of the transient response. Currently, the transient behavior is not part of the design but it should be considered for practical applications.

References

[AAA+07] F. Amato, R. Ambrosino, M. Ariola, C. Cosentino, and A. Merola. State feedback control of nonlinear quadratic systems. In *Proceedings of the 46th IEEE Conference on Decision and Control*, pages 1699–1703, 2007.

[ACM07] F. Amato, C. Cosentino, and A. Merola. On the region of attraction of nonlinear quadratic systems. *Automatica*, 43(12):2119–2123, 2007.

[AG64] Mark A. Aizerman and Feliks R. Gantmacher. *Absolute stability of regulator systems*. Holden-Day, San Francisco, 1964.

[AG12] Luis D. Alvergue and Guoxiang Gu. Feedback control for quadratic nonlinear systems. In *24th Chinese Control and Decision Conference*, pages 2566–2571, 2012.

[AGA11] Luis Alvergue, Guoxiang Gu, and Sumanta Acharya. A novel feedback controller for reduced order fluid flow models. In *30th Chinese Control Conference*, pages 711–716, 2011.

[AGA13] Luis Alvergue, Guoxiang Gu, and Sumanta Acharya. A generalized sector bound approach to feedback stabilization of nonlinear control systems. *International Journal of Robust and Nonlinear Control*, (`accepted`), 2013.

[AK99] Ahmad N. Atassi and Hassan K. Khalil. A separation principle for the stabilization of a class of nonlinear systems. *IEEE Transactions on Automatic Control*, 44(9):1672–1687, 1999.

[AK03] Ole Morten Aamo and Miroslav Krstić. *Flow Control by Feedback*. Springer, 2003.

[AKB01] O.M. Aamo, M. Krstic, and T.R. Bewley. Fluid mixing by feedback in poiseuille flow. In *Proceedings of the 2001 American Control Conference*, volume 3, pages 1930–1935, 2001.

[AR10] S. Ahuja and C.W. Rowley. Feedback control of unstable steady states of flow past a flat plate using reduced-order estimators. *Journal of Fluid Mechanics*, 645:447–478, 2010.

[BA11] Hessam Babaee and Sumanta Acharya. A semi-staggered numerical procedure for the incompressible navier-stokes equations on curvilinear grids. In *ASME 2011 International Mechanical Engineering Congress and Exposition (IMECE2011)*, pages 927–936, 2011.

[Bar85] B.R. Barmish. Necessary and sufficient conditions for quadratic stabilizability of an uncertain linear system. *Journal of Optimization Theory and Applications*, 46(4):399–408, 1985.

[Bew99] Thomas R. Bewley. Linear control and estimation of nonlinear chaotic convection: Harnessing the butterfly effect. *Physics of Fluids*, 11(5):1169–1186, 1999.

[BGFB94] Stephen Boyd, Laurent El Ghaoui, Eric Feron, and Venkataramanan Balakrishnan. *Linear Matrix Inequalities in System and Control Theory*. Society for Industrial and Applied Mathematics, Philadelphia, 1994.

[BGL06] John Burkardt, Max Gunzburger, and Hyung-Chun Lee. POD and CVT-based reduced-order modeling of Navier–Stokes flows. *Computer Methods Appl. Mech. Engrg.*, 196:337–355, 2006.

[BL99] Christopher J. Bett and Michael D. Lemmon. Bounded amplitude performance of switched LPV systems with applications to hybrid systems. *Automatica*, 35(3):491–503, 1999.

[Bla99] Franco Blanchini. Set invariance in control. *Automatica*, 35(11):1747–1768, 1999.

[BSS09] Alexandre Barbagallo, Denis Sipp, and Peter J. Schmid. Closed-loop control of an open cavity flow using reduced-order models. *Journal of Fluid Mechanics*, 641:1–50, 2009.

[BSSH09] Shervin Bagheri, Philipp Schlatter, Peter J. Schmid, and Dan S. Henningson. Global stability of a jet in crossflow. *Journal of Fluid Mechanics*, 624:33–44, 2009.

[BT06] D. G. Bogard and K. A. Thole. Gas turbine film cooling. *Journal of Propulsion and Power*, 22(2):249–270, 2006.

[BV04] S. Boyd and L. Vandenberghe. *Convex Optimization*. Cambridge University Press, 2004.

[CBA05] Pinaki Chakraborty, S. Balachandar, and Ronald J. Adrian. On the relationships between local vortex identification schemes. *Journal of Fluid Mechanics*, 535:189–214, 2005.

[Che97] Jie Chen. Frequency-domain tests for validation of linear fractional uncertain models. *IEEE Transactions on Automatic Control*, 42(6):748–760, 1997.

[Cor94] Martin Corless. Robust stability analysis and controller design with quadratic Lyapunov functions. In Alan Zinober, editor, *Variable Structure and Lyapunov Control*, volume 193 of *Lecture Notes in Control and Information Sciences*, pages 181–203. Springer Berlin / Heidelberg, 1994.

[CT89] Hsiao-Dong Chiang and James S. Thorp. Stability regions of nonlinear dynamical systems: A constructive methodology. *IEEE Transactions on Automatic Control*, 34(12):1229–1241, 1989.

[CWRM04] Tim Colonius Clarence W. Rowley and Richard M. Murray. Model reduction for compressible flows using POD and Galerkin projection. *Physica D*, 189:115–129, 2004.

[DBPL00] Raymomd A. Decarlo, Michael S. Branicky, Stefan Pettersson, and Bengt Lennartson. Perspectives and results on the stability and stabilizability of hybrid systems. *Proceedings of the IEEE*, 88(7):1069–1082, 2000.

[DHTZ09] Dan Dai, Tingshu Hu, Andrew R. Teel, and Lucca Zaccarian. Piecewise-quadratic lyapunov functions for systems with deadzones or saturations. *Systems & Control Letters*, 58(5):365–371, 2009.

[DKKO91] A. E. Deane, I. G. Kevrekidis, G. E. Karniadakis, and S. A. Orszag. Low dimensional models for complex geometry flows: Application to grooved channels and circular cylinders. *Physics of Fluids A*, 3(10):2337–2354, 1991.

[DLM99] J. P. Hespanha D. Liberzon and A. S. Morse. Stability of switched systems: A lie-algebraic condition. *Systems & Control Letters*, (37):117–122, 1999.

[Doe09] Charles R. Doering. The 3d navier-stokes problem. *Annual Review of Fluid Mechanics*, 41:109–128, 2009.

[DP00] Geir E. Dullerud and Fernando Paganini. *A Course in Robust Control Theory, A Convex Approach*. Springer, 2000.

[Fah00] Marco Fahl. *Trust-region Methods for Flow Control based on Reduced Order Modelling*. PhD thesis, Universitat Trier, 2000.

[GA94] Pascal Gahinet and Pierre Apkarian. A linear matrix inequality approach to $\mathcal{H}_\infty$ control. *International Journal of Robust and Nonlinear Control*, 4(4):421–448, 1994.

[Gah96] Pascal Gahinet. Explicit controller formulas for LMI-based $\mathcal{H}_\infty$ synthesis. *Automatica*, 32(7):1007–1014, 1996.

[GeHPB98] Mohamed Gad-el Hak, Andrew Pollard, and Jean-Paul Bonnet. *Flow Control: Fundamentals and Practices*. Springer-Verlag, 1998.

[GTV85] Roberto Genesio, Michele Tartaglia, and Antonio Vicino. On the estimation of asymptotic stability regions: State of the art and new proposals. *IEEE Transactions on Automatic Control*, 30(8):747–755, 1985.

[Gun03] Max D. Gunzburger. *Perspectives in Flow Control and Optimization*. Society for Industrial and Applied Mathematics, 2003.

[HaPH10] Kenji Hirata and Jo ao P. Hespanha. L_2-induced gains of switched systems and classes of switching signals. In *49th IEEE Conference on Decision and Control*, pages 438–442, Atlanta, GA, 2010.

[HB76] H.P. Horisberger and P.R. Bélanger. Regulators for linear, time invariant plants with uncertain parameters. *IEEE Transactions on Automatic Control*, 21(5):705–708, 1976.

[HDE00] Je-Chin Han, Sandip Dutta, and Srinath V. Ekkad. *Gas Turbine Heat Transfer and Cooling Technology*. Taylor and Francis, 2000.

[HHL04] Tingshu Hu, Bin Huang, and Zongli Lin. Absolute stability with a generalized sector condition. *IEEE Transactions on Automatic Control*, 49(4):535–548, 2004.

[HLB96] Philip Holmes, John L. Lumley, and Gal Berkooz. *Turbulence, Coherent Structures, Dynamical Systems and Symmetry*. Cambridge University Press, 1996.

[HM76] David Hill and Peter Moylan. The stability of nonlinear dissipative systems. *IEEE Transactions on Automatic Control*, 21(5):708–711, 1976.

[IA92] Alberto Isidori and Alessandro Astolfi. Disturbance attenuation and $\mathcal{H}_\infty$ control via measurement feedback in nonlinear systems. *IEEE Transactions on Automatic Control*, 37(9):1283–1293., 1992.

[IK95] Alberto Isidori and Wei Kang. $\mathcal{H}_\infty$ control via measurement feedback for general nonlinear systems. *IEEE Transactions on Automatic Control*, 40(3):466–472, 1995.

[Isi89] Alberto Isidori. *Nonlinear Control Systems*. Springer-Verlag, Great Britain, 1989.

[JH95] J. Jeong and F. Hussain. On the identification of a vortex. *Journal of Fluid Mechanics*, 285:69–94, 1995.

[JTP94] Z.P. Jiang, A.R. Teel, and L. Praly. Small-gain theorem for iss systems and applications. *Mathematics of Control, Signals, and Systems*, 7:95–120, 1994.

[KB07] John Kim and Thomas R. Bewley. A linear systems approach to flow control. *Annual Review of Fluid Mechanics*, 39:383–417, 2007.

[Kha02] Hassan K. Khalil. *Nonlinear Systems*. Prentice Hall, 3rd edition, 2002.

[Kir00] Michael Kirby. *Geometric Data Analysis: An Empirical Approach to Dimensionality Reduction and the Study of Patterns*. Wiley-Interscience, 2000.

[KK99] Petar V. Kokotović and Hassan K. Khalil. *Singular Perturbation Methods in Control – Analysis and Design*. Society for Industrial and Applied Mathematics, USA, 1999.

[KKK95] Miroslav Krstić, Ioannis Kanellakopoulos, and Petar V. Kokotović. *Nonlinear and Adaptive Control Design*. John Wiley & Sons, USA, 1995.

[KPZ90] Pramod P. Khargonekar, Ian R. Petersen, and Kemin Zhou. Robust stabilization of uncertain linear systems: Quadratic stabilizability and $\mathcal{H}_\infty$ control theory. *IEEE Transactions on Automatic Control*, 35(3):356–361, 1990.

[KSOE08] Coşku Kasnakoğlu, Andrea Serrani, and Mehmet Önder Efe. Control input separation by actuation mode expansion for flow control problems. *International Journal of Control*, 81:1475–1492, 2008.

[LA09] Hai Lin and Panos J. Antsaklis. Stability and stabilizabilty of switched linear systems: A survey of recent results. *IEEE Transactions on Automatic Control*, 54(2):308–322, 2009.

[Lab06] U.S. National Energy Technology Laboratory. The gas turbine handbook. `http://www.netl.doe.gov/technologies/coalpower/turbines/refshelf/handbook/TableofContents.html`, 2006.

[LH06] Kang-Zhi Liu and Rong He. A simple derivation of are solutions to the standard $\mathcal{H}_\infty$ control problem based on LMI solution. *Systems and Control Letters*, 55:487–493, 2006.

[LHC01] Alexander Leonessa, Wassim M. Haddad, and VijaySekhar Chellaboina. Nonlinear system stabilization via hierarchical switching control. *IEEE Transactions on Automatic Control*, 46(1):17–28, 2001.

[Lib03] Daniel Liberzon. *Switching in Systems and Control*. Birkhäuser, Boston, 2003.

[LL98] D. J. Leith and W. E. Leithead. Gain-scheduled controller design: An analytic framework directly incorporating non-equilibrium plant dynamics. *International Journal of Control*, 70(2):249–269, 1998.

[LMG02] Sanjay Lall, Jerrold E. Marsden, and Sonja Glavaški. A subspace approach to balanced truncation for model reduction of nonlinear control systems. *International Journal of Robust and Nonlinear Control*, 12(6):519–535, 2002.

[MH92] Iven .M.Y. Mareels and D.J. Hill. Monotone stability of nonlinear feedback systems. *Journal of Mathematical Systems Estimation Control*, 2(3):275–291, 1992.

[MIH12] Shervin Bagheri Miloš Ilak, Philipp Schlatter and Dan S. Henningson. Bifurcation and stability analysis of a jet in crossflow: onset of global instability at a low velocity ratio. *Journal of Fluid Mechanics*, 696:94–121, 2012.

[MK02] Xia Ma and George M. Karniadakis. A low-dimensional model for simulating three-dimensional cylinder flow. *Journal of Fluid Mechanics*, 458:181–190, 2002.

[MM07] Richard K. Miller and Anthony N. Michel. *Ordinary Differential Equations*. Dover Publications, 2007.

[Mor93] A.S. Morse. Dwell-time switching. In *Proceedings 2nd European Control Conference*, pages 176–181. Proceedings 2nd European Control Conference, 1993.

[NT73] Kumpati S. Narendra and James H. Taylor. *Frequency Domain Methods for Absolute Stability*. Academic Press, New York, 1973.

[NTM04a] Bernd R. Noack, Gilead Tadmor, and Marek Morzyński. Actuation models and dissipative control in empirical galerkin models of fluid flows. In *2004 American Control Conference*, pages 5722–5727, 2004.

[NTM04b] Bernd R. Noack, Gilead Tadmor, and Marek Morzyński. Low-dimensional models for feedback flow control. part I: Empirical galerkin models. In *2nd AIAA Flow Control Conference*, 2004.

[OSH11] Luca Brandt Onofrio Semeraro, Servin Bagheri and Dan S. Henningson. Feedback control of three-dimensional optimal disturbances using reduced-order models. *Journal of Fluid Mechanics*, 677:63–102, 2011.

[Pop62] V.M. Popov. Absolute stability of nonlinear systems of automatic control. *Automation and Remote Control*, 22:857–875, 1962.

[Raj98] Rajesh Rajamani. Observers for lipschitz nonlinear systems. *IEEE Transactions on Automatic Control*, 43(3):397–401, 1998.

[Rav07] S.S. Ravindran. Optimal boundary feedback flow stabilization by model reduction. *Computer Methods Appl. Mech. Engrg.*, 196:2555–2569, 2007.

[Row02] Clarence Rowley. *Modeling, Simulation, and Control of Cavity Flow Oscillations*. PhD thesis, California Institute of Technology, 2002.

[RS00] Wilson J. Rugh and Jeff S. Shamma. Research on gain scheduling. *Automatica*, 36(10):1401–1425, 2000.

[rW95] Karl J. Åström and Björn Wittenmark. *Adaptive Control*. Addison Wesley, second edition, 1995.

[SA90] Jeff S. Shamma and Michael Athans. Analysis of gain scheduled control for nonlinear plants. *IEEE Transactions on Automatic Control*, 35(8):898–907, 1990.

[Sir87] Lawrence Sirovich. Turbulence and the dynamics of coherent structures part i: Coherent structures. *Quarterly of Applied Mathematics*, 45(3):561–571, 1987.

[SJK97] R. Sepulchre, M. Janković, and P.V. Kokotović. *Constructive Nonlinear Control*. Springer, London, 1997.

[SL88] Michael G. Safonov and D.J.N. Limebeer. Simplifying the $\mathcal{H}_\infty$ theory via loop shifting. In *Proceedings of the* 27^th *Conference on Decision and Control*, pages 1399–1404, 1988.

[Son07] E.D. Sontag. *Nonlinear and Optimal Control Theory*, chapter Input to state stability: Basic concepts and results. Springer-Verlag, 2007.

[SWM+07] Robert Shorten, Fabian Wirth, Oliver Mason, Kai Wulff, and Christopher King. Stability criteria for switched and hybrid systems. *SIAM Review*, 49(4):545–592, 2007.

[vdS92] A. J. van der Schaft. $\mathcal{L}_2$-gain analysis of nonlinear systems and nonlinear state feedback $\mathcal{H}_\infty$ control. *IEEE Transactions on Automatic Control*, 37(6):770–784, 1992.

[vdSS99] A.J. van der Schaft and H. Schumacher. *An Introduction to Hybrid Dynamical Systems*. Number 51 in Lecture Notes in Control and Information Sciences. Springer-Verlag, 1999.

[Wil72a] Jan C. Willems. Dissipative dynamical systems part I: General theory. *Archive for Rational Mechanics and Analysis*, 45(5):321–351, 1972.

[Wil72b] Jan C. Willems. Dissipative dynamical systems part II: Linear systems with quadratic supply rates. *Archive for Rational Mechanics and Analysis*, 45(5):352–393, 1972.

[WIOv98] Teruyo Wada, Masao Ikeda, Yuzo Ohta, and Dragoslav Šiljak. Parametric absolute stability of lur'e systems. *IEEE Transactions on Automatic Control*, 43(11):1649–1653, 1998.

[XG89] Xiao-Hua Xia and Wei Bin Gao. Nonlinear observer design by observer error linearization. *SIAM Journal Control and Optimization*, 27(1):199–216, 1989.

[Zam66a] G. Zames. On the input-output stability of time-varying nonlinear feedback systems, part I: Conditions derived using concepts of loop gain, conicity, and positivity. *IEEE Trans. Automat. Contr.*, 11:228–238, 1966.

[Zam66b] G. Zames. On the input-output stability of time-varying nonlinear feedback systems, part II: Conditions involving circles in the frequency plane and sector nonlinearities. *IEEE Trans. Automat. Contr.*, 11:465–476, 1966.

Vita

Luis Donaldo Alvergue was born on March 1st, 1981 in San Salvador, El Salvador. He obtained the B.S. degree in engineering (concentration in electrical) in 2004 at McNeese State University. In 2005 he enrolled at Louisiana State University to pursue graduate studies in the Electrical and Computer Engineering Department with a focus in control systems. He is currently a candidate for the Doctor of Philosophy degree in electrical engineering which will be awarded in May 2012.